

PPPL-5448

Heating and Current Drive Analysis for the Electron Cyclotron System

F. Poli

Fiscal Year 2018



Prepared for the U.S. Department of Energy under Contract DE-AC02-09CH11466.

Princeton Plasma Physics Laboratory

Report Disclaimers

Full Legal Disclaimer

This report was prepared as an account of work sponsored by an agency of the United States Government. Neither the United States Government nor any agency thereof, nor any of their employees, nor any of their contractors, subcontractors or their employees, makes any warranty, express or implied, or assumes any legal liability or responsibility for the accuracy, completeness, or any third party's use or the results of such use of any information, apparatus, product, or process disclosed, or represents that its use would not infringe privately owned rights. Reference herein to any specific commercial product, process, or service by trade name, trademark, manufacturer, or otherwise, does not necessarily constitute or imply its endorsement, recommendation, or favoring by the United States Government or any agency thereof or its contractors or subcontractors. The views and opinions of authors expressed herein do not necessarily state or reflect those of the United States Government or any agency thereof.

Trademark Disclaimer

Reference herein to any specific commercial product, process, or service by trade name, trademark, manufacturer, or otherwise, does not necessarily constitute or imply its endorsement, recommendation, or favoring by the United States Government or any agency thereof or its contractors or subcontractors.

PPPL Report Availability

Princeton Plasma Physics Laboratory:

<http://www.pppl.gov/techreports.cfm>

Office of Scientific and Technical Information (OSTI):

<http://www.osti.gov/scitech/>

Related Links:

[U.S. Department of Energy](#)

[U.S. Department of Energy Office of Science](#)

[U.S. Department of Energy Office of Fusion Energy Sciences](#)

Heating and Current Drive Analysis for the Electron Cyclotron System

Work for Others Agreement

ITER Organization Reference No. 430000900
IO/RFQ/13/9550/JTR EC Analysis

between

Princeton University

and

ITER Organization

Francesca Maria Poli

Contents

1	Introduction	1
1.1	Objectives of the analysis and revision of deliverables	3
1.2	Summary of main results	5
2	Simulation assumptions and approach	9
2.1	Thermal transport	10
2.2	Boundary conditions for the pedestal pressure	10
2.3	Module for NTM control with EC feedback	11
2.4	Limits of the simulations for NTM control and stabilization	15
3	Heating and Current Drive sources	17
3.1	Electron cyclotron heating and current drive system	17
3.1.1	Electron cyclotron heating and current drive calculations	17
3.2	Neutral Beam heating and current drive system	20
3.2.1	Neutral Beam source models comparison	21
3.3	Ion cyclotron heating and current drive system	23
3.3.1	Ion Cyclotron source models comparison	24
4	Power management in the ELMy H-mode scenario	25
4.1	Reference simulation	25
4.2	Evolution of the (2, 1) and (3, 2)-NTMs	27
4.3	Control of NTMs in the ELMy H-mode plasma	28
4.3.1	Comparison of active search and pre-emptive control	28
4.4	IC heating	31
4.5	On the feasibility of sawtooth period pacing with the Equatorial Launcher	33
5	Operation at half-field	35
5.1	Neutral Beam heating	35
5.2	Electron Cyclotron heating	35
5.3	Ion Cyclotron Heating	38
5.4	General assumptions of simulations at half-field	39
6	H&CD power management in DT and DD plasmas	40
6.1	NTM control	41
6.2	Feasibility of sawtooth period pacing	45
7	H&CD power management in helium plasmas	47
7.1	IC heating schemes in Helium plasmas	50
7.2	NTM control in helium plasmas	53
7.3	Commissioning of the EC system	55
8	H&CD power management in hydrogen plasmas	56
8.1	IC heating in Hydrogen plasmas	58

1 Introduction

The heating and current drive (H&CD) systems of ITER are critical components to its successful burning plasma demonstration and deriving the capabilities for each of these systems is absolutely necessary. They provide heating to either electrons or ions (or both) that is critical for access to high confinement regimes, sustainment of performance, impurity control and volt-second consumption saving at startup. They provide current drive for ramp-up assist, plasma stability through current profile tailoring, which is critical for long pulse performance. Figure 1.1 summarizes the desired applications in a generic plasma discharge and highlights - for each system - the principal contributions. Thick arrows indicate where a system is going to provide a critical contribution that cannot be replaced by the other systems. For example, the Neutral Beams provide a broad current drive profile that cannot be provided by the other systems, especially at operation with low plasma current; they also provide external torque to the plasma, although much lower than in present day experiments because of the large plasma volume on ITER.

Contrary to present day experiments, ITER is dominated by electron heating and ions are predominantly heated by the electrons. At ITER burning plasma parameters, the role of the IC system should be revisited based on its synergy with the other systems. IC provides localized core heating for impurity accumulation control, which is particularly important in the plasma current ramp-up and ramp-down and across the transition to and from H-mode. However, this capability can also be covered by the EC system. The IC system has more flexibility in providing heating both to electrons and ions, but its role as the principal source of ion heating is more marginal compared to present day experiments. In particular, it will be shown that the dominant heating

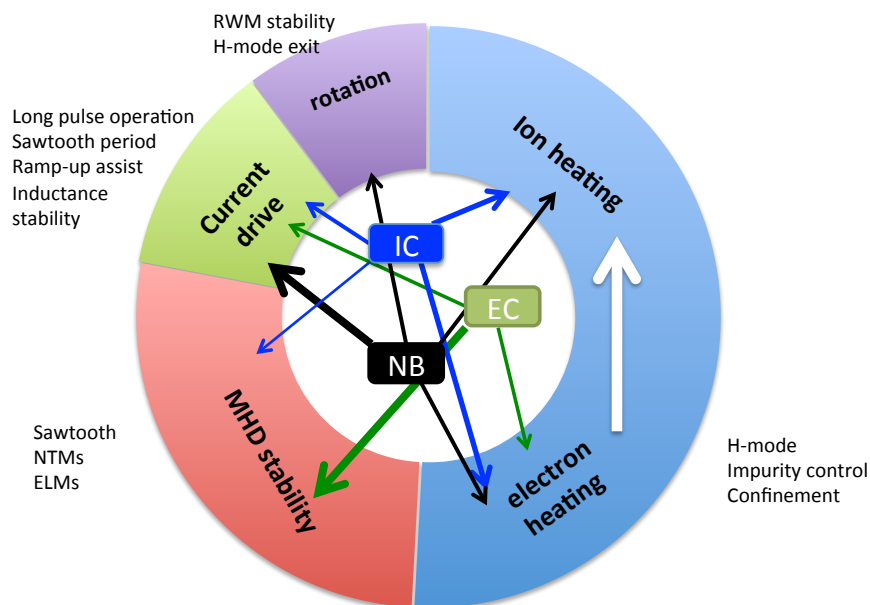


Figure 1.1: Schematics of the contribution of each H&CD source to a generic plasma application, based in part on the results of the analysis undertaken. Thicker arrows indicate where an individual source contributes the most compared to the others.

from the IC at half-field is to the electrons and a scheme with good ion absorption exists only in the ELMy H-mode at full field. In the plasma simulations undertaken here the IC is used in the ramp-up and in the ramp-down phase to provide core heating. It has been shown that IC can be successful to stabilize/destabilize the sawtooth cycle [?]. However, this requires fine tuning of the antenna frequency to provide absorption highly localized around the $q = 1$ surface. While this flexibility on ITER has to be demonstrated, this application might be incompatible with other combined applications, like core heating, which is critical for control of impurity accumulation. The availability of two antennas would overcome some of these limitations.

Among the planned external H&CD systems, the Electron Cyclotron system (EC) has the highest flexibility. By combining the equatorial and the upper launcher, the EC system can cover up to 85% of the plasma cross-section, missing about 10% of the edge and about 5%-10% near the axis, allowing for simultaneous functions like central heating, current profile tailoring, impurity control and MHD stability control of Neoclassical Tearing Modes and sawteeth [1–3]. Assessing the capability of the EC system for these combined functions, in a wide range of possible plasma scenarios from half-field to full-field, is critical to guarantee that sufficient power is available, engineering design is adequate and that a control strategy for simultaneous functions can be established. The dominant contribution of the EC system is to MHD stability, primarily NTM stabilization and suppression. It will be shown that - within the assumptions of the models used - the local modification of the magnetic shear that is used for sawtooth pacing with EC in present day experiments might not be as successful in ITER. Although the use of both co-current injection equatorial mirrors can modify the magnetic shear locally and induce an internal reconnection when the power is promptly removed from near the $q = 1$ resonant surface, the dominant mechanism for the sawtooth crash is still provided by fast ion effects not being sufficient to stabilize the internal kink instability.

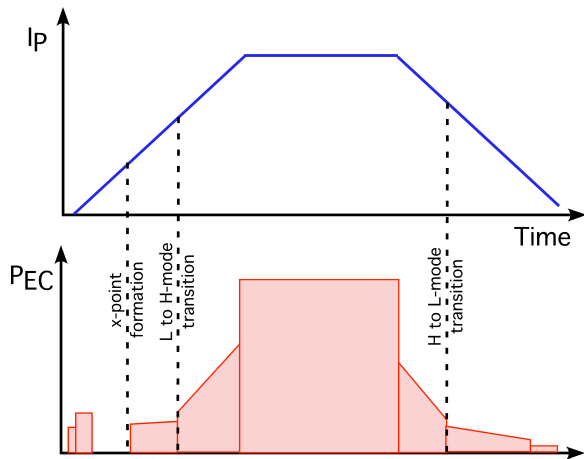


Figure 1.2: Schematics of the applications of the EC for a generic plasma discharge.

is turned-off after the H-L back transition because of the difficulty of tracking the plasma core during the rapid shrinking and downward drift that follows the H-L back transition. The EC might still be used during the current ramp-down in plasma discharges at reduced magnetic field and current that are terminated with a full-bore cross-section. These scenarios are not considered here, but might be of interest for assessment of vertical stability, heat load on the inner wall and test of the disruption mitigation system.

Figure 1.2 shows a schematics of possible applications of the EC system in a generic plasma discharge, with the expected power investment. They include (a) breakdown and burn-thru assist in a limited plasma for flux consumption saving, (b) ramp-up assist and H-mode access (c) MHD control and central heating in the flat-top phase (d) ramp-down assist and exit from H-mode and (e) plasma termination. Every application has to be accurately balanced with the other H&CD sources for optimization of the available resources.

The primary functions envisioned for the EC system are summarized in Table 1.1. The last two columns indicate which of these functions can be performed by the other systems.

Breakdown and burn-through are not examined here and all simulations use the EC system only after the X-point formation. Also, the EC

Impurity control is also not part of the analysis performed, since self-consistent impurity transport was not available at the time of defining the terms of the contract.

Sawtooth pacing with EC is achieved in present-day experiments by modifying the magnetic shear close to the $q = 1$ surface. The analysis undertaken here has addressed the effectiveness of the Equatorial Launcher on ITER to modify the sawtooth period in a similar way, both in scenarios at half-field and full-field. Instead, sawtooth stabilization/destabilization with IC waves is not discussed, because this analysis would require implementing a parametrization of the effects from IC fast ions in the sawtooth model, based on nonlinear MHD stability calculation.

The impact of coherent turbulence structures (blobs) and pellets on the broadening and scattering of the EC waves was originally included in the scope of the contract. This analysis has been dropped because it would require not only self-consistent simulations with a pellet module and an EC source model, but also coupling with a turbulence model (or an equivalent parametrization of the scattering effects), which was not available at the time of defining the scope of this contract.

1.1 Objectives of the analysis and revision of deliverables

The principal aim of this task was to provide time-dependent analysis of the EC H&CD deposition profiles for the various plasma scenarios to assess the EC system primary functional aims, as listed in Table 1.1, then couple the results with the functional capabilities of the other H&CD systems for revising the global power management for the ITER scenarios.

An EC system preliminary design review was performed in November 2012, wherein the review panel identified the need for additional EC H&CD analysis to ensure the EC system can achieve the desired objectives within reasonable delivered power limits. In addition, further analysis was required to assess the management of the injected power distributed over the various functions that may occur simultaneously in a plasma discharge.

The original workplan was organized in terms of a number of scenarios without taking into account that the aims and needs change depending not only on magnetic field and current, but also on background plasma species and how the different H&CD systems are used together. The EC power management and how the EC functions in synergy with the other H&CD systems has to be done case by case and this is one of the main conclusions of this work. There is no universal recipe to the choice of the phasing of the IC antenna and the balance of electron and ion heating depends on the phase of the discharge. It is common approach to assume that the IC is used with phasing for dominant heating rather than current drive; however, IC current drive provides an additional knob to the tailoring of the current profile not only in advanced scenarios, but also during operation at half-field. Time-dependent simulations for ITER scenarios usually target full energy beam sources, with the target of demonstrating access to H-mode and - at the same time - commissioning the system. However, changing the beam source energy modifies the fast ion contribution to the sawtooth stability; used in combination with the EC system with steering inside the $q = 1$ surface, the NBI system provides a passive approach to sawtooth pacing, by acting on the relaxation of the current profile during the sawtooth cycle. In addition, it provides flexibility for energetic particle studies studies and transport induced by fast ions, for which ITER will represent the only opportunity before DEMO-like experiments.

In the end, this analysis has not given the answers to the initial question of how much power is needed for each individual application, but it has replaced it with an alternate question of "how should the plasma discharge be designed" to achieve the target with the available resources and ensure that the use of these resources is optimized. More importantly, by focussing on the dynamics

task	Function	UL	EL	Scenarios	IC	NB
X	Ramp-up/down assist	X	X	all	X	X
	breakdown (X2 and O1)	X	X	all	X	
X	sawtooth control	X	X	L and H-mode	X	
X	NTM control	X		H-mode		
	impurity control		X	H-mode	X	
X	impact of blobs/pellets	X	X	all		
X	L-H mode transition	X	X	H-mode	X	X
X	current profile control	X	X	hybrid and advanced	X	X
X	bootstrap current optimization	X	X	advanced	X	X

Table 1.1: Primary functions envisioned for the EC system. The first column indicates which application was targeted (X), which has not been undertaken (X) and which was not planned but has been undertaken (X).

of the system, it has identified areas where further analysis is needed, it has lowered the priority of secondary applications like sawtooth control, it has identified phases of the discharge where plasma engineering is necessary to ensure that the use of available resources is optimized and it has identified what control schemes would be more appropriate for NTM control in ITER.

The major revision to the analysis of the EC functionalities concerns the control of NTMs with the UL. This functionality was not included in the original contract, with the agreement that prior, published results would have been used for the power management analysis. However, it was later recognized that assessing the power needed for NTM control in every phase of the plasma discharge is critical for actuator power sharing and that such a detailed analysis, including the onset of the NTM moving from half-field to full-field, has never been undertaken. Because the plasma profiles evolve in response to the external actuators, it is critical that the assessment of the power needed for NTM control, including potential limits of the EC feedback control, are assessed in time-dependent simulations. The approach undertaken and its limits are described in Sec.2.

Table 1.2 summarizes the scenarios and the analysis agreed upon at the time of signing this Task Agreement. At the face-to-face meeting in December 2015, the initial scope has been modified to accommodate the ITER research priorities: the hybrid and steady state scenarios have been dropped and assessment of operation at half-field has been raised in priority. Also, some scenarios have been dropped to avoid overlapping and duplication of efforts with the research undertaken by the Science and Operation Department (SCOD). These include (a) assessment of H-mode operation at 5.3 T and 15 MA in Helium and Hydrogen plasma (b) L-mode operation at half-field and full-field in Helium and Hydrogen plasmas. These scenarios have been studied as part of a joint ITPA-IO activity, led by Sun-Hee Kim (SCOD) [4]. The analysis of H-mode plasmas in He/H at half-field has been kept in the scope of work, but closely coordinated with SCOD as part of this IO joint activity. It should be noted that all ITER scenarios are continuously improved as new modeling capabilities are available and cross-compared among codes (TRANSP, CORSICA, JINTRAC) as part of joint ITPA-IO activities. The cases simulated and discussed in the following sections will be further improved as new physics modules become available, working in collaboration with SCOD and with the ITPA-IO group.

New compared to the joint ITPA-IO activity is specific analysis of the EC system, like an assessment of parasitic absorption on the third harmonics, which is strongly dependent of local values of the electron temperature and of details of the profiles inside the pedestal. This effect was

not identified in offline analysis based on temperature profiles rescaled from the baseline scenario [3], but is instead highlighted in the TRANSP simulations when the pedestal boundary conditions are calculated from interpolation over a look-up table of EPED1 and the thermal transport is evolved using a physics based model. Following this assessment, and within the limits of the models used herein, it is concluded that there is limited central access from power launched from the EC Equatorial Launcher at 2.65T, but that limitations can be avoided operating at magnetic field around 2.75T. Scenarios at intermediate values of the magnetic field were included in the original list of deliverables, like those at 3.3T and 4.3T. The assessment at 3.3T has indicated that radial accessibility of the EC inside the $q = 1$ surface is not possible and this scenario has not been analyzed for global power balance. A short description of the limitations of this operational point is provided in Sec.5. The scenario at 4.3T has been removed from the list of cases to be analyzed, having been assessed to be lower priority and because of the addition of new cases around half-field.

A significant amount of time has been spent during the first year of the contract on benchmarking between the H&CD modules in TRANSP against those in JINTRAC, which was not part of the original agreement. This code comparison has served for the calibration of the neutral beam geometry against ITER provided parameters and to ensure that the EC calculations in TRANSP are consistent with those currently used by the ITER Organization. Notable results of this exercise have revealed deficiencies - which have been fixed - in the code for neutral beam calculations ASCOT in helium plasmas (used in JINTRAC) and in the calculation of the EC current drive in TORBEAM (used in TRANSP). The comparison of the IC calculations is inconclusive, since all IC codes have their own limitations. While they are in fairly good agreement when used for thermal ion heating at the fundamental and first harmonics of the ion cyclotron resonance, they have very large uncertainties in the calculations of quasi-linear effects, because of different assumptions and approximations taken in the expansion of the Fokker Planck operator, which affect calculations of minority heating, absorption on fast ions and on alpha particles.

1.2 Summary of main results

The main conclusions from the analysis performed within this task agreement can be summarized as follows:

1. global power balance analysis should be done case by case. This is a cultural change compared to approaches previously undertaken based on profile rescaling, tabulated targets and time-slice analysis of H&CD sources. In particular, there is no universal recipe for the phasing of the IC antenna (it is common to use toroidal mode number of $n_\phi = 27$), since the balance between electron and ion heating, the absorption on the beam fast ions and the effect on the global evolution of the discharge need to be analyzed considering the synergy with the other sources. Thus, while the Neutral Beams provide the backbone for the evolution of the global parameters, the IC and the EC heating and current drive provide additional knobs for local modification of the temperature and current profile that affect the global performance and stability of the plasma, including the sawtooth cycle. In particular, the use of the IC as an actuator needs better characterization such that its potential usage for controlling plasma parameters and instabilities can be better exploited.
2. a self consistent time dependent simulation will likely be done for each ITER plasma discharge in advance, which will set up a ‘recipe’ for the input to the Plasma Control System. The latter will then provides a general plan for the discharge and an interactive analysis will be

	B_T (T)	I_P (MA)	gas mix	Notes
L-mode	2.65	7.5	He/H D	EC commissioning dropped
L-mode	5.3	15	He/H D	dropped dropped
L-mode	5.3	15.0	DT	dropped
H-mode	2.65	7.5	He/H D DT	done done new
H-mode	2.85	8.1	He/H D DT	new new new
H-mode	3.3	9.2	He/H	done
H-mode	5.3	15.0	DT	done
Hybrid	2.65	6.0	He/H D	dropped dropped
Hybrid	5.3	15.0	DT	dropped
steady state	2.65	3.0-4.5	He/H DT	dropped
steady state	5.3	6.5-9	DT	dropped

Table 1.2: List of scenarios analyzed in the task agreement, highlighting which has been dropped and which has been introduced as a consequence of the unknowns of the analysis in this task agreement.

used during the shot following this recipe. As a result the issue of how to power balance the available Heating and Current Drive sources will be performed on a shot to shot basis.

3. Good heating schemes for the Ion Cyclotron waves at half-field are limited to deuterium and tritium plasmas. The use of IC in Helium plasmas is possible with Hydrogen minority heating, provided the fraction of hydrogen does not exceed ten percent of the electron density. This is a challenge, because pellet injection will be needed in this plasmas to achieve densities where full energy Neutral Beam sources can be used. Moreover, the synergy of IC waves with fast ions needs to be assessed including orbit losses of accelerated particles from the wave electric field and this is arguably possible only in self-consistent time-dependent simulations. Because of the absence of good heating schemes in hydrogen plasmas, the use of IC at reduced field is possible only at 3.0T. However, the core accessibility of the EC at this field is significantly reduced. For this reason, it is very unlikely that H-mode access in hydrogen plasmas is possible at half-field unless the external power is increased.
4. pre-emptive control of NTMs is recommended on ITER, especially on the $q = 2$ surface. This conclusion is driven by the observation that the magnetic island may take only a few seconds to grow and lock. Since the detection threshold from the ECE diagnostics would be about 4 cm when the effect of fluctuations on the signal to noise ratio is taken into account, and the time required by the mechanical switch that re-directs the power between the Equatorial and the Upper Launcher can be up to 3 seconds, there would be not enough time to detect, track and suppress an NTM. Compared to previous assessments based on asymptotic calculations and standalone calculations, here the evolution of the magnetic island is calculated taking into account the mechanical response time of the EC system and the subsequent delays in the

feedback control.

5. Details of the evolution of the density and the timing of entry to H-mode do affect the growth rate of the magnetic island and how long it takes to lock. Plasma discharge engineering is here necessary to ensure that the entry to H-mode is optimized for MHD stability and NTM control and is an area where modeling should be guided by experiments for validation and by advanced MHD calculations for verification of the reduced models used in these assessments.
6. The EC power should be reserved for NTM control during the entire H-mode phase, with up to 13.4MW for the (2,1)-NTM at entry and exit from H-mode. During the flattop phase the power needed for pre-emptive control is reduced down to a maximum of 5-6 MW. Thus pre-emptive control minimizes the power needs for NTM stabilization and suppression, while at the same time maximizes the global performance of the discharge by potentially sustaining fusion gain close to the target.
7. The entry and exit from H-mode are the most critical phases of the discharge for NTM control. In the ramp-up phase the plasma surface is still expanding and tracking of the resonant surfaces is more challenging. In the ramp-down phase the EC deposition width broadens in combination with the plasma cross section being reduced, the EC current density peak decreases and therefore the power requirement for NTM control increases. The current ramp-up and current ramp-down phase might need to be re-designed regarding to H-mode access, current ramp-down duration and density evolution to ensure that the EC system can provide stabilization and suppression of NTMs, while at the same time ensure that sufficient core heating is available. In the ramp-down in particular, the use of the IC for core heating might be limited by the changing of the plasma cross-section.
8. Approaches to NTM control used in present-day experiments might not be as efficient on ITER. This includes not only an active search of the magnetic island (which would leave no time to the system to respond), but also combined sawtooth and NTM control. While on present-day experiments modification of the local magnetic shear provides a sufficient criterion for the triggering of a crash and thus localized EC heating and current drive (and prompt removal) close to the $q = 1$ surface is an effective method for sawtooth pacing, on ITER fast ion effects provide the dominant mechanism for stabilization of the sawtooth cycle and the EC system might not be effective for sawtooth pacing. The simulations indicate that deposition of the EC inside the $q = 1$ can alter the sawtooth period provided both co-current EL mirrors are used. However, removal of the power can trigger only an internal reconnection, but it is not sufficient to overcome the stabilizing effect of fast ions. In the ELMy H-mode scenario the sawtooth period converges to 40 seconds independently of the use of the EC. In plasmas at half-field, by appropriate choice of the beam energy and the electron density, the sawtooth period can be extended up to 100s, making these plasmas good candidates for demonstration of control of NTM triggered by long period sawteeth. This is particularly important for the commissioning of the NTM control system in helium and hydrogen plasmas where NTMs would otherwise be stable.
9. Operation at half-field needs to be optimized to avoid parasitic absorption of the EC on the third harmonics, which is inside the plasma at 2.65T. While operating around 2.75T would eliminate this problem, operation at 2.65T is still possible within a reduced range of poloidal steering angles for the EL and provided the wave polarization is changed from X-mode to O-mode after transition from L-mode to H-mode. Since changing the polarization requires about three seconds, the use of the NBI sources (energy and timing) needs to be optimized to

avoid back transitions to L-mode caused by the loss of localized heating. To ensure the full capability of the EC system and not loose accessibility inside mid-radius and - importantly - inside $\rho = 0.25$ for core heating and impurity accumulation control, the magnetic field should not be exceed 2.85T. This reduces the operation window originally proposed in the ITER research plan, which was extending up to 3.3T.

2 Simulation assumptions and approach

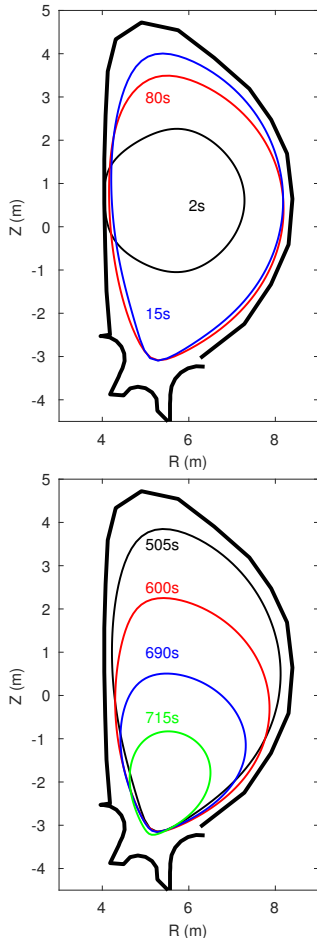


Figure 2.1: Plasma boundary from CORSICA during the ramp-up (top) and during the ramp-down (bottom) phase.

free-boundary simulations undergo vertical stability at the H-L transition and the plasma is lost either against the inner wall or because it becomes vertical unstable. Since optimization of shape and coil currents is not part of the analysis, and for the sake of computational time, all simulations - unless specified - are run as fixed-boundary. Plasma simulations at different values of magnetic field and current maintain the same cross-section shape and the same relative duration of the H-mode and L-mode phase in the current ramp-down.

All time-dependent simulations are run with the equilibrium and transport solver TRANSP [5]. The simulation is initiated as a full-bore, limited plasma, with current of 200 kA, which is grown to full size and diverted at about 12-15s. In the current ramp-down phase the plasma cross-section is maintained constant during H-mode, then the plasma is shrunk in size and guided downward during the L-mode and Ohmic phase, until the plasma current is reduced to 2 MA. The sequence of boundary shapes used as a reference has been provided by Sun-Hee Kim (ITER Organization, SCOD) from a CORSICA simulation of the baseline discharge and are shown in Fig.2.1. It is noteworthy that the duration of the ramp-up, of the flattop and of the ramp-down phase used in TRANSP are not the same as in CORSICA, thus there is no one-to-one correspondence between the times indicated in the figure and those in TRANSP. However, anchor points are the same, like the boundary shape at the X-point formation (around 12s in both cases), in the flattop phase, before and after the H-L transition and at 2MA current at the end of the termination phase. In the case of the ELMy H-mode plasma at 5.3T and 15MA, shown in Fig.2.1, the flattop phase starts at 60s in CORSICA and the plasma enters H-mode at the end of the current ramp-up phase. In TRANSP the flattop phase starts at 80s and the L-H transition is pre-programmed at about 65 seconds, towards two thirds of the current ramp-up duration. As it will be discussed in Sec.4, this choice is dictated by the evolution of the (2,1)-NTM island and by the time of locking. In CORSICA the current ramp-down phase starts at 500s, lasts for about 200s and the H-mode and L-mode phases have approximately the same duration, with H-L mode transition between 550s and 560s and the plasma being terminated at 720s. The TRANSP simulation is extending the duration of the flattop phase to 550s, with EOF at 630 seconds and it has reduced the duration of the H-mode in the current ramp-down because it was found that the control of NTMs in this phase is difficult. Thus the H-mode and the L-mode phase last about 35s each. However, the ramp-down phase requires optimization,

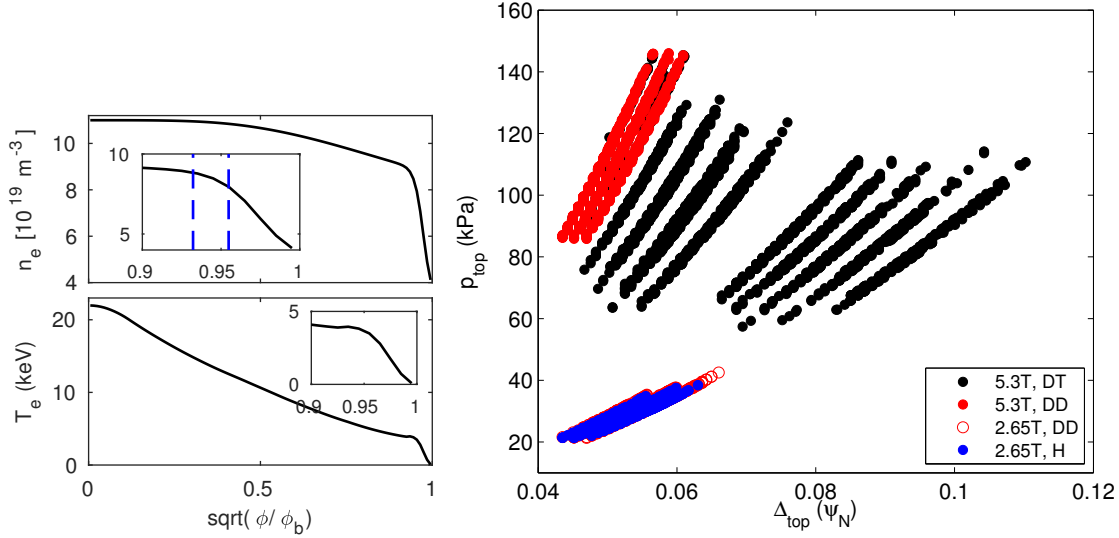


Figure 2.2: Left: analytic profiles assumed to shape the pedestal in the density and in the temperature profile. Right: database of EPED1 calculations, covering the operational space of ITER.

2.1 Thermal transport

The turbulence transport model GLF23 [6, 7] is used to predict thermal ion and electron, as well as momentum transport. Using GLF23 provides a good compromise between a physics-based model and computational time, as opposed to using TGLF [8] (physics based, but computationally intensive) and using semi-empirical models like Coppi-Tang [9] (fast and robust, but not physics-based). The electron density profile is prescribed in these simulations and the ion density profiles are calculated from particle balance assuming quasi-neutrality. Impurity profiles are assumed to be the same as electron density profiles, and rescaled according to fraction values that are prescribed in time. A self-consistent treatment of the impurity transport has recently been implemented in TRANSP, but was not available when these simulations have been performed. No assessment has been made on the effect of the choice of the turbulence transport model on the results of the simulations.

2.2 Boundary conditions for the pedestal pressure

The threshold for the L-H transition is calculated based on the ITPA scaling [10]:

$$P_{L-H} = 2.84 m_H^{-1} B_0^{0.82} \bar{n}_e^{-0.58} R a^{0.81} \quad (2.1)$$

The transition to H-mode occurs when the power across the separatrix is larger than the net power $P_{\text{loss}} - c_H P_{L-H}$, where the scaling factor c_H can be used to adjust the power threshold in those cases, like He plasmas, where the ITPA scaling would predict too high a threshold for transition compared to experimental evidence.

The pedestal height and width are calculated from a lookup table of peeling-ballooning stability limits provided by EPED1 [11]. Figure 2.2 shows the database of EPED1 calculations for the ITER operational space at half-field and full field and for hydrogen plasmas, deuterium plasmas and a mix of deuterium and tritium. The ion mass dependence - although an explicit input - is negligible in EPED1 so that results for different background plasma species (hydrogen, deuterium or a mix of

deuterium and tritium) are the same within less than 0.1%. Calculations for helium are not available at this time, since this implementation would require modifying EPED1 to allow calculations for non-hydrogenic species. The pedestal pressure calculated in this case is therefore the same as that of hydrogenic species plasmas.

Inputs to the EPED1 calculations are $B_T, I_P, n_{ped}, \beta_N, Z_{eff}, \kappa, \delta, R, a$. For ITER the major radius R and the minor radius a are fixed and the dominant parameters for the scaling are the pedestal density, the plasma current, the shaping parameters, the normalized pressure and the plasma composition Z_{eff} . The database includes about 6700 cases, of which 1500 are for the ELMy H-mode scenario at 15MA.

A multi-space interpolation is performed during the discharge at each time step of the H&CD source calculation, δt_{HCD} , to find height and width for a given pedestal density. When the density profile is prescribed in the simulations, the profile is constructed using the following parametrization [12]:

$$n_e(\psi) = n_{e0} \left((1 - r_2) \left(c_1 \left[H \left(1 - \frac{\psi}{\psi_{ped}} \right) \left(1 - \left(\frac{\psi}{\psi_{ped}} \right)^\alpha \right)^\beta \right] + c_2 \left[\tanh \left(2 \frac{1 - \psi_{mid}}{1 - \psi_{ped}} \right) - \tanh \left(2 \frac{\psi - \psi_{mid}}{1 - \psi_{ped}} \right) \right] \right) + r_2 \right) \quad (2.2)$$

The parameters c_1 and c_2 are defined as follows:

$$c_2 = \left(\frac{r_1 - r_2}{1 - r_2} \right) \frac{1}{2 \tanh 1} \quad (2.3)$$

$$c_1 = 1 - c_2 [1 - \tanh 1] \quad (2.4)$$

and $r_1 = n_{e,ped}/n_{e,0}$, $r_2 = n_{e,sep}/n_{e,0}$ define the values of the density at the pedestal and at the separatrix. The profile is thus fully characterized by four parameters, α, β, r_1, r_2 . The interpolation algorithm starts with an initial guess for the pedestal density as $n_{e,ped} = 0.61 \bar{n}_e$ and iterates over the lookup table until a solution is found that satisfies the dependence on all the input parameters. When the density is predicted, an additional condition is required after the L-H transition to setup a pedestal in the density profile. In this case, an initial guess over the ratio of the pedestal density to the density at the separatrix is provided as an input and the algorithm seeks for a converged solution starting from an initial guess of $n_{sep} = 0.35 n(0)$, consistent with the hypotheses made on the density profile shaping in the ELITE MHD calculations to derive the EPED1 scaling [11].

With this approach, variations in β_N in the discharge will be nonlinearly correlated to the pedestal height, as opposed to prescribing a value upfront, which is common procedure in time-dependent simulations. In the simulations shown in this report, where it is assumed that the heating and current drive sources have no unexpected failure and the input power is constant in time and where the density and impurity profiles are prescribed in shape and amplitude, the pedestal width and height are fairly constant during the entire discharge simulation.

2.3 Module for NTM control with EC feedback

In order to assess the EC control system requirements, it is important to simulate the evolution of the NTM island in combination with the plasma magnetic equilibrium and the kinetic profiles, as they evolve in response to the external heating and current drive sources. Approaches based on a modified form of the Rutherford Equation [13] are routinely used for calculations of NTM stability in real-time control oriented algorithms [14].

The TRANSP transport solver [5] has a unique capability of being used in conjunction with so-called ‘expert files’, external fortran codes that are linked to the main executable and that allow users to manipulate the simulations by including additional features. A direct application of expert files is for simulations dedicated to develop control algorithms and it has been applied on NSTX-U for control of the plasma performance [15, 16] and of plasma rotation [17] with Neutral Beam Injection. In this respect expert files can provide valuable inputs for control requirements, diagnostic sensitivity or development of shared power actuator control algorithms, because they allow to test the plasma response to external perturbations in the presence of high-fidelity physics models.

In order to provide a simulated response of the plasma, a Modified Rutherford Equation (MRE) [13] has been interfaced with TRANSP using an expert file, using the loop shown in Fig.2.3. The feedback control consists of two parts: one provides the evolution of the width and rotation frequency of the island and the other interfaces the calculation of the island stability with a feedback control of the poloidal steering mechanism and of the EC input power. Only cases with continuous EC injection are analyzed within this Task Agreement. In fact, the EC power modulation needed to synchronize the injection window with the island O-point is important only when the EC deposition width is larger than the magnetic island size [18–20], a situation that is not observed in the simulations performed and discussed here.

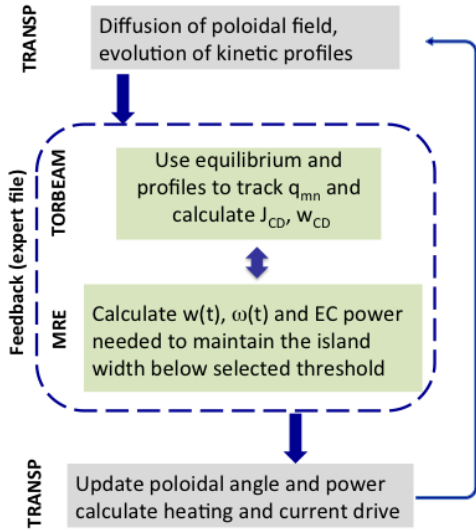


Figure 2.3: Schematic of the interface between TRANSP and the EC controller for NTM stabilization.

The part that deals with the control of the EC power and steering uses the beam tracing code TORBEAM [21, 22] and can be pre-programmed for combined applications, like sawtooth and NTM tracking and control. At each time step t_1 TORBEAM calculates the beam trajectory for a given poloidal steering angle and for given equilibrium and kinetic pressure plasma profiles and it aligns the beam with the resonant surface of interest, r_s , within a pre-selected tolerance dr_0 on the maximum allowed misalignment. The separation between successive time steps, δt_{HCD} , is pre-selected in TRANSP at the submission of the run. The longest time scale considered here for the feedback control is given by the mechanical switching of the EC transmission path between launchers, which has an upper limit of 3s. Other time scales of the hardware to be considered include (a) the time needed to turn-on and off a gyrotron, which is of the order of tens of milliseconds (b) the steering mechanism can scan the entire poloidal angle range of 30 degrees in about 2s, with steps of 0.02 degrees, therefore continuous mirror steering for tracking the island would require additional several milliseconds (c) the computation of real-time feedback control algorithm would be fast and of the order of a few milliseconds. These additional sources of delay were assumed not to impose any significant additional delay over the time-scale of switching the EC transmission path between EC launchers.

The second part in the EC feedback control deals with the calculation of the magnetic island width based on a MRE, using the implementation by E. Fredrickson [23], to which two terms for

the ECCD and for the ECH have been added:

$$\frac{dw}{dt} = 1.22 \frac{\eta}{\mu_0} [\Delta'_{m,n}(w) + \Delta'_{NC}(w) + \Delta'_{pol}(w) + \Delta'_{GGJ}(w) + \Delta'_{ECCD}(w) + \Delta'_{ECH}(w)] \quad (2.5)$$

where μ_0 is the magnetic permeability and η the neoclassical plasma resistivity, which is calculated in TRANSP using the NCLASS libraries [24]. For a given poloidal steering angle and input power TORBEAM calculates the driven current and heating profiles and the deposition width assuming a perfectly focussed, gaussian beam. These values are used in the $\Delta'_{ECCD}(w)$ and $\Delta'_{ECH}(w)$ terms. The procedure is iterated and the input EC power increased until the calculated $\Delta'_{tot}(w)$ drops to zero, indicating stabilization or suppression. The MRE evolves the magnetic island width and rotation frequency between t_1 and $t_2 = t_1 + \delta t_{HCD}$ with internal time steps of 25ms, under the effect of the EC for given input power, poloidal steering angle and calculated current density profile. The $\Delta'_{m,n}(w)$ term in Eq.2.5 represents the drive or damping on the tearing mode imposed by the external solution and it uses the so-called Δ' formalism to deal with the boundary layer physics inherent in tearing mode theory [25]. It has been shown that a full solution of the resistive magneto-hydrodynamic (MHD) equations is not necessary to determine the stability of a given current profile to tearing modes. In this approach the perturbed helical flux function $\psi_{m,n}$ is found through integration of the second order partial differential equation:

$$\left[\frac{\partial^2}{\partial r^2} + \frac{1}{r} \frac{\partial}{\partial r} - \frac{m^2}{r^2} - \left(\frac{\partial J_0}{\partial \psi_0} \right) \right] \psi_{m,n} = 0 \quad (2.6)$$

in the region between the plasma magnetic axis and the rational surface (the boundary layer) and in the region from the rational surface to the plasma boundary, subject to the constraint that $\psi_{m,n}$ matches across the rational surface. For the cylindrical case, $\partial J_0 / \partial \psi_0$ is just a function of $q_0(r)$. The code interfaced in TRANSP solves a quasi-cylindrical version of this equation by using both the unperturbed current density $J_0(r)$ and safety factor $q_0(r)$ profiles. Since TRANSP separately calculates the ECCD current, this term could be calculated excluding the contribution of the equilibrium perturbation to the total current, thus avoiding potential double counting [26]. The normalized discontinuity in the derivative at the resonant surface r_s :

$$\Delta'_{m,n} = \frac{\frac{\partial \psi_{m,n}^-}{\partial r} - \frac{\partial \psi_{m,n}^+}{\partial r}}{\psi_{m,n}} \Bigg|_{r=r_s} \quad (2.7)$$

represents the drive or damping for the island. For finite size islands, $\Delta'_{m,n}(w)$ is calculated by taking the discontinuity between the inner and outer island edges, with the perturbed flux, $\psi_{m,n}$ assumed constant across the island [23, 27–29]. As tearing modes are generally not predicted to be linearly unstable (with the possible exception of the (2, 1)), a ‘seed island’ that might originate from ELMs or sawtooth crashes is needed to trigger island growth. For convenience, the island evolution is calculated assuming a fixed minimum island size, $w_{min} \approx 10^{-3}a$, where a is the plasma minor radius. The island will only grow if $\Delta'(w_{min}) > 0$. This could be modified in the future by only making the seed island finite during ELMs or at sawtooth crashes, for example.

The approximations used in the calculation of the tearing stability have been shown to be accurate for magnetic islands with width up to 20% of the plasma minor radius [23].

The contributions from the EC heating and current drive have been implemented in the MRE using the formulation by Bertelli *et al* [19] and De Lazzari *et al* [30]. It should be noted that the TRANSP/MRE interface in its present state does not include a reduction of the global confinement with the island width.

The second term on the right hand side represents the destabilizing effect of the bootstrap current J_{BS} and is given by [31]:

$$\Delta'_{NC}(w) = k_1 \frac{16J_{BS}}{s \langle J \rangle} \frac{w}{w^2 + w_d^2} \quad (2.8)$$

where

$$w_d = 5.1k_d \frac{r_s}{\sqrt{\epsilon sn}} \left(\frac{\chi_{\perp}}{\chi_{\parallel}} \right)^{1/4} \quad (2.9)$$

measures the extent to which the cross-field transport can support a parallel temperature or density gradient [31]. Here s is the magnetic shear, r_s the radius of the rational surface, ϵ the local aspect ratio and k_1 and k_d two calibration coefficients. The correction to the w^{-1} dependence accounts for the existence of a threshold for instability of the tearing modes. The coefficient k_1 accounts for the fact that the derivation of the neoclassical term is not exact.

The third term on the right hand side is the polarization term [32]:

$$\Delta'_{pol}(w) = -k_2 \frac{\rho_{\theta i}^2 \beta_{pol} g}{w^3} \left(\frac{L_q}{L_p} \right)^2 \quad (2.10)$$

Here $L_{q,p}$ represent the local gradient scale length of the q and pressure profile respectively, β_{pol} is the plasma poloidal beta, $\rho_{\theta i}$ the ion poloidal gyroradius and the parameter $g \simeq \epsilon^{3/2}$ and it approaches unity in the limit of low collisionality [23]. The polarization term is important for small island sizes and it becomes a small contribution in the case of large island sizes.

The fourth term on the right hand side is the Glasser-Green-Johnson term [33]:

$$\Delta'_{GGJ}(w) \approx -5.4k_4 \frac{\beta_{pol} \epsilon^2 L_q^2 q^2 - 1}{r_s w |L_p| q^2} \quad (2.11)$$

The form used here is the derivation by Houlberg [24].

Finally, the last term is the stabilizing contribution of the localized EC current drive. There are several expressions for this term. The one used here is from Bertelli *et al* [19]:

$$\Delta'_{CD}(w) = k_6 16\pi^{1/2} \frac{\mu_0 L_q}{B_p} \frac{J_{CD,max}}{w_{CD}} F(\tilde{w}) M(\tilde{w}, D) G(\tilde{w}, x_{dep}) \quad (2.12)$$

with [19]

$$F(\tilde{w}) = 0.25 \frac{1 + 0.96\tilde{w}}{1 + \tilde{w}(1.5 + \tilde{w}(0.43 + 0.64\tilde{w}))} \quad (2.13)$$

where $\tilde{w} = w/w_{CD}$ is the island width normalized to the EC deposition width. The term $M(w)$ represents the effect of modulation [19]. In the cases discussed herein no power modulation is assumed and $M(w) = 1.0$. The term $G(w)$ represents the effect of misalignment of the EC deposition with the resonant surface. The expression used in TRANSP uses the derivation in De Lazzari *et al* [30]:

$$G(\tilde{w}) = 1 - 2 \frac{x_{dep}}{g(\tilde{w})} e^{-\left(\frac{x_{dep}}{g(\tilde{w})}\right)^2} \int_0^{x_{dep}/g(\tilde{w})} dt e^{t^2} \quad (2.14)$$

with

$$g(\tilde{w}) = \frac{0.38\tilde{w}^2 + 0.26\tilde{w} + 0.5}{\tilde{w} + 1} \quad (2.15)$$

where $x_{dep} = (r_{dep} - r_s)/w_{dep}$ represents the deposition location relative to the resonant radius, normalized to the EC deposition width. We note that there is a typo in Eq.15 of Ref. [30], although

the figures in that paper have been derived using the correct formulation. This term is important for the studies undertaken herein, which aim at assessing the effects of systematic misalignments or the effect of transient misalignments, like those caused by a sawtooth crash. The effect of the EC heating is included in the MRE using the formulation of Bertelli et al [19], with the effect of misalignment $G(\tilde{w})$ from De Lazzari et al [30]. This term is not discussed here, because it contributes less than a fraction of a percent compared to the current drive contribution under ITER conditions.

2.4 Limits of the simulations for NTM control and stabilization

Although the approach described in the previous section for the simulation of NTM feedback control with EC is more advanced than previous, parametric studies based on asymptotic calculations, there are still several limitations that introduce large uncertainties in the results. The MRE is evolved at this time within an external interface, thus the evolution of the island is calculated using the magnetic equilibrium and kinetic profiles at time t_1 , while the magnetic equilibrium and kinetic profiles are evolved in TRANSP over shorter time scales. If the control interface decides to update the input power in order to suppress the island, then the new value is given to TRANSP, which will update and use the new power and current for the equilibrium and temperature profile evolution. This is consistent with what would be done during feedback control experiments, where ray-tracing calculations would be performed based on real-time reconstruction of the magnetic equilibrium and of the density and temperature profiles at a given time and where there is a latency between the time the new EC power and steering angle are communicated to the Plasma Control System and the time these parameters are actually updated. However, the plasma would evolve over MHD time scales under the presence of the magnetic island and this is not described accurately in the interface yet. More consistent calculations should evolve the island over the faster time scales of transport, as well as include the effect of a finite island width on the temperature (and density) profiles, for example by increasing artificially the conductivity (and diffusivity) profile locally to reduce the neoclassical drive. Also, in TRANSP both the steering angle and the input power are updated during the same time scale δt_{HCD} , while the time required to turn-on/off a gyrotron and to make small adjustments to the poloidal angle are much shorter than the time required to switch between transmission lines. In practice, all simulations described here have an uncertainty on the results that is equal to the time step used for the update of the EC parameters, δ_{HCD} . While some of these effects, like the evolution of the magnetic island over transport time scales, the inclusion of toroidal effects in the calculation of the tearing stability term, and corrections in the calculation of $\Delta'_{m,n}(w)$ to avoid counting the EC current twice [26], will be accounted for in future work, we note here that a self-consistent approach would be possible only within the context of 3D nonlinear MHD simulations coupled with a ray tracing code.

Because of the large number of simulations required for statistics on variations of the results for small variations of the input parameters, the simulations are run with the fix-boundary solver for the sake of saving time. Cross-check with free-boundary calculations for each operating value of the magnetic field and current, indicate that the results are reproducible from start-up to the H-L back transition during the plasma current ramp-down, but they fail across the H-L transition.

TRANSP is a framework in continuous evolution. As such, not all predictive capabilities were available at the time this research has been undertaken and not all those available have been used for this analysis. The first case includes pellet ablation, whose implementation has started in the fall of 2016 and self-consistent impurity transport, which is currently under test. The second case includes density predictions, since for the ITER simulations it would require a fully functional pellet

ablation module and boundary conditions for the density and temperature at the separatrix derived from parametrized scaling or from the full coupling with an edge transport model.

A self-consistent simulation of the plasma scenario, including the termination phase, should evolve self-consistently all transport channels. We found that the free-boundary simulations fail at the H-L back transition because of either too large impurity radiation or inward shift of the plasma, or both, and that this problem is intensified each time the EC feedback control is turned-on (thus always in this analysis). Because some of the plasma background profiles are prescribed, it was deemed not essential for the scope of this contract to optimize free-boundary simulations across the entire discharge. The optimization of the ITER plasma termination is a joint activity coordinated under the ITPA-IOS by the contractor, which will work closely with control experts in SCOD to further develop these plasma simulations from startup to termination.

3 Heating and Current Drive sources

All simulations assume 73MW of external power available, with 33MW of NBI, 20MW of EC and 20MW of IC, but they assess scenario performance with a 15MW deficit input power. This is done under the assumption that auxiliary power must be available for replacement in order to sustain H-mode plasmas, for example if one of the Neutral Beam sources fail, which is the case with operation at half-field, where there is no contribution from the α s.

This section summarizes the geometry setup of the H&CD sources and the source modules used in TRANSP, including a discussion of the assumptions and approximations made in each physics module and of the limitations in the models used. As part of the analysis, a benchmarking of the source modules has been undertaken. In the case of the NBI module, the focus was to verify the correct geometry and the deposition profiles at the tangency radius and at the wall location. In the case of the EC modules the goal was to verify that the calculations are consistent with GRAY [34], a state-of-the-art code for Electron Cyclotron calculations. In the case of the IC module only a qualitative comparison has been done, since all codes used for IC calculations in time-dependent transport solvers have their own limitations and deficits; in particular none of them provides a self-consistent calculation of the minority heating, of the interactions with neutral beam fast ions and alpha particles and of propagation and losses in the Scrape-Off-Layer. For this reason, conclusions on the IC heating schemes used and on the synergy with the other heating and current drive sources are never stressed as conclusive in this report.

3.1 Electron cyclotron heating and current drive system

An important application of the EC system is for NTM control, for which the Upper Launcher (UL) has been specifically designed to provide localized deposition down to 2% of the minor radius [1–3, 35–37]. The power is provided by 24 gyrotrons, connected to 24 transmission lines, operating at a frequency of 170 GHz and power of 1 MW each, of which 0.83 MW are delivered to the plasma on account of transmission losses from the gyrotron diamond window to the plasma boundary. The UL is located in four upper ports, each housing eight beam lines, arrayed in an upper and lower row of four waveguides each, dubbed Upper Steering (USM) and Lower Steering (LSM) mirror. The combined four UL can deliver the total 20MW of power, with up to two thirds on either steering mirror. In the configuration with 20MW of power, 24 switches direct the power to either the EL or the UL and eight switches direct the power between the USM and the LSM. Table I reports the coordinates (R, z) of injection of the mirrors used in the simulations, the toroidal angle β , which is fixed, the range of poloidal steering angle α , the initial beam waist as an elliptical section and the curvature of the mirror.

3.1.1 Electron cyclotron heating and current drive calculations

Electron Cyclotron heating and current drive calculations have been run with the beam tracing code TORBEAM [21], which has been implemented specifically for the purposes of this Task Agreement, because it offers some advantages over the other two codes for electron cyclotron

Table 3.1: Geometry of EC launchers used in the simulations.

Mirror	R(m)	z(m)	w _{ox} (mm)	d _{ox} (m)	w _{oy} (mm)	d _{oy} (m)	β	α (min,max)
TOP	9.394	1.192	12	0.505	23.2	0.618	-20	-20, +15
MID	9.394	0.62	12	0.505	23.2	0.618	25	0, 35
LOW	9.394	-0.004	12	0.505	23.2	0.618	25	-10, 25
USM	6.99871	4.41441	29.0	2.134	29.0	2.134	20	40, 65
LSM	7.05392	4.17821	21.0	1.62	21.0	1.62	20	30, 55

calculations, TORAY and GENRAY, also implemented in TRANSP. First, TORBEAM uses realistic settings, such as the mirror curvature and the beam waist, to evolve the beam trajectory, while the beam width is set by a divergence parameter in the other two codes, which therefore need to be calibrated. Second, TORBEAM uses coordinates defined in the frame of the EC launcher instead of the tokamak frame. Since the toroidal angle is fixed and the poloidal angle is steerable, the settings for the EC control are therefore straightforward, because no conversion to the equivalent azimuthal and poloidal angle is needed.

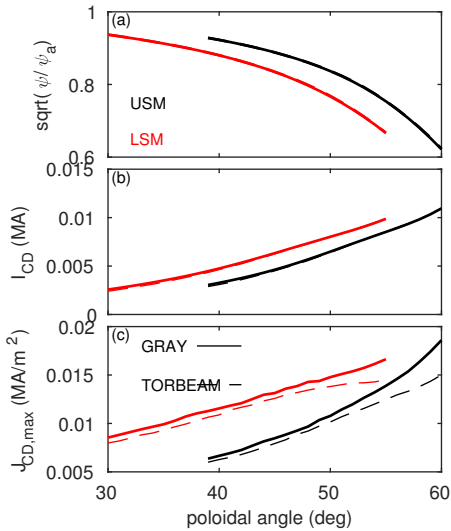


Figure 3.1: Results of benchmarking between TORBEAM/TRANSP and GRAY for the baseline scenario. Input profiles and equilibrium are from a CORSICA simulation.

The calculations with TORBEAM have been compared to those with GRAY over time slices for the O-mode injection at full field and for the O-mode and X-mode injection at half-field. Although ray tracing and beam tracing codes have been extensively verified against each other and validated by the EC community and TORBEAM and GRAY - in particular - have always demonstrated very good agreement, the comparison is repeated here to evaluate the effect of using a coarse grid for the kinetic profiles and for the equilibrium in TRANSP on the reconstruction of the magnetic field in TORBEAM and therefore in the ray trajectories as opposed to the calculations of GRAY, which has more robust reconstruction of the magnetic field. Differences in the ray trajectories and in the deposition profiles are sensitive to the internal reconstruction of the magnetic field inside the EC codes and the agreement typically improves when the comparison is done using equilibria with finer spatial resolution. Here, the comparison has been done on purpose using a coarse grid for both the density and electron temperature and for the equilibrium, which are representative of typical TRANSP time-dependent simulations. Under these conditions, a difference up to 3% exist in the peak current density at the two resonant surfaces of interest.

A positive and unexpected outcome of the benchmarking was the finding of conceptual error in the calculation of the current drive in the algorithm of Lin-Liu [38] that is used for the calculation of the current drive in TORBEAM and in most EC codes used worldwide (but not in GRAY). The error has been fixed and will be reported in a separate publication by E. Poli (IPP) [22].

Figure 3.1 shows the results from the comparison in the baseline scenario, with O-mode polarization and absorption at the fundamental resonance, for a scan over the poloidal steering angle for both the upper steering mirror (USM) and the lower steering mirror (LSM). The reference

profiles and equilibrium in the flattop are taken from a CORSICA simulation, provided by Sun-Hee Kim (ITER Organization, SCOD). The agreement on the deposition location, identified by the maximum in the current density profile, is excellent for the entire range of poloidal angles and so is the integrated driven current. Differences exist in the peak value of the current density, as shown in Fig.3.1(c), that increase with increasing poloidal angle, *i.e.* when the ray trajectory becomes more vertical and tangent to the magnetic flux surfaces.

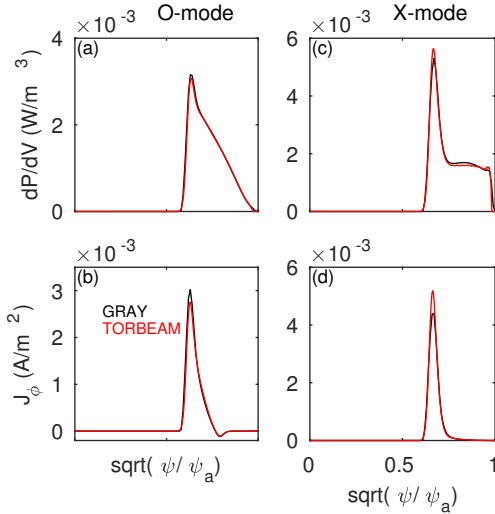


Figure 3.2: Results of the benchmarking between GRAY and TORBEAM for a hydrogen plasma at 2.65T/7.5MA. Input profiles and equilibrium are from TRANSP.

These angles correspond to situations where the UL is steered close to mid-radius, a configuration that is not used in the simulations discussed in this report, where the USM and the LSM are steered respectively on the $q = 1.5$ and the $q = 2.0$ resonant surface. Figure 3.2 shows the comparison between TORBEAM and GRAY in a hydrogen plasma at magnetic field of 2.65T and plasma current of 7.5MA, for both O-mode and X-mode polarization, after the correction of the error in the Lin-Liu algorithm. The calculations are done here for the EL-bot mirror and for poloidal angle of 25 degrees, at which the loss in absorption in O-mode is only 20%. The magnetic equilibrium, electron density and temperature profile, are from a TRANSP simulation (see Sec.8). At 2.65T the third harmonics of the electron cyclotron resonance is inside the plasma and close to the plasma edge, resulting in parasitic absorption near the plasma edge, as shown in Fig.3.2(c). This effect is sensitive to the local value of the temperature profile and - in this case where the resonance is close to the plasma edge - to the pedestal structure. Since a physics based model for the transport inside the pedestal is not available, it should be assumed that uncertainties in the EC calculations are large. It will be shown in Sec.5 that increasing the magnetic field to 2.75T eliminates the problem by moving the Doppler-shifted resonance outside the plasma.

3.2 Neutral Beam heating and current drive system

Three Neutral Beam systems are planned on ITER, two of which available in the baseline operation, whose geometry is reported in Table 3.2. The grounded grid is at $z_0 = 1.443$ m above midplane (Machine Center Line: MCL) and each beam is aimed downwards at a nominal angle of $\theta_0 = 2.819^\circ$, which corresponds to 49.2 mrad. Relative to this nominal angle the beam can be steered downward or upward by 9 mrad, with a ± 1 mrad accuracy in the measurement. With these settings the beam power can be deposited between $z = -417$ mm and $z = +156$ mm relative to the MCL. The actual steering is subject to limits imposed on the First Wall, which is designed to sustain $4\text{MW}/\text{m}^2$. The presence of a gap between tiles limits the power load to $2\text{MW}/\text{m}^2$. These numbers provide reference values for an upper limit to the shine-through power, which - in turn - limits the maximum energy and power that can be used in a specific scenario for a given density. Each source can deliver up to 16.5 MW of power, with power and energy scaling according to $P_{MW} = 16.5 E_{MeV}^{2.5}$. For deuterium beams the energy varies between 200 keV and 1 MeV. The beam power can be changed in three ways: (a) by varying the beam voltage in between pulses (b) by modulating the power during pulse operation in the range of 2 - 7 Hz (c) by $\pm 25\%$ power variation during the pulse (to be confirmed on MITICA).

Neutral Beam calculations in TRANSP are performed with the MonteCarlo code NUBEAM [39]. NUBEAM uses a representation of the rectangular source and aperture, whose values and reported in Table 3.2. In addition, NUBEAM needs information on the distance between the source and the tangency radius along the beam line of flight d_{s-tg} , the distance between the source and the aperture d_{s-ap} and the elevation of the beam source at the starting point and at the tokamak entrance. The width and height of the beam, the starting point, the beam tangency radius and the tilting range are summarized in Table 3.2. The table also reports the footprint width and height of the beam at the tangency radius, and the beam center vertical coordinate for the on-axis and for the off-axis injection. The last two parameters are used as a reference and sanity check on the accuracy of the geometrical model used in NUBEAM.

The distance between source and tangency radius is calculated as $L_{s-tr} = x_0 / \cos(\alpha)$ where α is the steering angle and (x_0, y_0, z_0) are the cartesian coordinates of the beam starting point. The beam footprint vertical location can be calculated from L_{s-rt} as $z_{fp} = z_0 + L_{s-rt} \cos(\pi/2 + \alpha)$,

Table 3.2: NB system layout

$R_{tan} = 5.3102$ m
$y_0 = -R_{tg}$
$z_0 = 1442.61$ mm (Grounded Grid height)
$z_{MCL} = 1490.85$ mm (machine centerline at operating temperature)
$\theta_0 = 2.819^\circ$
Tilting = $2.306 \div 3.331$ deg (downward) $\rightarrow (49.2 \pm 9)$ mrad
Footprint @ R_{tan} : $z=0.156$ m (on-axis), $z=-0.417$ m (off-axis)
Footprint @ R_{tan} : $\Delta z = 0.6$ m, $\Delta r = 0.4$ m
beam starting point: $(x_0, y_0, z_0) = (31.95214, -5.3102, 1.44261)$ m
source width: 56.0 cm
source height: 151.8 cm
aperture width: 58.4 cm
aperture height: 122.6 cm
equivalent vertical focal length of beam: 2256.668 (cm)
equivalent horizontal focal length of beam: 1869.02 (cm)

which gives $z_{fp} = 0.156\text{m}$ for on-axis injection and $z_{fp} = -0.4171\text{m}$ for off-axis injection, in agreement with the reference footprint values. The distance between the source and the aperture is calculated from $L_{s-ap} = d_{s-ap}/\cos(\alpha)$, where $d_{s-ap} = x_0 - 6.49918\cos(\alpha)$ is the distance projected on the horizontal plane. The value of d_{s-ap} has been inferred from the CAD designs and is our best estimate from the available information. The resulting values are $L_{s-ap} = 25.4789\text{m}$ for on-axis injection and $L_{s-ap} = 25.5013\text{m}$ for off-axis injection. The distance between the source and the wall is calculated from the above formulas to be $L_{s-w} = 38.4125\text{ m}$.

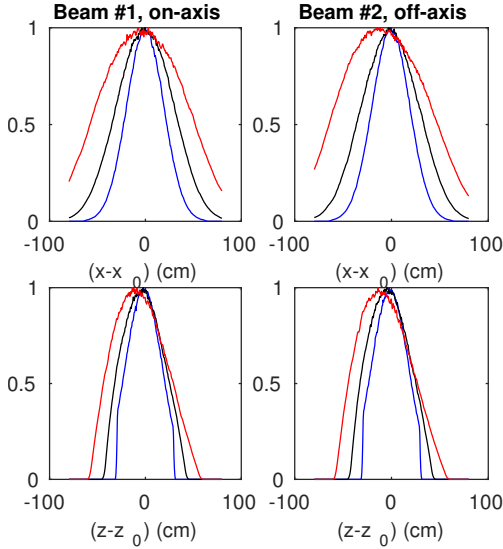


Figure 3.3: Footprint of the 1MeV beam source in a baseline plasma, for on-axis and off-axis injection. The three curves represent the integral of the number of particle per volume over a region of xxxcm around the coordinates - along the beam path - of the entry point (blue), the tangency radius (black) and back wall (red).

zonal and for the vertical width at the tangency radius respectively, the deposition profile calculated by NUBEAM is about 50% wider in both directions. These differences are likely due to the focal length approximation and can over-estimate the integrated power that shines through to the wall.

3.2.1 Neutral Beam source models comparison

The Neutral Beam codes used in this comparison are ASCOT and PENCIL, implemented in JINTRAC, and NUBEAM, implemented in TRANSP. Reference profiles, calculated with OFMC and kindly provided by T. Oikawa, are used as a reference to assess the geometry of the NBI system in the respective workflows from a comparison of the radial location of the maximum current for on-axis and off-axis deposition, and of the total current. The calculations use two beams, one steered on-axis and one steered off-axis.

This is not direct input to NUBEAM, but it is used in dedicated calculations to extract the beam footprint in the plasma for comparison with OFMC, respectively at the wall, at the tangency radius and at the port entry. It is a useful test also to check that the focal length of the beam and the divergence are set correctly. In fact, the beam divergence and the focal length are defined for individual beamlets to be equal to 8 mrad. Since NUBEAM models the entire beam rather than integrating over individual beamlets, it uses an equivalent representation of the focal length over a convolution of individual beamlets. The focal length used in NUBEAM and reported in Table 3.2 has been provided by Sun-Hee Kim (ITER Organization, SCOD). Although a representation of the beam with a unique focal length in the horizontal and vertical plane is not technically correct, these numbers are the best representation that is consistent with the geometry of the ITER beamline. Figure 3.3 shows the beam profiles at the three locations, indicating the broadening of the beam along the beam line of injection. An integral of the profiles along the radial and vertical plane is shown in Fig.3.3. The equilibrium and pressure profiles used for these calculations are the same used for the EC calculations. Compared to the reference value of 40cm and 60cm for the horizontal and for the vertical width at the tangency radius respectively, the deposition profile calculated by NUBEAM is about 50% wider in both directions. These differences are likely due to the focal length approximation and can over-estimate the integrated power that shines through to the wall.

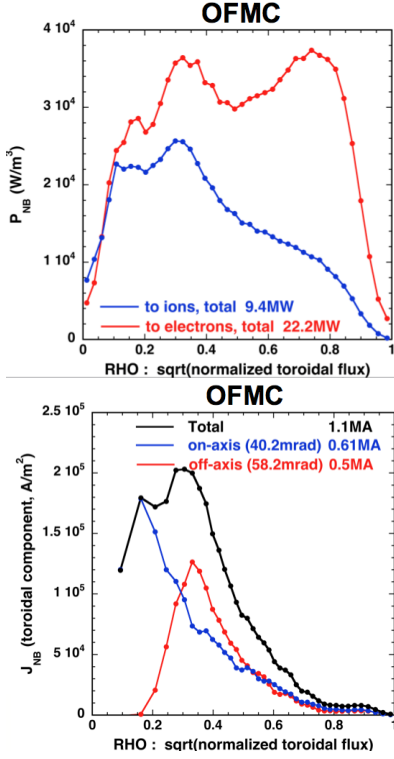


Figure 3.4: Power and current density profiles for on-axis and off-axis injection, calculated with OFMC. Input profiles and equilibrium are from a CORSICA simulation.

The calculations with OFMC for the baseline are shown in Fig.3.4 for the on-axis and off-axis beam. Since Oikawa did not provide ASCII files with the data, these profiles are reported in separate figures. The comparison has been done on two scenarios: the baseline scenario at full field and the helium scenario at half-field, in both cases without the IC heating. Both JINTRAC and TRANSP are running simulations in interpretive mode, reading the equilibrium and the profiles of electron, ion and impurity density, and the profiles of electron and ion temperature. Figure 3.5 shows the comparison for the total and individual beam power density and current profiles. Since the heating profiles of ASCOT contain the electron heating from alpha thermalization, these are not reported in the figure for the baseline scenario. Good agreement is found among codes in the baseline scenario. The current calculated by ASCOT (1.10 MA) and PENCIL (1.11 MA) is in very good agreement with the OFMC calculations (1.1 MA), while NUBEAM is underestimating the total current by about 20%, with a calculated value of 0.9 MA. The difference is accounted for by shine-through losses (likely over-estimated), orbit losses and charge-exchange losses, which are not included in the standalone calculations. In the helium plasma, the current predicted by ASCOT is about half the value predicted by PENCIL and NUBEAM, while the power density is in very good agreement. It was found that the difference is due to an error in the algorithm for the calculation of the current drive in ASCOT for non-hydrogenic species. After the fixing of the bug, the agreement among the three codes has been recovered.

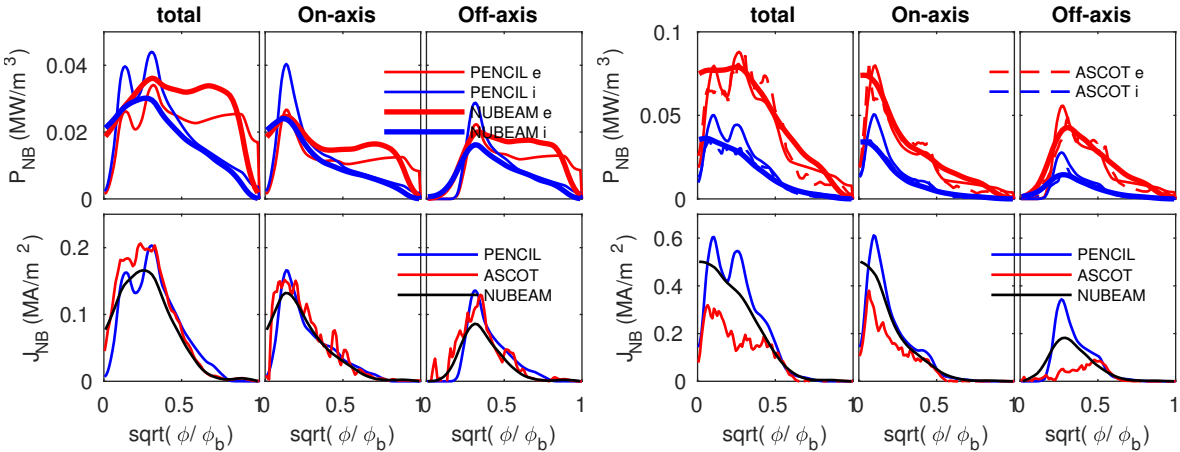


Figure 3.5: Comparison between PENCIL, ASCOT and NUBEAM for the baseline scenario (left panel) and for a Helium plasma (right panel). No power density profiles are reported from ASCOT for the DT case because the power deposition profile contains the heat deposition from the alpha thermalization.

3.3 Ion cyclotron heating and current drive system

The main requirements of the ICRF system include (a) coupling 20MW of power for heating and current drive (b) cover operation at the nominal and at half-field (c) perform IC wall conditioning at low power between pulses (d) be resilient to rapid antenna loading variations, for example during the L-H(-L) transition and during ELMs.

Two identical ICRF antennas are part of the baseline H&CD configuration. The antennas operate at frequency in the range of 40-55 MHz to cover the operational space. Each antenna is designed to deliver 20MW of power, however the baseline configuration distributes the power on the two antennas. Having two antennas, independently operated, reduces risks associated with uncertainties in the plasma edge profiles that affect the coupling of the power to the plasma. It also increases versatility, for example operating with two frequencies, and reduces drawbacks associated with failure of one of the antennas. Each antenna consists of six poloidal by 4 toroidal straps, which can provide arbitrary toroidal phasing spanning from pure heating to heating and current drive. Based on the analysis performed with ANTITER [40], there are three phasing that maximize the heating (case 1 to 3), and two that maximize the current drive (case 4 and 5), summarized in Table 3.3. Case 2 has been recommended as the case that provides the best coupling, as well as the optimal heating, with one dominant peak (symmetric) and negligible side contributions, while case 4 provides the best spectrum for current drive. We will be using the ICRF antennas mostly in heating configuration, with spectrum from the case 2. TORIC uses an equivalent representation in terms of toroidal mode number, which is reported in the table for each value of k_{\parallel} .

A critical parameter is the maximum power coupled to the plasma as a function of the frequency. Since this is sensitive to the assumptions on the SOL density, a parameterization would be needed for the correct accounting of losses outside the separatrix. Such a parametrization has never been provided. According to simulations with TOPICA, for operation at 53MHz it can be assumed that the power coupled to the plasma is near to 100%; for operation at 42MHz, assumptions are of 8MW after the L-H transition, then full power in flattop. This said, the antenna design focuses on conservative profiles with low far SOL transport, while uncertainties on the ITER SOL profiles are large. Modeling of propagation of IC waves from the antenna to the plasma core with realistic, coupled core and edge plasma transport, are still at their infancy. This is an area where IC modeling is still very immature and uncertainties in the scenario predictions can be significant.

	toroidal phasing	k_{\parallel} (m^{-1})	n_{ϕ}
case 1	0 π 0 π	± 7.5	47
case 2	0 0 π π	± 3.1	19
case 3	0 π π 0	± 4.6	29
case 4	0 $\pi/2$ π $3\pi/2$	-3.65	-24
case 5	0 $-\pi/2$ $-\pi$ $-3\pi/2$	3.85	25

Table 3.3: Antenna toroidal phasing, corresponding wave vector (k_z) and equivalent toroidal mode number used in TORIC (n_{ϕ}).

3.3.1 Ion Cyclotron source models comparison

The ion cyclotron codes used for this comparison are PION, implemented in JINTRAC, and TORIC5, implemented in TRANSP. Comparison between IC codes is complicated by how Fokker Planck solvers are implemented in the workflow, and how the solvers themselves are simplified. Both PION and TORIC5 in TRANSP use a 1D Fokker Planck solver.

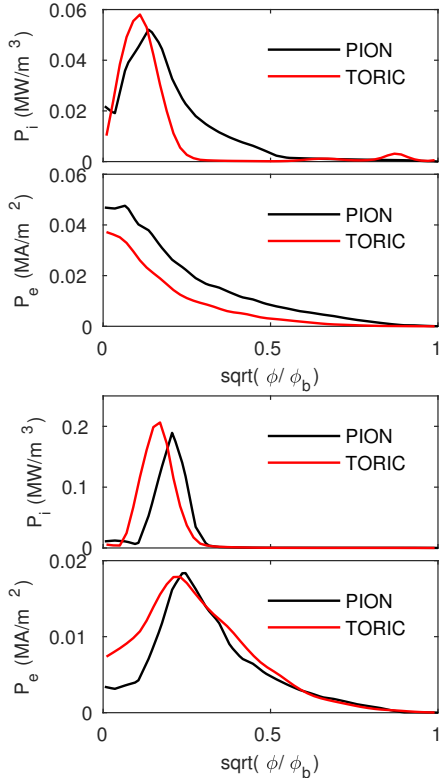


Figure 3.6: Top: comparison between PION and TORIC for the baseline scenario in the case of heating on the tritium second harmonics. Bottom: comparison for the half-field He scenario, in the case of 3% hydrogen minority heating.

absorption profiles. A correct benchmarking should be done outside of the transport-solvers; the ITER Modeling and Analysis Suite, with a common data structure, provides an ideal platform that would facilitate such benchmarking effort.

Figure 3.6 shows a comparison between PION and TORIC5 for the two scenarios in the case of absorption on the thermal species. TRANSP is assuming no minority, while JINTRAC is using a very small fraction, namely 10^{-5} for the ^3He minority and 3×10^{-2} for the H minority. All the ion absorption is on the thermal species, which are the second harmonic Tritium in the case of the baseline and thermal Helium in the half-field case. The small fraction of minority used in the JINTRAC calculations results in an absorption that is about 500 times smaller than the absorption on the thermal species at the peak value. This is very small and does not explain the differences in the maximum amplitude of the power density profiles. The heating profiles are in good agreement, with differences in the radial location of the peak power density, likely due to the reconstruction of the magnetic field internally in PION and in TORIC, which may cause differences in the position of the resonance.

Differences are larger when the minority species are introduced and this is a direct consequence of the assumptions in the Fokker Planck solvers. An extensive effort is being undertaken under EuroFusion to benchmark Ion Cyclotron codes and Fokker Planck solvers. Here, we have been comparing the codes within their respective frameworks JINTRAC and TRANSP, which is not an appropriate way of proceeding. In order to satisfy the required ratio of 20% hydrogen to 80% helium density, the electron density has been rescaled in JINTRAC while maintaining the same impurities and the same Z_{eff} . This results in discrepancies already in the input profiles that are used by TORIC and PION and therefore in the output

4 Power management in the ELMy H-mode scenario

The target of operation in DT at 5.3T and 15MA is to demonstrate up to 500MW of fusion power and fusion gain of $Q = 10$, the challenges include doing so while ensuring MHD stability, ELM control, disruption avoidance and low power heat load to the divertor.

The simulations discussed here focus on (a) assessing an upper and lower limit on the EC power needed for NTM stabilization in all phases of the discharge (b) qualitative assessment of how these limits depend on the conditions of H-mode access (c) assessment of a suitable control scheme that optimizes the use of the EC system for shared applications and (d) assessment of the effectiveness of the Equatorial Launcher in affecting and eventually controlling the sawtooth period.

The main difference with previous assessments of the power needed for NTM stabilization and suppression is that the analysis here undertaken is based on time-dependent calculations rather than on asymptotic solutions. However, similar to previous calculations, toroidal effects are not included in the calculation of the tearing stability term and the threshold for the onset of the NTM is based on analytic approximations, since reduced models based on nonlinear MHD calculations are not available yet. These are limitations intrinsic in all approaches based on a Modified Rutherford Equation (MRE) that introduce large uncertainties on the triggering of NTMs. The results of these simulations should be regarded as upper limits on the instability and growth rate of the NTMs, obtained under assumptions that likely overestimate the neoclassical drive and under-estimate the triggering threshold of the (2,1)-NTM. It is therefore advised that these results be interpreted qualitatively, for example looking at trends, and that the simulations be further optimized as the physics modules are improved.

4.1 Reference simulation

Figure 4.1 shows a TRANSP simulation of the ITER 15MA ELMy H-mode, which will be used as a reference for the NTM analysis. The current ramp-up phase is 80s long, with the plasma being diverted at about 12s and the radio-frequency heating and current drive being turned-on shortly after for flux saving [41, 42]. The electron density is built-up rapidly to $2 \times 10^{19} \text{m}^{-3}$ within the first 20s to provide a background plasma for good absorption of both Electron and Ion Cyclotron waves. The EC power is turned-off in the flattop to provide a reference case for the NTM stability and for the sawtooth period in the absence of any control.

The time step for the H&CD sources calculations, δt_{HCD} , is relaxed here to 5 seconds. The electron density profile is prescribed in time, using the parametrization described in Sec.2.2, while the electron and ion temperature profiles are evolved using the GLF23 [6, 7] turbulence transport model. The pedestal width and height are interpolated from a lookup table, as described in Sec.2.2. Because the pedestal width and height are interpolated at each time step, the discharge evolution and the core profile evolution are nonlinearly coupled to the pedestal structure and evolve during the simulation, responding to variations in β_N , shape and Z_{eff} . The shape of the impurity profiles are the same as the electron density profile, rescaled according to a fraction that is prescribed in time; impurity fraction levels assumed here in the flattop phase are Berillium at 2% of the electron density, Argon 0.1% and Tungsten up to 10^{-5} of the electron density. For a given electron density and impurity fraction, the ion density is derived from particle balance, while satisfying quasi-neutrality.

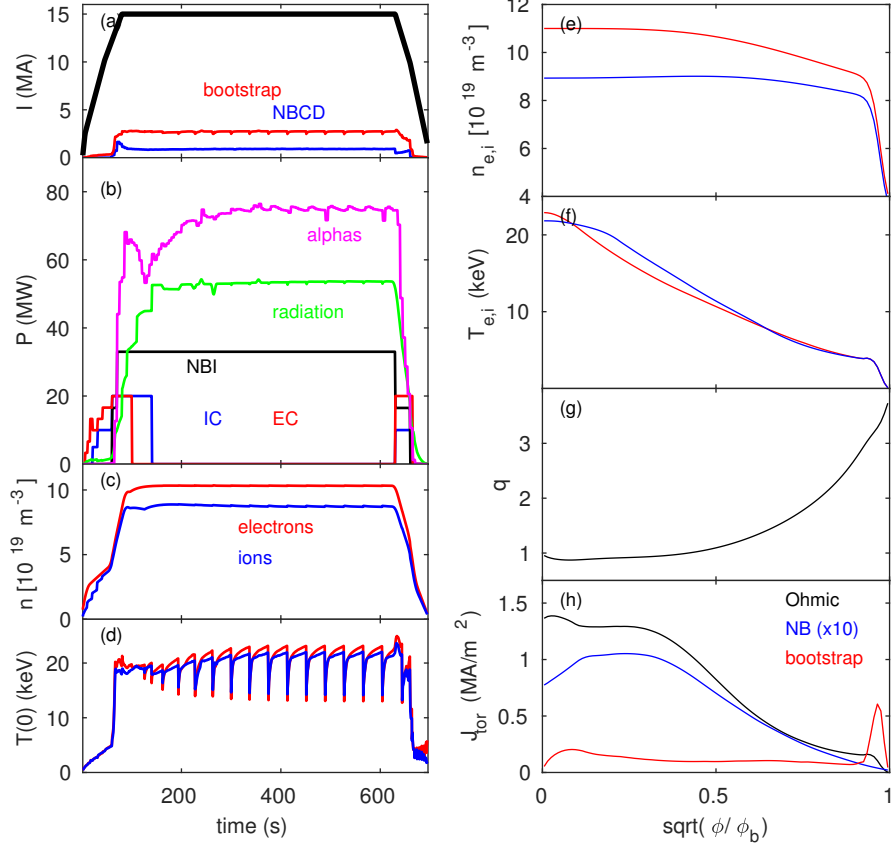


Figure 4.1: Reference simulation of the ITER baseline scenario. Left column: (a) plasma current, NB driven current and bootstrap current (b) injected external power, radiated power and α power. (c) line integrated density for electrons, ions and impurities, (d) electron and ion temperature, central value. Right column: profiles at 560s, before a sawtooth crash. (e) electron and ion density (f) electron and ion temperature (g) safety factor (h) ohmic current, NB current and bootstrap current (i) total electron and ion heating (thick) and electron and ion heating from the alphas (thin).

The transition from L- to H-mode is set by increasing the level of injected power above the threshold power provided by the ITPA scaling [10] and by changing the density profile from a more peaked to a more flat profile with a pedestal. In this simulation the L-H transition is pre-programmed at 65s, at which time the electron density is half the Greenwald density n_G . After the L-H transition the electron density rapidly builds-up to the flat-top value of $0.85n_G$. The density at the pedestal and at the separatrix are respectively 75% and 35% of the central density, according to the boundary conditions used in the derivation of the EPED1 pedestal pressure [11].

The IC power is turned-off in the flat-top phase in this reference simulation, although its effects on the scenario are assessed, under different assumptions on the IC heating scheme, as discussed in Sec.4.4. Although impurity transport is not modeled self-consistently, it is assumed in these simulations that IC heating is needed both in the current ramp-up and ramp-down phase for impurity control and for H-mode access. Self-consistent calculations of the effect of IC and EC central heating on tungsten accumulation in the core should be undertaken to assess global actuator power sharing in every phase of the discharge. In the flat-top phase the IC could be used for sawtooth control thru fast-ion destabilization. This effect is not currently self-consistently modeled in the sawtooth model in TRANSP and this application of the IC system is therefore not considered here. Because of the large Ohmic current contribution, the effect of the IC centrally peaked current drive on the

relaxation of the $q = 1$ surface is negligible and no effect on the sawtooth period is observed in response to the IC current drive, thus this discussion is also not included here and the IC antennas are used with a phasing that provides only heating.

4.2 Evolution of the (2, 1) and (3, 2)-NTMs

The triggering and evolution of NTMs, their width and frequency, depend on the plasma discharge parameters. In addition, the analysis with the MRE depends on the simplifications in the model and on the coefficients used in front of the individual contributions. The evolution of the width of the (3, 2)-NTM, in particular, is found to be highly sensitive to the choice of the coefficients that calibrate the amplitude of the neoclassical contribution and of details of the pressure and current profiles; this mode is predicted to be either stable or unstable for small variations in the plasma parameters. The evolution of the width of the (2, 1)-NTM is instead more reproducible, although the threshold size for the triggering is likely underestimated. The focus is therefore limited to the study of the stability of the (2, 1)-NTM.

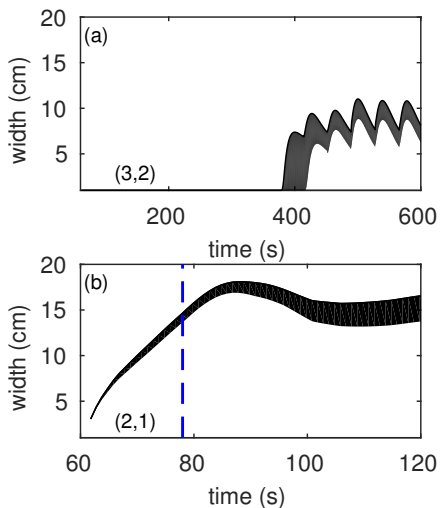


Figure 4.2: Evolution of the island width for two assumptions on the multiplier in the neoclassical driving term for the (3,2) and the (2,1) mode.

Figure 4.2 shows the evolution of the (2,1) and of the (3,2) NTM in the reference scenario simulation for two choices of the multiplying coefficient in the neoclassical term $\Delta'_{NC}(w)$ in Eq.2.8, namely $k_1 = 0.20$ and $k_1 = 0.16$, which correspond respectively to the values of 3.2 and 2.6 used by Sauter [43] and derived in the case of large aspect ratio tokamaks [31, 32] and geometrical effects [44]. In the case of the (2, 1)-NTM is shown the time at which the island is predicted to lock. Small variations in the pedestal pressure and/or in the time of entry to H-mode will affect the island evolution, so that this mode is predicted to lock within seconds after its trigger.

Considering that the upper limit to the time required for switching the transmission lines between the equatorial and the upper launcher is about 3s, which is comparable to the time required to steer the UL from mid-radius to the $q = 2$ surface, that the threshold for the detection of an island with the ECE diagnostic is about 3-4cm when turbulence effects on the signal to noise ratio are taken into account, that the resonant surfaces are still evolving after the L-H transition, and that uncertainties on the evolution of the density, temperature and bootstrap current are large

in this phase, it is concluded that uncertainties in the analysis are very large. The original question of how much power is needed for NTM stabilization is herein reformulated as (a) how can the discharge be designed to ensure that the EC system can stabilize the NTMs within the limits imposed by the hardware and by the detection diagnostics and how can the power needed for NTM stabilization be minimized to enable shared applications with the EC system?

The pressure profile flattening inside the magnetic island leads to a relative degradation of the confinement τ_E , which can be estimated using the *belt* model [45]:

$$\frac{\Delta\tau_E}{\tau_E} = -4\rho_s^3 \frac{w_{sat}}{a} \quad (4.1)$$

where ρ_s is the value of normalized minor radius where the NTM appears. The confinement degradation would increase from 4% in the case of a (3,2)-NTM at $\rho_s \simeq 0.65$ and with $w_{sat} \simeq 7\text{cm}$, to about 7% for a (2,1)-NTM at $\rho_s \simeq 0.80$ and with similar size. Assuming this is a reasonable upper limit on the maximum reduction of confinement that can be sustained in the baseline scenario, while avoiding at the same time mode locking, the analysis has focussed on identifying under what conditions the width of the (2,1)-NTM can be prevented from growing above 7cm.

4.3 Control of NTMs in the ELMy H-mode plasma

Approaches to NTM control can be divided into two categories: control of modes that have grown above the detection threshold size and prevention of the triggering of instabilities. The first approach relies most on the sensitivity of the ECE diagnostic, the SXR diagnostic and the Mirnov coils; the second approach relies most on the accuracy of the magnetic equilibrium reconstruction.

This section describes simulations where the input power is adjusted in response to the measured NTM width and growth rate and where a constant amount of power is maintained on each resonant surface for pre-emptive control. It is shown that the requested power is significantly lower in the latter case, provided an alignment of the EC deposition with the resonant surface within half the EC deposition width is maintained. It is also shown that broadening the EC deposition profile up to 6 cm favorably helps the stabilization of the (2,1)-NTM.

The time scales relevant to simulations of control in the ITER baseline scenario are the following:

- The switch mechanism that redirects the power between transmission lines has a mechanical upper limit of 3s in the response
- 24 switches direct the power to either the EL or the UL, thus the entire 20MW can be redirected between the EL and the UL in $\leq 3\text{s}$.
- 8 switches direct the power to either the USM or the LSM, thus additional power can be re-directed to the mirror tracking the $q = 2$ surface in $\leq 3\text{s}$, if needed (up to maximum of 13.4MW total on either mirror)
- the steering speed of the upper and lower steering mirror is 13 degrees in 2 seconds, thus the mirror can potentially be used for combined sawtooth and NTM control.

4.3.1 Comparison of active search and pre-emptive control

We describe herein simulations run with EC feedback control, where the EC input power is updated in real-time in response to the island width in order to either suppress the NTM or to reduce its width below a threshold value. The time step used here for the EC calculations is $\delta t_{HCD} = 3\text{s}$, which corresponds to the limit imposed by the switch that redirects the power from one mirror to another. For example, if the EC power is directed to the Equatorial Launcher for core heating and current profile tailoring and an NTM is detected, then three seconds are needed for the power to be available on the Upper Launcher from the time the feedback control activates the EC mechanical system. The time step used in the simulations mimics such delay in the response of the system.

The calculated magnetic island width w_{NTM} and $\Delta'_{tot}(w)$ are used as proxies for the detection of the NTM from the ECE diagnostics and from the magnetic measurements. The MRE evolves

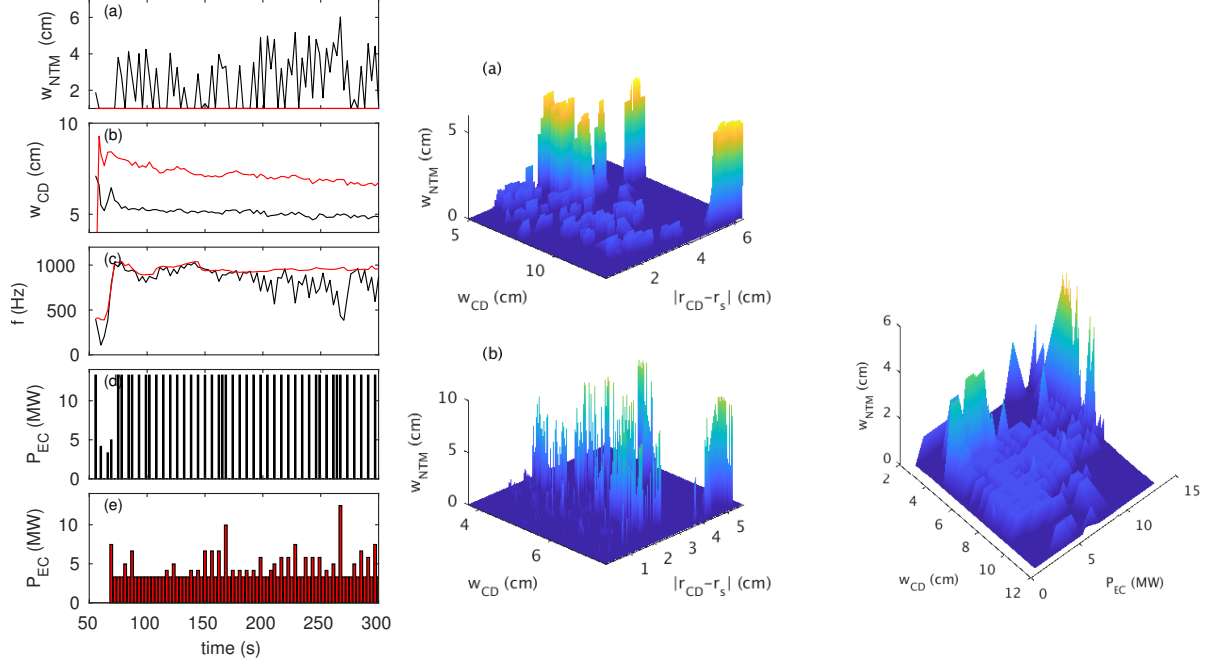


Figure 4.3: Left: Simulations with active search for a mode already developed on the $q = 2$ surface, for two choices of the EC deposition width. The EC power is turned-off after suppression of the (2,1)-NTM. Central panel: Simulations with pre-emptive control for the (3,2)-NTM (top) and the (2,1)-NTM (bottom). Right panel: simulations that combine pre-emptive control and feedback response on the EC power, for two choices of the EC deposition width and for three assumptions on the pre-emptive power on the $q = 2$ surface. Right panel: Histogram that summarize the results of a number of simulations with active search and with pre-emptive control under different assumptions on the EC broadening. The width of the island is plotted in function of the injected power on the $q = 2$ surface and of the EC deposition width.

forward the magnetic island width and rotation frequency between t_1 and t_2 with internal time steps of 25ms, under the effect of the EC for given input power, poloidal steering angle and calculated current density profile. The feedback control procedure is programmed as follows: (a) the EC power is turned-on only when the island width grows above the detection size w_{det} (b) if the island width has shrunk below w_{det} and $\Delta'_{tot}(w) \leq 0$ the input power is dropped to zero, this case corresponding to a fully suppressed island (c) if $\Delta'_{tot}(w) > 0$ and $w > w_{det}$ the MRE calculates how much power is needed to reduce $\Delta'_{tot}(w)$ to zero and feedbacks this power level to TRANSP (d) if $\Delta'_{tot}(w) > 0$ and $w < w_{det}$ the EC input power is maintained constant.

Figure 4.3 shows two simulations of control of the (2,1)-NTM run under different hypotheses on the EC power management. In one case the EC power is turned-off as soon as the island has been suppressed, in the second case a minimum amount of power is maintained always on the $q = 2$ surface and the power increased only when an island is detected. It should be noted that the minimum threshold size for detection is set here very low (about 1cm) and the maximum tolerance on the alignment of the EC with the $q = 2$ resonant surface is assumed to be 2 cm, consistently with the requirements of the PCS [46]. The EC deposition profile has been broadened with respect to the case of an ideal, perfectly focussed gaussian beam, by modifying the beam waist at the launching location. Both simulations avoid the locking of the (2,1)-NTM. However, in the former case the NTM grows again above its threshold size for onset as soon as the EC power is removed from the resonant surface, while in the second case additional power is required only a finite number of times. Increasing the pre-emptive power on the resonant surfaces reduces the number of these occurrences.

It has been observed that the large β on ITER would make NTM metastable and susceptible of being triggered not only from sawtooth crashes, as observed in present-day experiments, but also from other external or internal disturbances, like ELMs and pellets [43], or possibly electromagnetic turbulence [47–50]. However, it is very likely that the continuous triggering of modes observed in these simulations is an effect of the reduced models used in the MRE; thus, in practice, it is like these simulations are assuming a ‘sea’ of islands with width just below the critical size for onset, ready to be triggered at the appearance of any perturbation. Although these simulations are likely overestimating the number of triggering events, by overestimating the neoclassical drive in the MRE and underestimating the threshold for triggering of the mode, they indicate that an approach of this type might challenge the EC system. This said, pre-emptive control would minimize the need of continuously turning-on and off the gyrotron power and it might be preferable for the lifetime of the system.

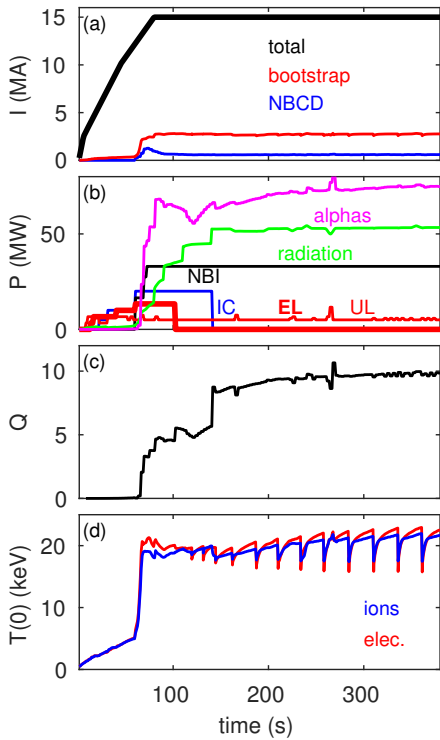


Figure 4.4: Simulation of the baseline scenario, with pre-emptive NTM control on the $q = 2$ surface. (a) plasma current and non-inductive contribution (b) heating power from fusion α s, external sources and impurity radiation (c) fusion gain (d) central temperature.

lution of the island width, similarly to the cases shown in the left panel. The broadening has been increased from 4cm to 12cm, while maintaining the maximum misalignment below 2.5cm, under the assumption of (a) maintaining a constant level on the $q = 2$ surface, between 1.66MW and 6.67MW (b) turning the power to zero after suppression. The island size is large and above the limit for locking for deposition width below 6 cm. In the limit of narrow deposition width the input power needs to be increased up to the maximum available power on the mirror that is tracking the $q = 2$ surface, which is 13.4 MW, i.e. two third of the total available EC power. Outside these limits an

A number of simulations have been run where the pre-emptive power is changed for a given broadening of the EC deposition profile and for given tolerance on the alignment of the EC with the $q = 1.5$ and the $q = 2$ rational surface [51]. Figure 4.3 summarizes the main results in a histogram of the magnetic island width with respect to the misalignment $|r_{CD} - r_s|$, to the EC deposition width w_{CD} and to the input EC power. The cases shown in the central panel refer to simulations where the power on each resonant surface is constant, w_{CD} is broadened up to three times the width at the resonance that would be given by the geometry of the mirror, $|r_{CD} - r_s|$ is varied between 1cm and 6cm. The results in the case of the (3, 2)-NTM show that (a) for narrower deposition width and large misalignment, typically $|r_{CD} - r_s| \geq 0.5w_{CD}$, even pre-emptive control is not sufficient to suppress the NTM. Ideal conditions for suppression correspond to $w_{CD} > 5$ cm and $|r_{CD} - r_s| \leq 0.5w_{CD}$. When the deposition profile becomes too broad, for example as a result of fluctuations, and the misalignment is larger than 4cm, suppression is no longer possible. Increasing the injected power does not change the results, since the critical parameter for success is maintaining good alignment between the EC current density peak and the resonant surface.

The right panel of Fig.4.3 shows the results from simulations that combine the injection of a constant amount of power on the $q = 2$ resonant surface with adjustment of the power level in response to the evolution of the island width, similarly to the cases shown in the left panel.

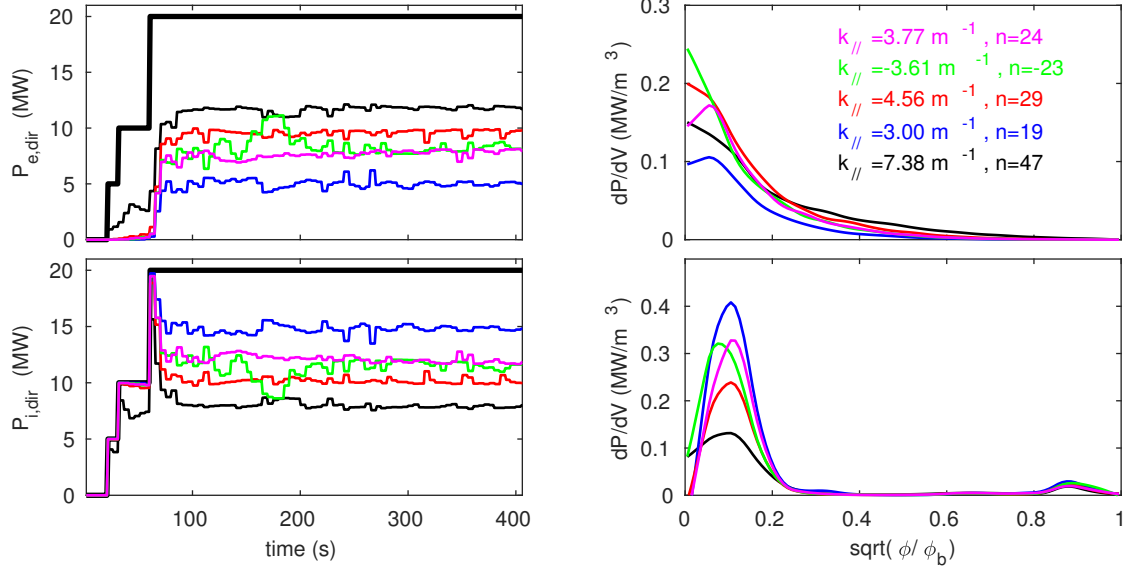


Figure 4.5: Direct IC heating on electrons and ions for different assumptions of n_ϕ in TORIC. The equivalent parallel wavenumber is reported for reference.

island of about 2-5 cm, below the locking size, can be sustained with power up to 7 MW provided the deposition width is at least 6cm wide.

NTMs cause a degradation of the confinement that can be recovered with suppression and/or stabilization with ECCD. However, increasing the input power will reduce the fusion gain, which is calculated as $Q = 5P_\alpha/P_{ext}$. Figure 4.4 shows a simulation that puts together everything learnt from the simulations discussed in this work. Here it is assumed that the LSM is tracking the $q = 2$ as soon as the plasma enters H-mode, that the combined effect of using multiple waveguides and turbulence broadens the EC deposition width up to about 7cm and that the EC power is reserved to the UL in the flattop. The EC power is used in the ramp-up for H-mode access, with up to 20MW, combining the equatorial and the upper launcher. The Upper Launcher starts tracking the $q = 2$ surface at the entry to H-mode with constant 5MW of power for pre-emptive control. At 100s the power on the Equatorial Launcher is redirected to the Upper Launcher and reserved for NTM control. The reserved gyrotrons are promptly turned-on when the diagnostics detect an island (i.e. when the width calculated by the MRE satisfies $w > w_{ECE} = 4cm$), as indicated by the occasional spikes in the EC waveform. This simulation achieves $Q = 10$, but it does so only by turning-off the IC power in the flattop. With 50MW of radiated power, 40MW of injected power, 80MW of self-heating from the alphas, the total power crossing the separatrix is about 30MW above the H-mode threshold power. However, the alpha power depends on the density peaking profile, which is prescribed herein, and the radiation is calculated assuming impurity profiles rescaled from the electron density profile and with constant fraction in time.

4.4 IC heating

Figure 4.5 shows the results of simulations that use up to 20MW of IC heating in the flattop phase. The toroidal mode number is changed to reproduce the parallel wavenumber corresponding to the different phasing configurations of the IC antenna reported in Table 3.3. All cases are considering

direct absorption on Tritium on the second harmonics resonance. The case with $n = 19$ provides the best ion heating. This is the closest to Case II analyzed by Messiaen et al [40] and indicated as the configuration with the best coupling to the plasma. The case with the largest toroidal mode number has the lowest ratio of ion to electron heating and the others, including the two cases corresponding to current drive, have comparable contributions to the ions and to the electrons.

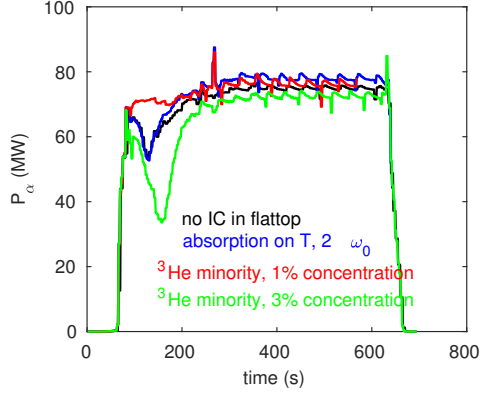


Figure 4.6: Self-heating alpha power for different assumptions on the IC heating scheme.

Interestingly, the effect of IC heating on the ion temperature and on the alpha power is only marginal, as shown in Fig.4.6 for the case of $n_\phi = 19$ and for 10MW of IC power in the flattop phase. Although the electron and ion temperature increase in the core by about 25%, the increase in alpha power in the flattop phase is modest and it depends on the heating scheme. The largest differences are observed during transient phases, like between the entry to H-mode and the first 100 seconds of the flattop phase. However, since the electron density profile is prescribed and the ion density profile is calculated from quasi-neutrality, these results should not be considered conclusive. Fusion power depends on the density profile peaking, which should be calculated self-consistently from particle transport models. Within the limits of the simulations and of the models used, it is found that adding 10MW of IC power with dominant direct ion heating on the Tritium lengthen the sawtooth period by about 30%,

from 35s to 45s, which would provide a direct seeding for NTM triggering from sawtooth crashes. Future simulations should evolve all transport channels and use fast wave solvers that account for the synergy between the RF waves and beam fast ions to address the following open questions:

- how is the sawtooth period affected when the effect of the RF electric field on the beam distribution function is taken into account to modify the fraction of the passing to trapped particle, by changing the frequency of the antenna.
- what is the flexibility of the ITER IC antenna in adjusting the IC frequency to ensure absorption close to the $q = 1$ surface and what is maximum tolerance that is allowed on the distance from the $q = 1$ in order to see an effect on the trigger of a sawtooth crash.
- is the use of the IC antenna for sawtooth pacing compatible with the need for deep core heating for avoidance of impurity accumulation in the core and how does the latter compare to using the EC instead?
- Given that the phasing corresponding to a parallel wavenumber of $k_{\parallel} = 3.1 \text{ m}^{-1}$ provides the best coupling of the power to the plasma under typical flattop conditions, is this phasing still the best option for access to H-mode and exit from H-mode with reduced core impurity accumulation?

4.5 On the feasibility of sawtooth period pacing with the Equatorial Launcher

The simulations described in the previous sections assume that NTMs in ITER would either be triggered spontaneously because of the large β_p . In present day experiments, NTMs are observed in many cases to be triggered by sawtooth crashes. It has been estimated that on ITER the sawtooth period for triggering NTMs should exceed 40s. The simulations described in this section try to reproduce experiments done on TCV where the EC power is injected inside the $q = 1$ and then promptly removed on demand to trigger a crash via modification of the local shear. On TCV the EC was then moved to the $q = 2$ surface for NTM pre-emptive control. Here, we instead assume that the power is transferred from the EL to the UL. This is for two reasons: first, it takes approximately the same time to steer the UL from the $q = 1$ to the $q = 2$ surface; second, it is conservatively assumed that some power might be needed on the UL at all time to track the $q = 2$ surface, for pre-emption; third, the current density of the EL is higher than that of the UL inside the $q = 1$ surface, thus providing a better control knob. The question is whether the current drive efficiency of the EL is sufficient for modifying the sawtooth period and triggering a crash on demand.

Figure 4.7 shows the results of these simulations. The different curves compare the sawtooth period in the reference simulation (black curve), which is about 40 seconds in the flattop phase, with cases where both the EL-bot and EL-mid are steered inside the $q = 1$ surface (blue curve) or only one of the two is steered inside the $q = 1$ surface. If we exclude the first large sawtooth after the L-H transition, the sawtooth period is affected only when both mirror are steered inside the $q = 1$.

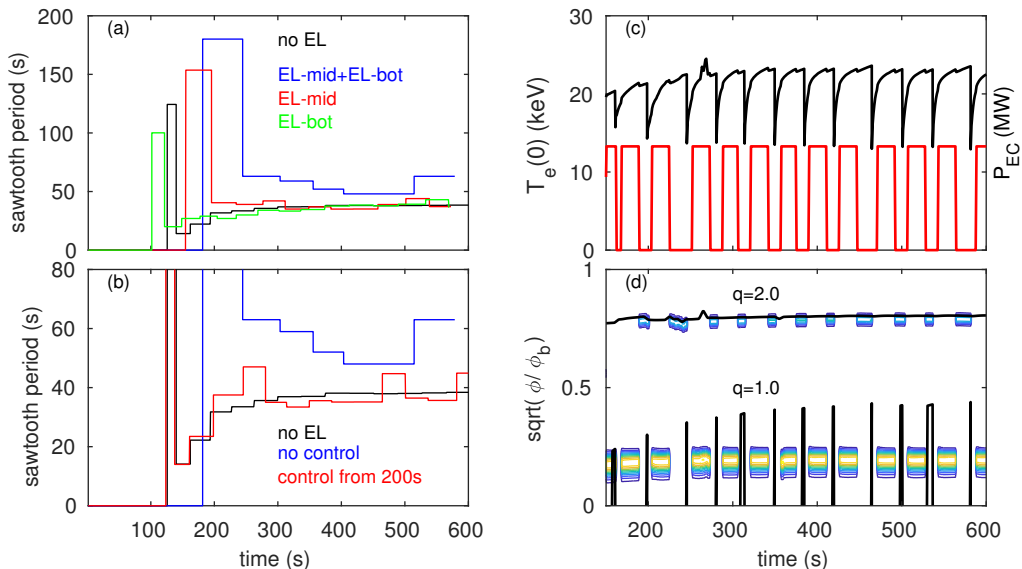


Figure 4.7: (a) sawtooth period in the case of the reference simulation (no EC in flattop) and with the equatorial launcher steered inside the $q = 1$ surface, each mirror delivering 6.67MW of power. (b) Comparison between the sawtooth period in the reference discharge, when both the EL-mid and EL-bot are steered inside the $q = 1$ surface and when the power is removed from the EL for trigger of a sawtooth on demand. (c) central electron temperature in the case with control shown on the left and waveform of the power on the EL. (d) contour plot of the power delivered on the EL and then redirected on the LSM, the position of the $q = 1$ and of the $q = 2$ surfaces are shown for comparison.

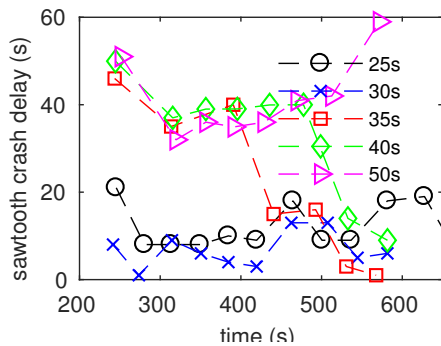


Figure 4.8: Delay between the trigger of a sawtooth crash and the time the EC power is removed from inside the $q = 1$ surface for different values of the requested sawtooth period.

the time of a sawtooth crash for a scan of the requested sawtooth period. In all cases analyzed the sawtooth period is 40s independently of the requested pacing period. As shown in the figure, when the requested period is summed to the delay $t_{crash} - t_{EC,off}$, the total is comparable to 40s, which is the natural sawtooth period without any EC power, suggesting that pacing is inefficient. This also suggests that the only way of manipulating the sawtooth period is by modifying the fast ion population, rather than by trying to modify the local magnetic shear. It will be shown that the neutral beam energy provides an effective way of manipulating the sawtooth period at half-field, which is desirable for demonstration of NTM control in helium plasmas, where NTMs would otherwise be stable.

Figure 4.7-(b) shows a simulation where the controller is programmed to switch the power from the equatorial to the upper launcher when the sawtooth period exceeds a critical value, in this case 25s, which is shorter than the natural period. Although the control fails in sustaining the requested period, the timing of the power turn-off and the time of crash is quite well aligned. It is noted that the removal of power causes a minor internal reconnection, which is followed by the major crash after a few seconds, indicating that the EC current is not sufficient to modify the local magnetic shear to a level that can trigger a sawtooth crash. This is different from what observed in present-day experiments with sawtooth pacing. Under ITER conditions the crash is triggered when stabilizing fast ion effects cannot overcome the internal kink stability term. Figure 4.8 compares the delay between the time the EC power is removed from inside the $q = 1$ surface and

5 Operation at half-field

Operation around half-field aims at demonstrating H-mode access in plasmas with all gas mixtures and each of these configurations has its own limitations as of how to optimize the heating schemes. Operation in hydrogen and helium, in particular, will serve the commissioning of the heating and current drive systems, of Edge Localized Modes mitigation schemes, disruption mitigation, divertor heat loads and detachment, controlled plasma termination, NTM control. In these plasmas NTMs are predicted to be stable because of the low poloidal beta (including fast ion contributions) thus they are good candidate for demonstration of NTM control with sawtooth pacing.

Plasmas are simulated assuming electron density in the range of 40% to 75% of the Greenwald limit (the Greenwald density at 7.5MA is $n_G = 6.0 \times 10^{19} \text{ m}^{-3}$), with hydrogen and helium plasmas typically close to the lower limit and deuterium and DT plasmas close to the upper limit, depending on the power threshold for H-mode transition.

5.1 Neutral Beam heating

Simulations use deuterium neutral beam sources in deuterium and D-T plasmas and hydrogen beam sources in helium and hydrogen plasmas. The beam source energy is selected each time taking into account both the tabulated admissible density, provided by the IO, and safety margins for the uncertainties in the evolution of the plasma kinetic profiles. For example, even at the lower operational density, the line averaged density is above the shine-thru limit for deuterium beams, allowing nominally the use of full energy beam sources. However, since the effective shine-thru is a function not only of the line-integrated density but also details of the profile peaking and of the plasma composition Z_{eff} , all of which are not constant during the discharge and unknown, it might be advised to operate below the tabulated shine-thru limits, for operational safety margin, by using lower beam energy sources. Simulations indicate that this is the case for hydrogen and helium plasmas. The simulations are not limited to the use of the maximum energy beam, but explore scenarios with lower energy beam to assess the effect of the current drive on the sawtooth cycle for a given line averaged density. This is done with the purpose of identifying trends in the sawtooth period and conditions under which the sawtooth period can be lengthen sufficiently to trigger an NTM in plasmas that would be otherwise stable. The lowest beam energy is constrained by the threshold power for sustaining H-mode and the highest beam source energy is constrained by the shine-through power. Impurity seeding is considered in hydrogen and helium plasmas to reduce the shine-thru power.

5.2 Electron Cyclotron heating

At 2.65T, which is the nominal magnetic field for operation in the pre-fusion operation 2, the third harmonics of the electron cyclotron frequency is inside the plasma, close to the plasma edge, as shown in Fig.5.1. The power and current profiles from the Equatorial Launcher are affected by parasitic absorption on the third harmonics for all steering angles, whose effect is sensitive to details of the local temperature and therefore to details of the profiles inside the edge transport

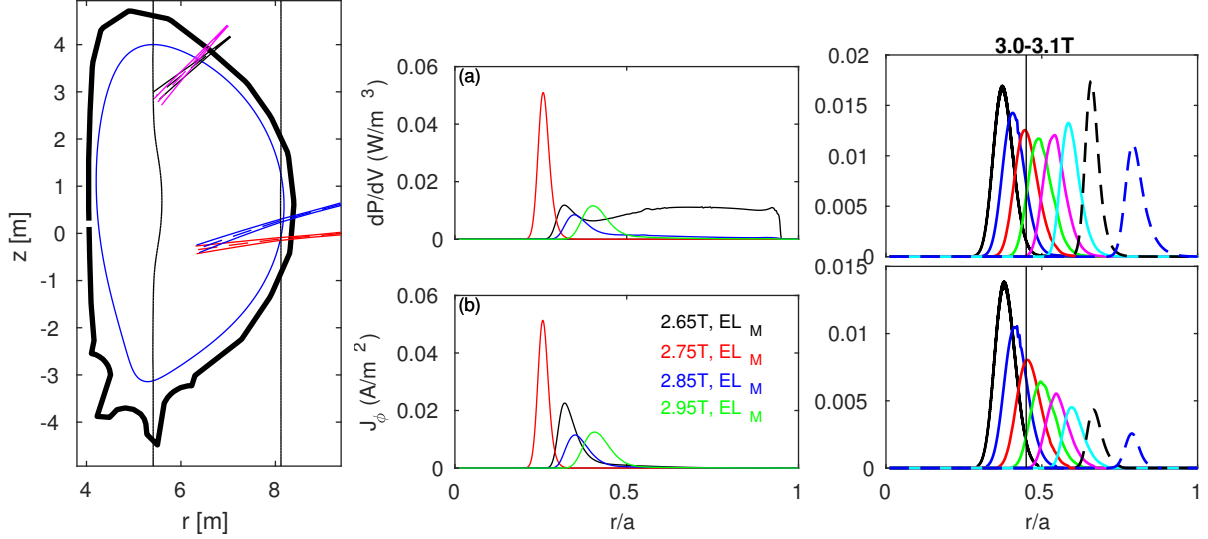


Figure 5.1: Left: beam trajectories from the EL-mid and EL-bot, which intersect the 2^{nd} and 3^{rd} harmonics of the electron cyclotron resonance, and from the UL, which does not intersect the 3^{rd} harmonics. Center: power and current density profiles from the EL-mid, for a poloidal angle of 15 degrees, in plasmas with different values of the magnetic field on-axis. Right: Power and current density profiles from the EL-bot over the available poloidal steering range, for magnetic field of 3.0-3.1T.

barrier. Since none of the physics-based transport models available is valid outside $\rho = 0.75$ and no model exists to describe the so-called "no-man's land" inside the pedestal, the thermal diffusivity profile and the temperature profile are calculated imposing a continuity both in the value and in the first derivative of the transport solution between the core and the pedestal. Boundary conditions for the pedestal are commonly based on peeling-ballooning stability limits, which do not include effects of turbulence and of the presence of coherent structures in the SOL on the transport across the separatrix. Uncertainties in the temperature profiles in the outer 25% of the radial profile are therefore very large. Previous calculations performed offline from profiles of temperature derived from semi-empirical transport models (thus valid over the entire radial region) did not observe any problem [2].

As shown in Fig.5.1, the third harmonics parasitic absorption can be eliminated by increasing the magnetic field to 2.75T. It should be noted that the position of the magnetic axis depends on the global discharge parameters and on the Shafranov shift, so the profiles indicated for 2.65T and 2.75T are using the same target input value of $B_0 R_0$, but they evolve to flattop magnetic equilibria that have different position of the magnetic axis and different minor radius, resulting in a magnetic field on axis of 2.64T in one case and 2.77T in the other case. The latter does not display any parasitic absorption on the third harmonics. Thus operating at a nominal magnetic field of 2.75T would completely eliminate the problem of parasitic absorption. This is a minor variation in the desired operational point, which has a minor impact on the power threshold for access to H-mode in deuterium, DT and helium plasma.

The heating and current drive profiles become broader with increasing the magnetic field in the range of 2.75T to 2.95T and the deposition location moves outward. For magnetic field higher than 3.0T the innermost radius that can be reached by the EL is $\rho = 0.6$, outside the $q = 1$ surface, which typically expands to a maximum of $\rho = 0.46$. Although accessibility to the inner half-radius is still possible up to 2.9-3.0T, the operational window between 3.0T and 3.3T is not recommended, because it would compromise the full accessibility of the EL and the capability of providing core heating,

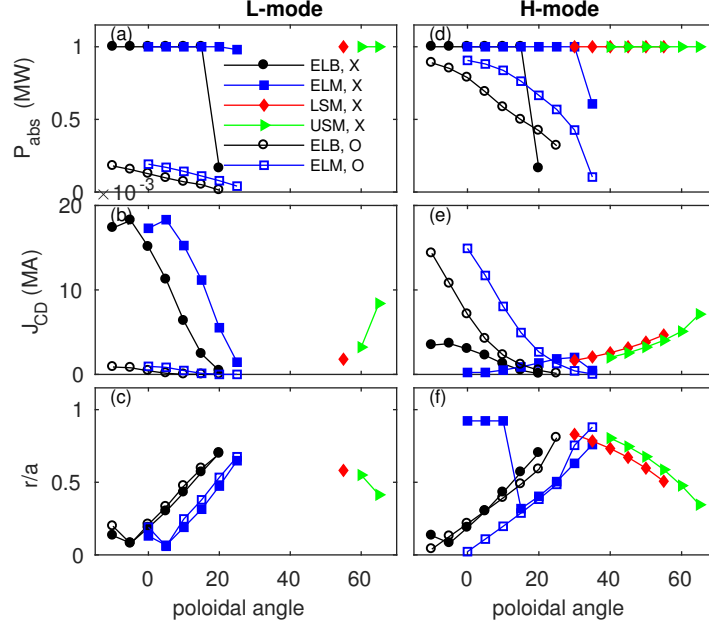


Figure 5.2: Total absorbed power and driven current from the co-current EL and from the UL over the available range of poloidal steering angles for L-mode (left) and H-mode (right).

which is critical for avoidance of impurity accumulation. Scenarios at 2.65T will be analyzed anyway for NTM control, operation at 2.85T will be analyzed for sawtooth control, and recommendation will be provided on how to operate the EC system at 2.65T by taking advantage of both the O-mode and X-mode polarization.

Figure 5.2 shows offline calculations with TORBEAM in L-mode at 25s and H-mode at 300s for the same plasma discharge at 2.65T that is shown in Fig.5.1. In the case of the two co-current EL mirrors both X and O polarization have been analyzed, while in the case of the UL only X polarization has been considered, since this launcher never intersects the region affected by the Doppler-shifted third harmonics resonance.

Since the UL is crossing more peripheral regions, there is a minimum value of the local density at which the beam trajectory does not shine through the plasma and first pass absorption becomes significant. At 25s, only the largest poloidal steering angle can provide full absorption.

The difference between X-mode and O-mode absorption is maximized in L-mode, where the EL loses almost 70% of the injected power when injected with O-mode polarization. Current drive is maximized for poloidal steering inside mid-radius, which also optimizes core-heating inside $\rho = 0.25$.

After transition to H-mode, localized EC absorption is compromised by the Doppler-shifted third harmonic resonance. Interestingly, the difference between O-mode and X-mode polarization depends on the poloidal steering angle and is minimized for small values of α , which correspond to the innermost deposition. For these angles, not only the EL can reach inside $\rho = 0.4$, but the driven current would be higher than the current driven in X-mode polarization.

While operation at 2.75T would completely eliminate the problem of parasitic absorption, operation at 2.65T is still possible, provided the polarization of the EL is changed from X-mode in L-mode to O-mode in H-mode. The range of suitable poloidal steering angles is limited to span about 15 degrees maximum out of the full steering range by the absorbed power rapidly decreasing when the deposition moves outward. This would limit the ability of using the EL for sawtooth control and current profile tailoring, but it still allows demonstration of access and sustainment of

H-mode with good core-heating. Since the change in polarization takes about three seconds, the entry to H-mode has to be feed-forward controlled for density build-up, time of entry to H-mode, timing and energy of the neutral beam sources to ensure that the plasma does not undergo a back transition during this time window and that shine-through does not exceed limits.

5.3 Ion Cyclotron Heating

Figure 5.3 shows the position of Ion Cyclotron resonances for magnetic field of 2.65T in the range of frequency covered by the ITER IC antenna. Helium, hydrogen and deuterium all have a resonance in the core at 40-45 MHz, beryllium, argon and neon have also a resonance at the second harmonics inside mid-radius, while ^3He heating in the core would require increasing the frequency up to 53MHz.

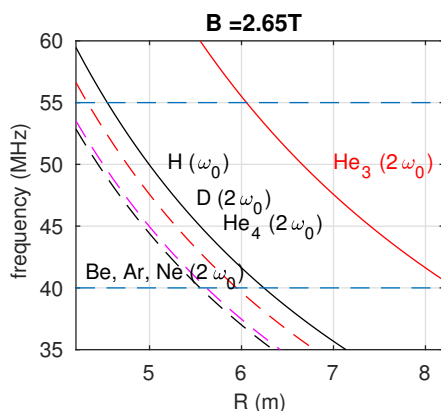


Figure 5.3: IC resonance inside the plasma at 2.65T.

It is expected that at this magnetic field the distribution function of neutral beam fast ions is modified by the RF electric field both for deuterium and hydrogen beam sources. Simulations should therefore take into account the synergy of the RF waves and the fast ions, as well as assess orbit losses due to acceleration of the fast ions by the RF waves. As of today there is no capability of such a self-consistent simulation in a time-dependent fashion, since every code has its own limitations. Ion Cyclotron calculations are performed in TRANSP with the full wave solver TORIC and the effect of the electric wave field on the beam fast ions is accounted for by a kick model that follows the orbits of resonant fast ions and accelerates them giving a "kick" in the energy. This approach is not self-consistent yet, since TORIC is still assuming an equivalent maxwellian distribution function instead of using the distribution function calculated by NUBEAM. The feasibility of a self-consistent loop is currently under test and will be available in the near future.

The feasibility of a self-consistent loop is currently under test and will be available in the near future. It has been observed that first pass absorption of IC waves is very low in hydrogen plasmas and no good heating scheme exists [4, 52]. If the purpose is demonstration of access to H-mode, it probably does not matter whether the fraction of first pass is low, provided there is sufficient power inside the edge transport barrier to sustain the high confinement regime. Since the EC will be used in combination with the IC for core heating and H-mode access, high confinement would be sustained by the localized EC core heating. However, compatibility of the IC heating in this plasma with the SOL losses should be addressed to assess the coupling of the IC power to the plasma.

Operation in hydrogen might be compromised by the lack of sufficient power for access and sustainment of H-mode, if ITER wants to operate at a density sufficiently high for the commissioning of the hydrogen Neutral Beam sources up to full energy. It has been suggested that increasing the magnetic field up to 3.0-3.3 T and injecting a very small fraction of ^3He would significantly improve the first pass absorption of IC waves, operating at 40MHz [53]. By using a mix of hydrogen and helium with up to 10-15% fraction of helium would benefit from the three-ion scheme heating that has been recently proposed [54]. However, operation at magnetic field around 3.0T and above would compromise the full functionalities of the EC system, by preventing accessibility inside mid-radius.

5.4 General assumptions of simulations at half-field

Plasma operation at half-field does not benefit from the self-heating alpha power and the sustainment of H-mode entirely relies on the external heating. When possible, the reference plasmas use only Neutral Beam injection. The assumption behind this choice is that the EC power is needed for NTM control and the IC power is reserved in case one of both the neutral beams fail, to sustain H-mode. In deuterium and D-T plasmas the threshold power is sufficiently low to allow sustainment of H-mode with the available NBI power, while in hydrogen plasmas all sources need to be used. It is also assumed that pellet injection will allow to achieve the target of 75% of the Greenwald density, although these assumptions have to be verified with self-consistent simulations that evolve coupled core and edge plasma with a model for the pedestal pressure and radial structure that includes both MHD and turbulence effects. Contrary to the baseline scenario, where the H-mode is sustained during one third of the current ramp-down phase, it might be advisable to have a transition to L-mode shortly after the end of the flattop phase. As discussed in the following section, this is due to the presence of NTMs in DT and DD plasmas and the the combination of a narrow EC deposition profile and broadening in the ramp-down phase, which would limit control more than they would in the baseline scenario.

The power threshold for access to H-mode is unfavorable in hydrogen plasmas, since it depends on the inverse of the hydrogenic mass species. At 2.65T and 7.5MA, the power threshold from the ITPA scaling [10] is 40MW for densities of $n_e \simeq 2.7 \times 10^{19} \text{m}^{-3}$ ($0.45n_G$), and increases up to 60 MW for densities of $n_e \simeq 4.7 \times 10^{19} \text{m}^{-3}$ ($0.75n_G$). At magnetic field of 3.0T and higher the threshold power would be about 10% higher. Access to H-mode would not be possible at this magnetic field if ITER cannot rely on all the H&CD system in the baseline for core heating.

The maximum NBI power that can be used in this plasma, to stay below tabulated values of shine through power, is 13 MW at the lower density and full power at the higher density, although impurity seeding might be needed to reduce the shine-through.

On account of radiation losses, and to maintain sufficient power margin above the H-mode power threshold, operation at $0.45n_G$ would need the full available power of 20MW of EC and 20MW of IC in addition to the NBI. This would leave no reserved power for emergencies, like in case one of the systems fail, to sustain H-mode operation. Operation at higher density can benefit from the use of full energy beam sources, but it also has higher threshold power and it thus needs the full available power to sustain H-mode, leaving no reserved power for handling of system failures.

If the effectiveness of IC heating is proven to be low at these values of the magnetic field, then H-mode operation in a pure hydrogen plasma cannot be demonstrated if ITER has to rely only on 33MW of NBI and 20MW of EC power. Polluting the plasma with helium would decrease the power threshold. The question is: how much helium would be needed in order to demonstrate H-mode operation with the available power and would this be a sensible approach as opposed to operate in helium plasmas instead?

Electron Cyclotron and Ion cyclotron power are used in the ramp-up phase, up to full power, to access H-mode and in the ramp-down, while the Neutral Beam power is stepped-down. Similar to the baseline scenario, the EC is turned-off after the back transition to L-mode, because the plasma is shrinking and moving downward and it would be difficult for the system to keep heating the core during this phase.

6 H&CD power management in DT and DD plasmas

The deuterium and D-T plasmas have similar characteristics in the flattop phase within the assumptions and approximations done in the simulations and are therefore discussed together. The power threshold for H-mode in DT plasmas varies between 20.5 and 24.5MW for densities between 60% and 77% of the Greenwald density and it decreases down to 16.5 MW for operation at 40% of n_G . In deuterium plasmas, the power threshold is about 5MW higher, but there is no contribution from the fusion alphas, which is about 5MW in the DT plasma. Since the radiated power, under the approximations taken here on the impurity profiles, is comparable in the two cases, sustainment of H-mode is subject to an additional 10 MW of power in the deuterium plasma for the same given density profile.

Figure 6.1 shows the reference case for the DT plasma. The neutral beam source is 1.0MeV, since the density is well above the shine-through limit of $2.2 \times 10^{19} \text{m}^{-3}$. The integrated power that shines-through - as calculated by NUBEAM in these plasmas is about 1% of the total injected power - or 250kW. Electron density profiles are prescribed in shape and amplitude, with moderately broad peaking, with values at the separatrix and at the pedestal respectively of 35% and 75% of the central value, similarly to the assumptions made for the baseline scenario. These assumptions should be verified against self-consistent simulations that account for gas and pellet fueling. The stabilization of the alphas leads to a slightly longer sawtooth period in the DT plasma, of $\tau_{SAW} = (17.1 \pm 0.7)\text{s}$ compared to the $\tau_{SAW} = (13.1 \pm 0.4)\text{s}$ in the deuterium only plasma. This is about one third to half the natural sawtooth period predicted at full field, under the same hypotheses in the Porcelli model.

Similarly to the simulations for the ELMy H-mode plasma at full field, also these plasmas are not using EC and IC in the flattop phase, to have a reference for both the NTM stability and the sawtooth period without any additional localized source of current drive inside the $q = 1$ surface. It is assumed that the Ion Cyclotron is needed during the ramp-up and ramp-down phase for avoidance of core impurity accumulation across the transition between L and H-mode. The effectiveness of EC as opposed to IC for core heating and impurity control should be assessed in self-consistent simulations as well as in experiments and is still subject of research. It should be noted that, at this operating density of $\bar{n}_e = (4.7 \pm 0.1) \times 10^{19} \text{m}^{-3}$, the power threshold for entry and sustainment of H-mode, which is $(24.2 \pm 0.8)\text{MW}$ in the case of the DT plasma and $(30 \pm 1)\text{MW}$ in the deuterium plasma, is satisfied by the use of EC and the NB full energy sources only. Should one neutral beam fail during the discharge, there is still enough backup power to sustain an H-mode plasma with either the EC or the IC system.

P_{NB} (MW)	E_{NB} (keV)	n_e [10^{19}m^{-3}]	
16.5	1000	2.2	SHT 2.4 MW/m ² (off gap)
12.7	900	1.7	
9.4	800	1.55	
6.8	700	1.85	SHT 0.8 MW/m ² (on gap)
4.6	600	1.45	
2.9	500	1.2	

Table 6.1: Shine-thru limits for deuterium beams, as a function of the target density and neutral beam source energy and injected power.

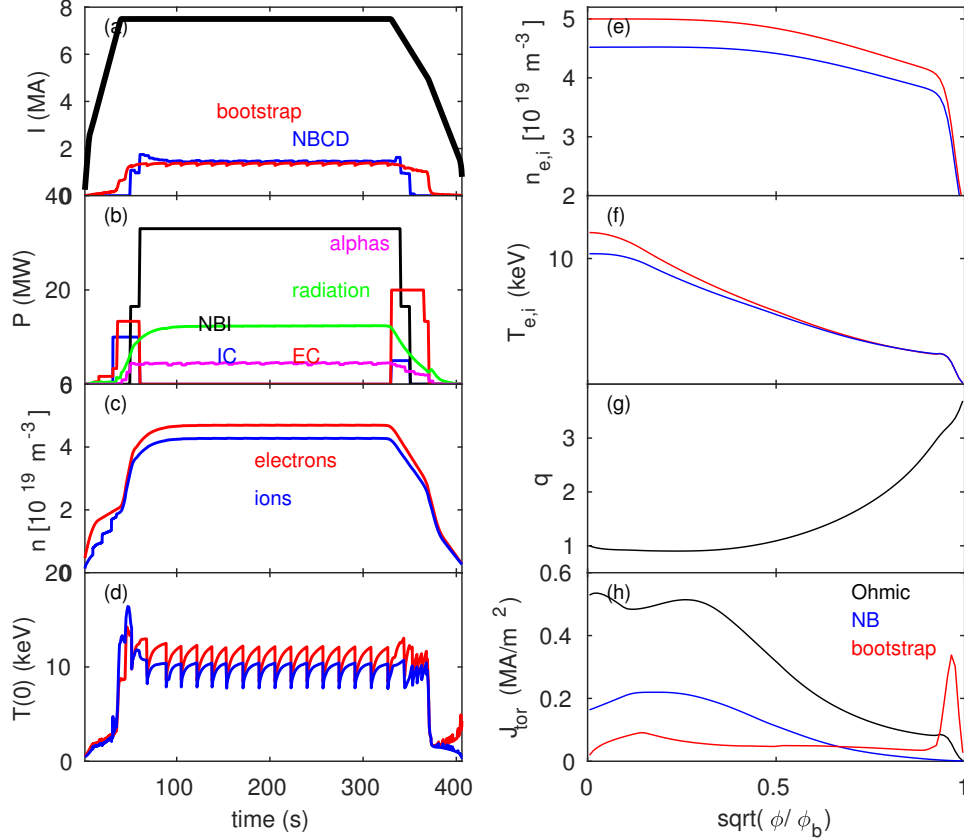


Figure 6.1: Reference simulation for a plasma with D-T mix. The plasma current is 7.5MA and the toroidal field 2.65T. Left column: time traces of current, power, line averaged density and central temperature. Right column: profiles at 290s of (e) electron and ion density (f) electron and ion temperature (g) safety factor (h) beam current, bootstrap current and ohmic current.

6.1 NTM control

NTMs are predicted to be unstable both in the deuterium and the DT plasma simulations, with similar features to those observed in the ELMy H-mode plasma, which can be summarized as follows: (a) the (2,1)-NTM is triggered shortly after the H-mode transition and locks within seconds from its onset (b) the stability of the (3,2)-NTM is sensitive to the plasma parameters but this islands never gets larger than about 6-8 cm and it never locks.

Similarly to the approach taken in the analysis of the baseline scenario, we have run simulations that combine pre-emptive injection of a small amount of EC power on the $q = 2$ surface with an active control of those islands that grow above a threshold size. The EC deposition width has been varied around the optimal value of 5 cm [18] and the tolerance on the maximum misalignment has been set to 2.5cm, which is a realistic assumption based on diagnostics uncertainties and signal to noise ratio.

Figure 6.2 shows the results of simulations run in the reference plasmas discussed in the previous section where the feedback control loop is activated. The left panel refers to a DT plasma and the right panel to a deuterium plasma. We have run scans of the EC deposition width, from the value that is given by the tabulated values of the mirror curvature and of the beam waist, up to a factor three broadening. Thus, the narrower case corresponds to the FWHM value of a perfectly focused,

gaussian beam, injected with $d_{ox} = 4.813$, while the wider case corresponds to $d_{ox} = 0.963$, which is very broad at the resonant location.

It should be noted that the natural width of the beam injected with X2 polarization in these plasma at half-field is narrower than the natural width of the beam injected with O1 polarization in plasma at full field. Thus, the requirements on the alignment between the EC current density profile and the $q = 2$ resonant surface for stabilization and suppression of NTMs at reduced magnetic field are expected to be higher than at full field.

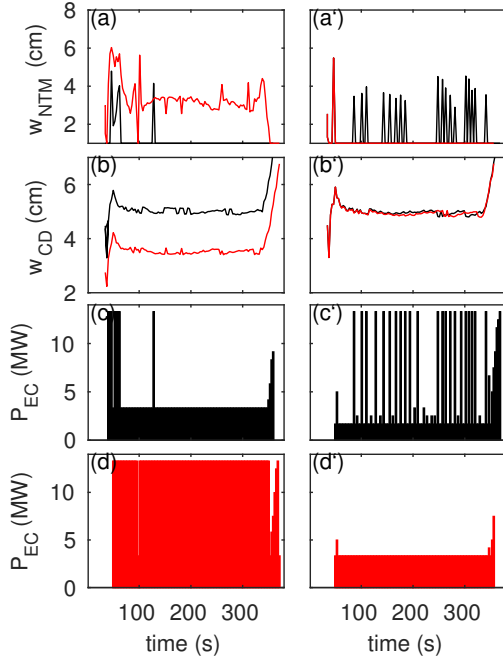


Figure 6.2: Left: simulations of NTM control in the reference discharge, under two assumptions on the EC beam waist. (a) island width, (b) width of the EC current profile (c) EC power from the feedback control in the case with broader beam waist (d) EC power from the feedback control for the case with narrower beam waist. Right: simulation in the case of a discharge operating at $0.40n_G$, for two assumptions on the minimum EC power that is maintained on the $q = 2$ surface. (a') island width, (b') width of the EC current profile (c') EC power from the feedback control in the case where two gyrotrons are maintained on the $q = 2$ surface (d') EC power from the feedback control for the case where four gyrotrons are maintained on the $q = 2$ surface.

In the case of the DT plasma two cases are shown with different assumptions on w_{CD} . With wider EC deposition (black) the island would be fully suppressed with about 4MW of power on the $q = 2$ surface. The entry to H-mode and the ramp-down phase require the largest power investment; in the former case the position of the resonant surfaces is still moving outward, in the latter case the deposition naturally broadens because the rays are more tangent to the resonant surfaces. In the case with narrower deposition, additional power is required during the entire flat-top phase, up to the maximum available to the LSM. However, this is not sufficient to stabilize the island, which is predicted to lock after a few seconds after triggering. Steering both the USM and the LSM to the $q = 2$ resonant surface would provide the needed power.

The plasma in deuterium, shown in the right column, shows qualitatively similar features. In this case, two cases with the same w_{CD} are shown, but with different assumptions on the amount of power used for pre-emptive control on the $q = 2$ surface, respectively two and four gyrotrons. While the case with lower power needs additional gyrotrons to be turned-on frequently, the case with higher power can prevent the NTM from growing above the threshold size. Considering the limits in the reduced models used for the calculation of the width and frequency of the magnetic islands, the number of times the power needs to be turned-on is probably over-estimated. We will assume that four gyrotrons is an upper limit for the pre-emptive power needed for NTM control in DD and DT plasmas operating at 75% of the Greenwald density and with full energy beam sources. These conclusions are valid within the limits of the models used here and provided the EC beam deposition width is at least 5cm, a condition that can be satisfied by

selecting individual waveguides and because of the presence of turbulence fluctuations that broaden the beam during its propagation.

It is found that, both in DT and in DD plasmas, even the maximum available power would not be sufficient to stabilize and suppress the (2, 1)-NTM when no broadening is taken into account.

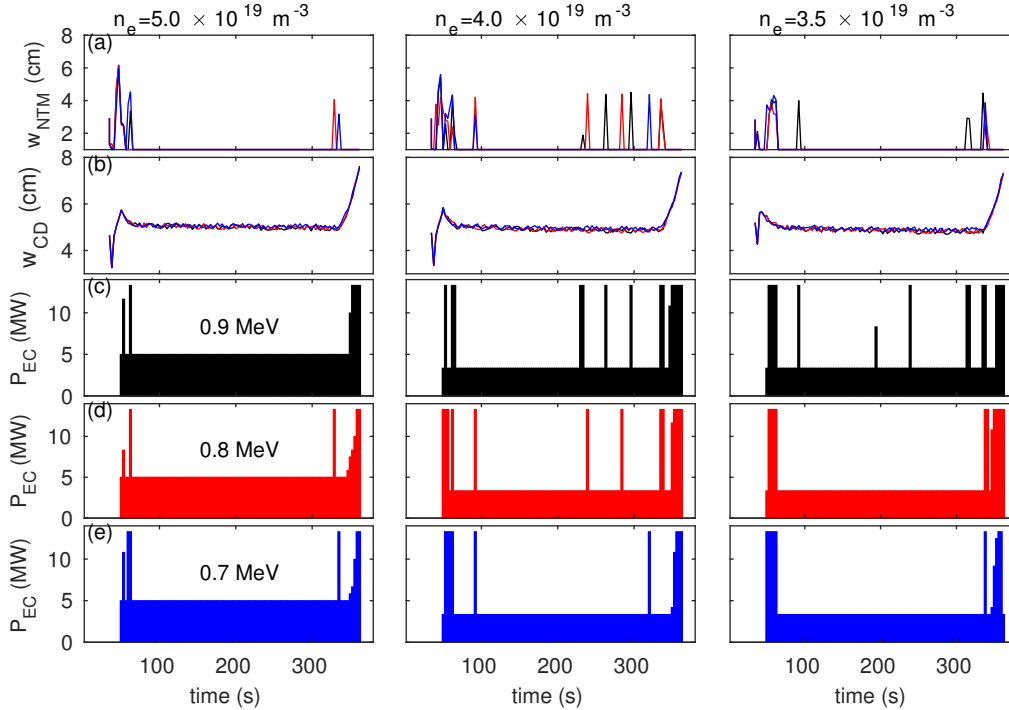


Figure 6.3: Simulations of EC feedback control for three values of the electron density and for three values of the beam source energy: 0.9 MeV (black curves), 0.8 MeV (red), 0.7 MeV (blue). (a) island width (b) width of the EC current profile (c-e) EC power from the feedback control.

Under these ideal geometry conditions, the (2,1)-NTM would lock within seconds from its onset, at a width that is about half the value of the locking size that is predicted at full field. The presence of fluctuations will naturally spread the beam, which might help, but blobs and pellets would scatter the beam, which is deleterious because it increases the misalignment with the resonant $q = 2$ surface, which has been identified to be critical parameter for the success of NTM stabilization and suppression. The positive effect of broadening by turbulence fluctuations on the stabilization of NTMs might sound counter-intuitive in the light of previous assessments. However, there is no contradiction when it is considered that previous calculations were assuming a fully developed island, which is the typical situation in control-oriented experiments in present-day tokamaks. Under the hypothesis of pre-emptive control, where the resonant surface is constantly tracked, a magnetic island would always fall ‘under the shadow’ of the EC current profile if this is sufficiently broad; moreover, broadening would reduce the negative effects of misalignment. Future work might include the use of parametrization for the effects of turbulence fluctuations, based on standalone calculations over a range of parameters, including the width of the magnetic island and the EC beam deposition width. They should also evolve self-consistently the plasma density with a model for pellet ablation and assess the effect of pellets on the EC beam trajectory and - as a consequence - the effect of deflections from the original path on the NTM stabilization. They should assess the feasibility of scenarios that exit H-mode at the end of the flattop phase for MHD, NTM stability and control and compatibility with plasma shape and vertical control, density decay, impurity accumulation, disruptivity, power loads to the divertor.

Figure 6.3 show simulations with lower electron density and with beam source energy between 0.7 and 0.9MeV, for a qualitative assessment of how the power needs for NTM control change when

either of these parameters is modified. The three columns refer to plasmas with density of $5.0 \times 10^{19} \text{ m}^{-3}$, $4.0 \times 10^{19} \text{ m}^{-3}$ and $3.5 \times 10^{19} \text{ m}^{-3}$, respectively. For each value of the plasma density, three values of the beam source energy are considered, equal to 0.9 MeV, 0.8MeV, 0.7MeV, as indicated in the frames. All cases have the same tolerance on the maximum misalignment of 2.5cm and assume an EC deposition width of 5-5.5cm, which is obtained by rescaling the beam waist at the injection point by a factor two. All cases achieve NTM stabilization and suppression with comparable investment of EC power used pre-emptively, independently of the beam source energy. Operation at the lowest density requires lower power for given beam energy, but the amount of power is independent of the beam energy. Thus, by progressively increasing the density from 40% to 75% of the Greenwald value, provides a step-wise approach to demonstration of pre-emptive control in plasmas with deuterium and DT at half-field. Up to 5MW of EC power should be used for pre-emptive control. Provided the deposition width is broad enough, namely at least 5cm, pre-emptive control should be a sufficient condition for the NTM stabilization, given that these simulations - as discussed in Sec.2 - are likely overestimating the neoclassical drive and under-estimating the threshold size for triggering. Also, at given density, increasing the beam source energy would provide another step-wise approach for the demonstration of NTM control with active feedback, by gradually increasing the bootstrap current and the fast-ion contribution to the total plasma β .

Since the UL is not affected by the presence of the Doppler-shifted third harmonics inside the plasma, pre-emptive NTM control can be demonstrated in these plasmas at 2.65T. However, the use of the EL for core heating is limited to a reduced range of poloidal steering angles, as discussed in Sec.5. Moreover, the L-H transition phase needs to be controlled to avoid a back transition to L-mode during the 3 seconds time window where the polarization of the EL is changed from X-mode to O-mode. Since the power threshold for transition to H-mode is so low in deuterium and DT plasmas, one might want to use the top mirror from the Equatorial Launcher to heat inside $\rho = 0.25$ and the USM with the largest poloidal steering angle to provide heating inside mid-radius, while at the same time track the $q = 2$ surface with the LSM and 6.67MW until both the neutral beams have been turned on and the plasma has entered into a stable H-mode phase. The USM can then be steered to the $q = 2$ surface for additional broadening or the power can be made available to the LSM when needed. This way, while the polarization of the EL is changed from X-mode to O-mode, heating is provided by the USM which can operate with X-mode polarization during the entire plasma discharge. These scenarios should be assessed and a suitable path for demonstration of access and sustainment of H-mode should be provided that minimizes the fatigue of the EC system.

6.2 Feasibility of sawtooth period pacing

Figure 6.4 shows the sawtooth period, averaged in the flattop between 50s and 350s, for the reference DT plasma simulation (black) and for the cases shown in Fig.6.3. No EC power is used in the flattop phase to isolate the effect of the beam source energy from the effect of localized EC current drive.

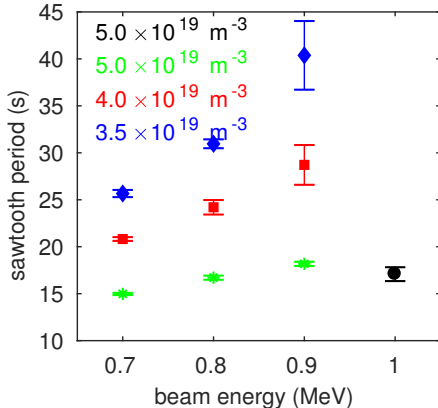


Figure 6.4: average sawtooth period in the flattop phase for plasma simulations in DT for the reference plasma (black) and for three values of density and three values of energy beam source.

For a given density, the sawtooth period increases with increasing beam energy, because of the increasing stabilizing contribution from the fast ions. For given beam source energy, the period increases with decreasing density because of the indirect effect of having more efficient heating. Although the radial position of the $q = 1$ surface in these plasmas at half-field is slightly outward compared to full field plasmas, the UL still cannot be moved inside the $q = 1$ or close enough while maintaining current density large enough to modify the sawtooth period. Simulations that attempted sawtooth period pacing using the UL have failed and are not discussed here.

Figure 6.5 shows simulations at 2.85 T and 8.1MA, with density of $4.0 \times 10^{19} m^{-3}$ and $4.0 \times 10^{19} m^{-3}$ respectively and with neutral beam sources between 0.8 MeV and 1.0 MeV. For each value of density and for each beam energy source, the requested pacing period τ_{req} has been varied between 25s and 60s. The EC controller is pre-programmed to steer both the EL-bot and the EL-mid inside the $q = 1$ surface at about $\rho = \rho(q = 1) - 0.05$ five

seconds after the triggering of each sawtooth. The EL mirror is maintained inside the $q = 1$ surface until the sawtooth period exceed τ_{req} , then the power is removed. If a sawtooth crash happens before the requested pacing period τ_{req} , the EC power is promptly removed from inside the $q = 1$ surface. It is assumed that each time the power is removed from the $q = 1$ surface it is re-directed to the UL for NTM control. This is mimicking a combined sawtooth-NTM control, although this approach might not be applicable in ITER because fast ion effects would still dominate the effect of the ECCD on the modification of the local magnetic shear and because NTMs might appear spontaneously.

We note two interesting features. First, the EC current drive is sufficiently large to modify the bulk current plasma profile, so that at lower density and with full beam energy the sawtooth period can be lengthened up to over 60 seconds. Second, in all cases the EL can modify locally the magnetic shear and induce a partial reconnection, as indicated by the smaller amplitude crashes, but not large enough to trigger a major crash. The fast ion stabilization is still large enough to stabilize the internal kink and the major crash is thus caused by the internal kink instability. Similarly to the case of the ELMy H-mode plasma, also at half-field sawtooth pacing with EC might not be possible because the stabilizing effects from fast ions dominates. However, at half-field the EC is more effective in modifying the sawtooth period and can be used as an actuator to achieve a very long sawtooth period. Although a sudden crash cannot be triggered by the prompt removal of the EC power from inside the $q = 1$ surface, assuming that there is a delay of at least five seconds before the crash occurs provides enough time to re-direct the power to the $q = 1.5$ or the $q = 2$ surface. It is noteworthy that the (3,2) and the (2,1) islands are observed to be mutually exclusive

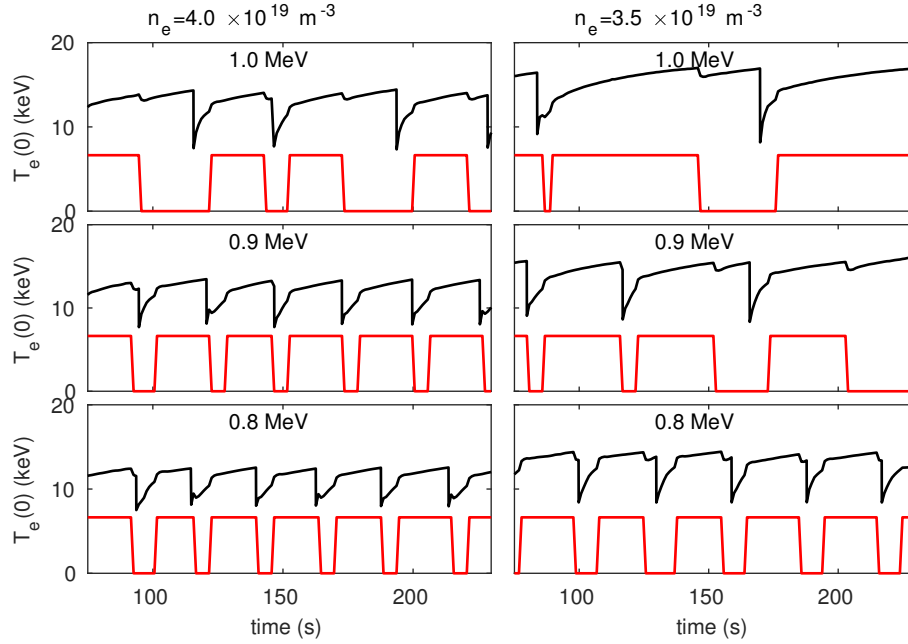


Figure 6.5: Simulations of sawtooth pacing with the EL in deuterium plasmas, for two values of the electron density and for three values of the beam energy source.

in experiments, for example on DIII-D, where it is observed that - as soon as the (2,1)-NTM is suppressed - the (3,2) appears. If one assumes that this is a standard situation that might occur on ITER as a way for the plasma to conserve free energy, then these examples provide good case for testing pre-emptive control with constant tracking of the $q = 2$ resonant surface and - at the same time - combined sawtooth period pacing and control of both the (3,2) and the (2,1)-NTMs. All these combinations should be further analyzed with MHD codes that can model interactions between the internal kink and the NTM as well as interactions between magnetic islands.

7 H&CD power management in helium plasmas

Operation at half-field with helium and hydrogen plasmas has common problems related to shine-through of the hydrogen source beams. Table 7.1 shows the minimum admissible line averaged density to inject sources of given energy and power, respectively in pure helium and hydrogen plasmas (table on the left) and how this density changes for a given fraction of hydrogen over helium (table on the right) [55].

Fueling in helium plasmas will be provided by helium gas injection and by hydrogen pellets. Experiments on C-Mod show that the power threshold for H-mode transition in pure helium plasmas is close to that of deuterium plasmas, while experiments on ASDEX-U indicate a favorable power threshold [56]. Based on these results and on previous, recent modeling activity of the ITER non-active phase [4, 57], it is assumed a reduction of 0.7 over the power threshold predicted by the ITPA scaling for plasmas in Helium with a small fraction of Hydrogen.

It has been demonstrated in time-dependent simulations with self-consistent core-edge transport modeling within the JINTRAC suite of codes that there is an upper limit to the line-averaged electron density that can be achieved with helium gas puffing alone, which is around $2.7 \times 10^{19} \text{ m}^{-3}$ [57]. With reference to table 7.1, at this density the maximum beam source energy would be limited to 800 keV. For safe operation, it is advised that the energy be maintained lower, because of variations in time of the target line-averaged density, of the profile peaking, of effectiveness in pellet fueling and variation in the plasma composition are taken into account.

In order to achieve the density admissible for use of full energy neutral beam sources, injection of hydrogen pellets will be needed to raise the electron density. To ensure sustainment of good quality H-mode, the dilution from hydrogen pellets in helium plasmas should not exceed 20% of the helium density. On the other hand, to ensure good hydrogen minority heating and avoid mode conversion the fraction of hydrogen should be higher than 1%, but not exceed 8%. Thus, hydrogen minority heating would be possible only in helium plasmas with densities up to 45% of the Greenwald density, which is a stronger constraint on the operational space if IC waves have to be used with hydrogen minority heating. If the goal is to sustain H-mode it probably does not matter whether the IC waves have good or poor first pass absorption, provided losses in the Scrape-Off layer are low and

P_{NB} (MW)	E_{NB} (keV)	He	H	f_H	n_e [10^{19} m^{-3}]	Z_{eff}
		n_e [10^{19} m^{-3}]	n_e [10^{19} m^{-3}]			
16.5	870	3	4.3	0	2.9	2
13.4	800	2.5	3.75	0.2	3.1	1.8
11.4	750	2.3	3.4	0.4	3.3	1.6
9.6	700	2	3.1	0.6	3.6	1.4
8.0	650	1.7	2.75	0.8	3.9	1.2
6.5	600	1.5	2.35	1	4.3	1
5.2	550	1.25	2			
4.1	500	1	1.6			

Table 7.1: Left: admissible density for injection of hydrogen beams in pure helium and hydrogen plasmas. Right: admissible density for injection of full energy hydrogen beams as a function of the fraction of hydrogen to helium.

the heating profiles are peaked inside mid-radius. Only advanced simulations with full wave IC codes, coupled to finite-element models of the ITER antenna and a realistic model for the SOL can answer the question of the coupling of IC waves in ITER plasmas, an approach that is currently being undertaken by the RF community in the US.

The simulations described in this section compare different background plasmas and IC heating schemes as follows:

- Helium plasma, with up to 8% dilution from hydrogen, with dominant hydrogen minority heating. These plasmas have typically lower density because have to rely mostly on gas puffing and use therefore neutral beams sources with reduced energy.
- A mix of 80% helium and 20% hydrogen at higher density and with full energy beam sources, with IC heating on thermal ions at frequency of 42MHz and ^3He minority heating at frequency of 53MHz.

It will be shown that changing the neutral beam source and operating at low density has a strong impact on the sawtooth period. Since these non-activated plasmas are predicted to be otherwise stable against NTMs, having the capability of modifying the sawtooth period over a wide range of values is a critical knob for the demonstration of NTM control with the EL system during PFPO-2.

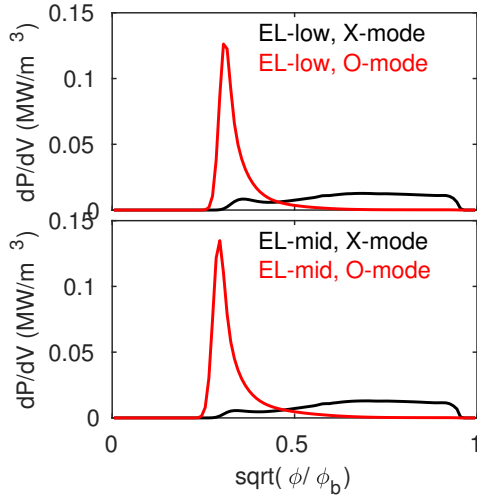


Figure 7.1: power density profiles in the flattop phase, calculated at 290s, for X and O polarization.

background electron temperature profiles. Since the Neutral Beam and the Ion Cyclotron heating is highly localized inside $\rho = 0.4$, changing the beam source energy also has no effect in modifying the temperature in the outer mid-radius to reduce the parasitic absorption. In order to gain the full accessibility of the Equatorial Launcher over the radial region, the magnetic field should be increased to 2.75T.

Figure 7.2 shows two TRANSP simulations for a helium plasma, with 8% hydrogen dilution and 10 MW of IC in the current flattop phase. The beam sources have 650 kV acceleration in one case (16MW delivered power) and 800 kV acceleration in the other case (26.8 MW delivered power).

The polarization of the UL is maintained in X-mode during the entire duration of the discharge, while the polarization of the EL is changed from X to O-mode after the L-H transition to avoid parasitic absorption on the third harmonics.

In the example shown in the figure all the mirrors except the USM are depositing between $\rho = 0.35$ and $\rho = 0.5$, which causes the large peak in the total current off-axis and a hollow current profile. This can be avoided by distributing the EC current over the minor radius, an optimization that is not done here where the focus is on trends in the global characteristics of the discharge for variation of the beam source energy and of the plasma density. Similarly to the analysis done in DT and deuterium plasmas, increasing the beam energy at constant electron density lengthens the sawtooth period. With the same EC and IC settings and the same electron density, increasing the beam energy from 650keV to 800 keV can lengthen the sawtooth period at the point that there is only one single sawtooth cycle in the flattop, as shown in Fig.7.2. These simulations need to be verified and to be repeated with all transport channels active, including impurity transport and self-consistent evolution of the background plasma density with gas puffing and with pellet injection. Regardless, they suggest that there might be some flexibility in the choice of how to use the external actuators to manipulate the sawtooth cycle by controlling the current profile evolution with appropriate use of off-axis current drive. Distribution of the current from the EL over the minor radius is another knob that can be used together with the beam source energy to manipulate the sawtooth period by acting on the total plasma current profile. In these plasmas where the NTMs would be otherwise stable, this approach to enforce the triggering of an NTM is required for the commissioning of the NTM control system.

The integrated power that shines thru the plasma - as calculated in TRANSP/NUBEAM with the present focal length - is 2.7MW in the flattop phase, *i.e.* about 13% of the injected power, with beam sources of 800 keV and it drops down to about 7% by reducing the beam source acceleration to 650keV, while still providing enough power to access and sustain good quality H-mode and reserving

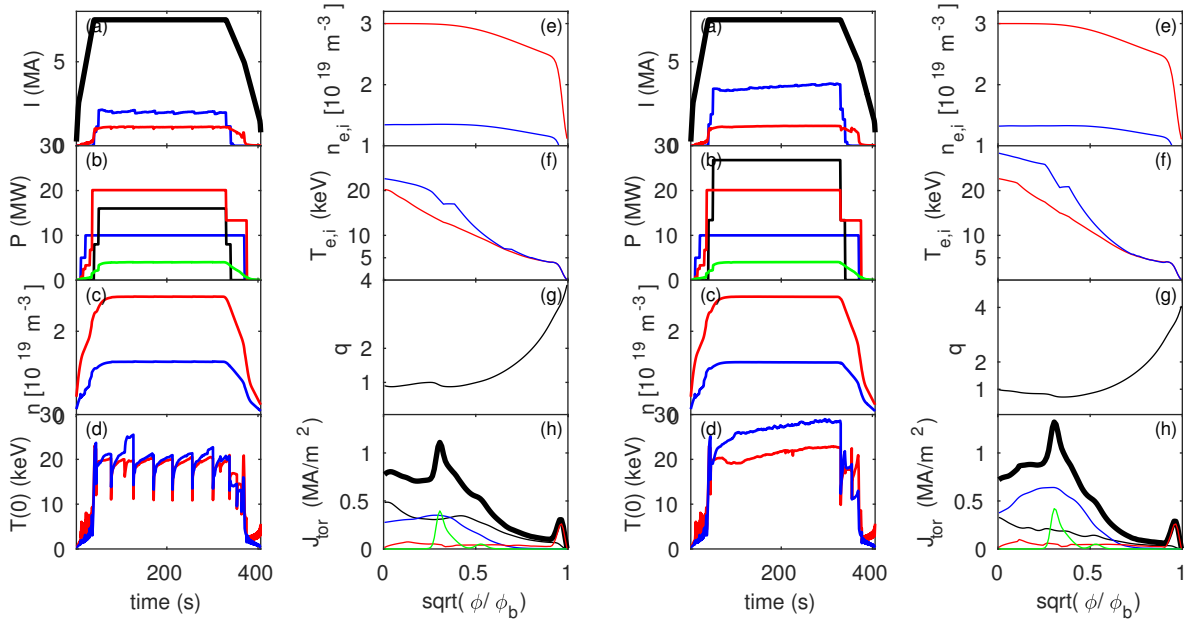


Figure 7.2: Simulation of a helium plasma, with 8% dilution from hydrogen pellets for 600 keV beam sources (left panel) and for 800 keV sources (right panel). Profiles are calculated at 290s.

P_{NB}	Ar, Ne	P_{sh}	P_{rad}	Z_{eff}
26.8000		3.4772	3.9515	2.0318
26.8000	Ar, 1.0×10^{-3}	2.2896	4.6789	2.3168
26.8000	Ar, 5.0×10^{-3}	0.7189	7.5237	3.4699
26.8000	Ne, 5.0×10^{-3}	3.2754	4.0720	2.1116
19.2000		1.9335	3.9466	2.0424
19.2000	Ar, 1.0×10^{-3}	1.2323	4.6758	2.3281
19.2000	Ne, 5.0×10^{-3}	1.8054	4.0646	2.1207
16.0000		1.1956	3.9497	2.0454
16.0000	Ar, 1.0×10^{-3}	0.7407	4.6724	2.3310

Table 7.2: Shine-thru power for three values of the NBI source energy, under different assumptions on the impurity seeding. The electron density is $2.8 \times 10^{19} \text{m}^{-3}$.

at the same time EC and IC power for emergency replacement in case one of the beams fail. Impurity seeding, with argon or neon, provides another way of reducing the shine-through power. With reference to Table 7.2 the shine-through power is reduced by about 17% with Argon injection up to a fraction of 10^{-3} of the electron density and reduced of 80% from its value with injection up to 5×10^{-3} of the electron density, with an increase of Z_{eff} from 2 to about 3.5. Neon injection is not as effective as argon injection. With a lower effect on the purity of the plasma and on the total radiated power, the reduction of the shine through power is only marginal for an equivalent density fraction. It should be noted that the radiation is dominated by tungsten line radiation, thus little variation is observed in the total radiated power when the fraction of impurities with intermediate atomic number is increased. However, since impurity transport is not calculated self-consistently in these simulations, but the impurity density profiles are rescaled from the electron density profiles the calculated radiation power is affected by large uncertainties.

7.1 IC heating schemes in Helium plasmas

The heating scheme envisaged for operation at half-field in helium plasmas is hydrogen minority. However, in order for this to be effective, the fraction of hydrogen should not exceed about 10%. Figure 7.3 compares the IC heating in simulations that use the same EC and NBI configuration. The simulations differ in the toroidal mode number, which is $n_\phi = 19$ in one case and $n_\phi = 27$ in the other case. The equivalent parallel wavenumber calculated by TORIC is $k_{||} = 3.00 \text{m}^{-1}$ in one case and $k_{||} = 4.5 \text{m}^{-1}$ in the other case; these correspond respectively to Case 2 and 3 in the paper by Messiaen [40]. The case with the lower n_ϕ provides the best absorption on the hydrogen minority. The total heating on electrons and ions is comparable, since the lower direct heating on the electrons in the case with $n_\phi = 19$ is compensated by a larger heating from the minority species. The figure also shows the heating on electrons and ions from the hydrogen neutral beams. While the total heating is the same, the heating profiles are different in the core because of the contribution of the IC on the electron and ion temperature profiles.

Commissioning of full energy beam sources in safe conditions must be done at higher densities, which can be achieved by increasing the fueling from hydrogen pellets. Figure 7.4 compares simulations with a background ion composition of 80% helium and 20% hydrogen and electron density (prescribed) of $4.5 \times 10^{19} \text{m}^{-3}$. The EC and NBI settings are the same, namely 870keV

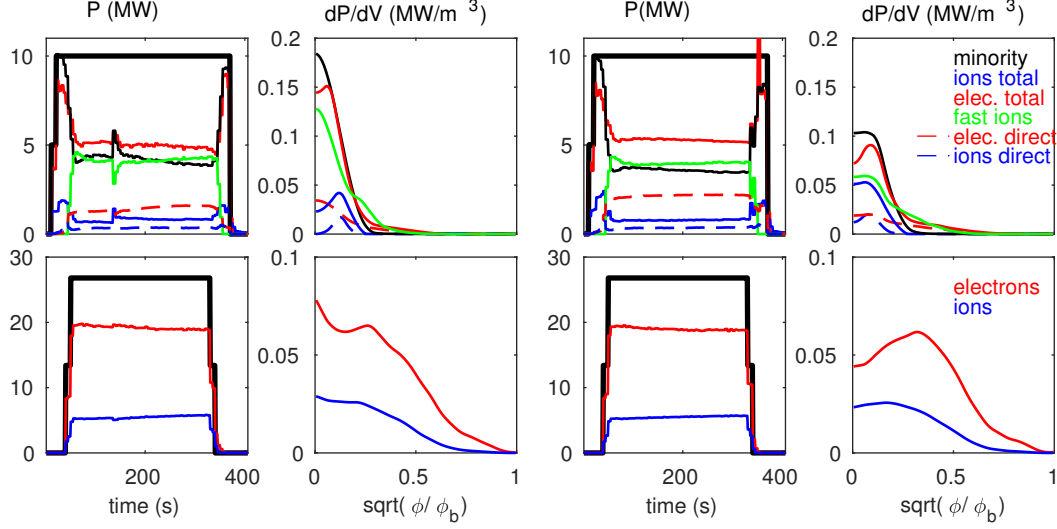


Figure 7.3: (a) time traces of the heating contribution from the IC waves for 10MW of injected power in the flattop. Dashed lines indicate direct absorption on the ions (blue) and on the electrons (red), solid lines indicate total heating on ions (blue) on the electrons (red), on the hydrogen minority (black) and on the beam fast ions (green). (b) neutral beam power absorption on electrons (red) and on ions (blue). (c) Profiles of the IC heating contribution, calculated at 290s. (d) neutral beam heating profiles.

hydrogen beam sources and all EC mirrors steering inside mid-radius, while different hypotheses are made for the IC heating scheme. The first simulation is assuming $n_\phi = 19$, $f_{IC} = 53\text{MHz}$ and 1% ^3He minority, the second is using the same toroidal mode number, but no minority heating and $f_{IC} = 42\text{MHz}$, so the dominant heating is on thermal ions; the third simulation is also assuming dominant absorption on the thermal ions, but is using a phasing suitable for both heating and current drive, with $n_\phi = 24$. The minority absorption is very effective and accounts for about 90% of the total absorbed power, which goes predominantly to the electrons. The two simulations with lower IC frequency and no minority heating do maximize the heating on the thermal ions, they also have a large fraction of the power absorbed by the beam fast ions, which accounts up to 50% of the total power in the configuration with no current drive. In all cases the damping of the IC waves is very good, as indicated by the fast decrease of the real component of the electric field.

There is no single optimal configuration for the use of the IC heating, as there is no single optimal configuration for the use of the EC or the Neutral Beams. Ion Cyclotron wave coupling and absorption depend on the background plasma parameters and on the density and temperature in the Scrape-Off-Layer plasma in addition to the chosen phasing of the antenna. Calculations of IC heating with full wave codes are usually done on time slice and - in most cases - on given analytic profiles in the core plasma and in the SOL and this includes computational extensive calculations with realistic models of the ITER antenna. The spectra that result from these calculations and the calculated coupling efficiency are valid only within the limits of the input parameters that have been used, while plasmas are nonlinear systems that evolve in time in response to external actuators and internal dynamics. IC calculations for ITER have historically been performed in TORIC with a toroidal number of $n_\phi = 27$ because this was recommended as the optimal configuration for heating based on standalone calculations. The simulations discussed here and in the previous Sec.4 indicate that this is not the case, but that the choice of the phasing needs to be selected case by case depending on the target plasma and on the applications. It has been shown that a toroidal

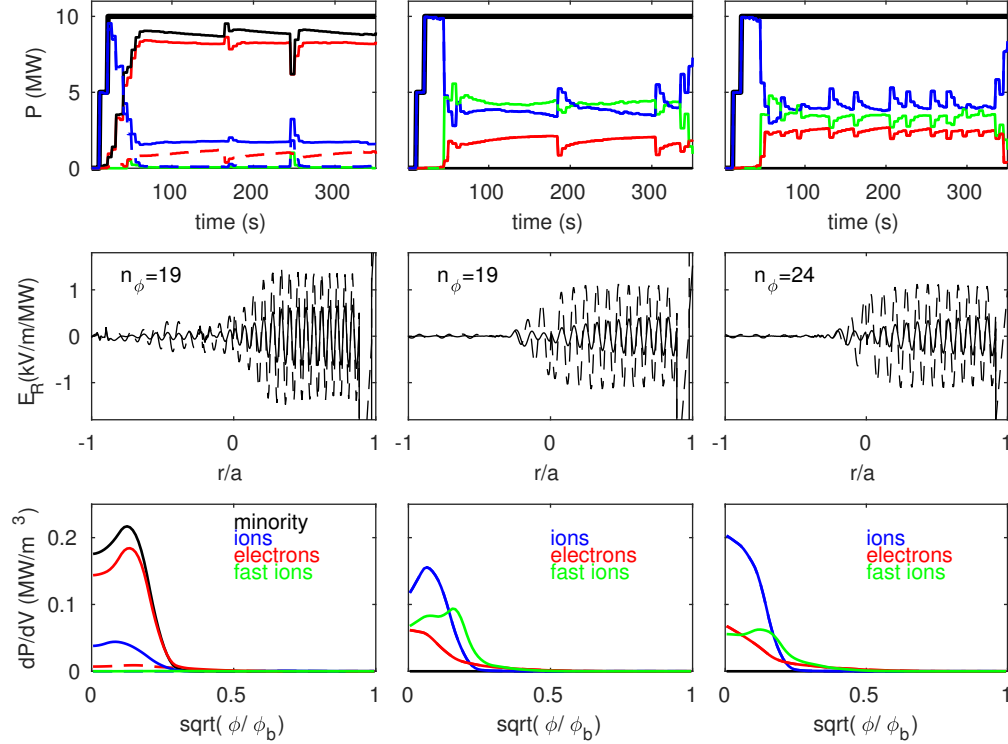


Figure 7.4: (a) time traces of the heating contribution from the IC waves for 10MW of injected power in the flattop. Dashed lines indicate direct absorption on the ions (blue) and on the electrons (red), solid lines indicate total heating on ions (blue) on the electrons (red), on the hydrogen minority (black) and on the beam fast ions (green). (b) neutral beam power absorption on electrons (red) and on ions (blue). (c) Profiles of the IC heating contribution, calculated at 290s. (d) neutral beam heating profiles.

mode number of $n_\phi = 19$ provides the best ion heating in the ELMy H-mode plasma, but also the best minority heating scheme in the helium plasma at half-field. The choice of n_ϕ and thus of the phasing of the antenna is not a universal solution that can be defined from standalone calculations, but requires a time-dependent analysis that evolves the plasma with the other H&CD sources and with the background plasma to find an optimal solution for the various phases of the discharge. The work undertaken here is by far not conclusive for the use of the H&CD in the ITER plasmas, but open interesting avenues for further investigation and for optimization of the use of the IC heating and current drive in synergy with the other systems.

7.2 NTM control in helium plasmas

NTMs are predicted to be stable in the helium plasmas simulated herein, calling for strategies for destabilization from external seeding, for example inducing a sawtooth crash or lengthening the sawtooth period. As discussed in the previous section, for a given configuration of the IC and EC system, the sawtooth period in helium plasma can be lengthen from about 50s to 200 s and longer only by increasing the neutral beam energy from 650 keV to 800 keV operating at a density of $0.45n_G$. The IC frequency and phasing provides an additional way of modifying the total current density profile, as shown in Fig.7.4, where the simulations that uses a phasing for current drive results in the shortest sawtooth period.

Note that the discussion here on the use of IC on sawtooth destabilization ignores approaches used on present-day experiments and based on IC fast ion effects, because these are not properly accounted for in the Porcelli model used for the triggering conditions. Approaches to sawtooth destabilization with IC rely on tuning the frequency to ensure absorption as close as possible to the $q = 1$ surface, which might be incompatible with the need for core heating for impurity accumulation control. Similarly, the discussion ignores also common approaches to sawtooth pacing based on EC destabilization by modification of the local shear, because our simulations indicate that this does not provide a sufficient criterion to trigger a crash. These cases might be analyzed in the future, as part of joint ITPA-IOS modeling activities, as the necessary modeling tools become available.

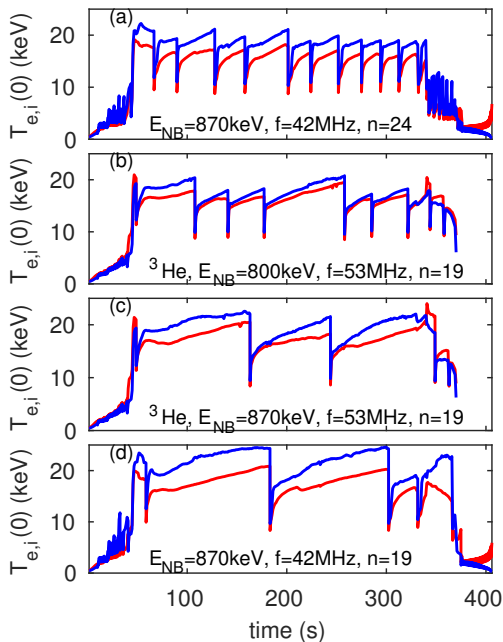


Figure 7.5: Central value of the electron (red) and ion (blue) temperature in a helium plasma with up to 20% dilution from hydrogen pellets and for two different values of the hydrogen beam energy source.

Figure 7.5 compare the evolution of the central electron and ion temperature in simulations of a Helium plasma with 20% dilution from hydrogen pellets for two values of energy of the neutral beam source, and for different values of IC frequency and of the toroidal mode number n_ϕ . The plots are ordered from top to bottom according to the simulated sawtooth cycle, from the shortest to the longest period. The final, simulated, plasma discharge is the result of how the plasma parameters evolve nonlinearly under the action of the H&CD sources and additional simulations, including comparison of turbulence transport models, should be undertaken before any firm conclusion is made on the best configuration for the EC or for the IC. These two systems provide fine-tuning of the current and temperature profiles on the top of the neutral beams and - at the same time - affect details of the beam deposition profile and of the fast ion distribution function.

The simulations discussed herein are using the EL over a reduced range of poloidal steering angles to avoid loss of absorption in O-mode (see Fig.5.2), which is the main cause for the large off-axis current that is observed in Fig.7.2. While this might be a way of tailoring a reverse shear in the core and lengthening the sawtooth period for purposes of commissioning of the NTM control, it limits the radial accessibility

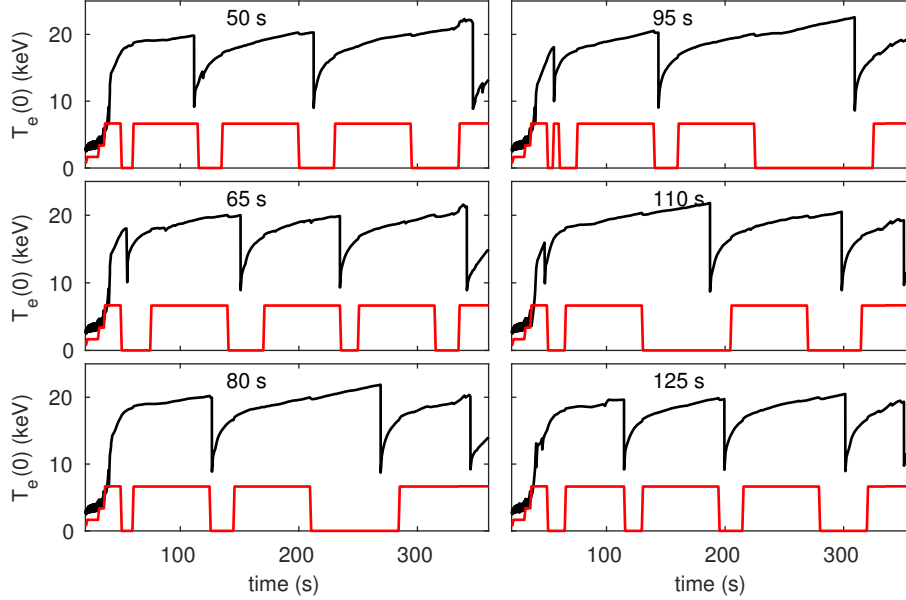


Figure 7.6: Time evolution of the central electron temperature when both the EL-bot and EL-mid are steered inside the $q = 1$ resonant surface, for requested pacing period between 50 seconds and 125 seconds.

of the EL for current profile tailoring. Core impurity accumulation should not be a problem because the IC system can be used in these plasmas with good absorption in the core, but other applications (like avoiding the peak in the current at mid-radius) would not be possible.

Increasing the magnetic field to 2.75T would avoid parasitic absorption of the EC waves at the third harmonics and allow the use of the EC system with full radial accessibility. However, similarly to the plasmas in deuterium and a mix of deuterium and tritium, also in helium plasmas simulations indicate that steering the EL inside the $q = 1$ surface can lengthen the sawtooth period, although the results are not clear. Also, switching off the EL does not modify the local magnetic shear sufficiently to overcome the stabilizing effect of the fast ions. Figure 7.6 shows simulations where both the co-current mirrors are steered inside the $q = 1$ surface and the requested pacing period increases from 50s to 125s. The EL is power is turned-on in the simulation about 15 seconds after the previous sawtooth crash under the assumption that - should an NTM be triggered by a crash - at least 15 seconds are needed for its stabilization and therefore the power would be allocated on the UL during this time window. If a sawtooth crash occurs before the requested time, then the EC power is promptly turned-off, since it is expected that an NTM is triggered and the power must be and re-directed on the resonant surfaces $q = 1.5$ and $q = 2.0$. Otherwise the EC power is maintained inside the $q = 1$ until the delay from the previous crash equals the desired pacing period. As shown in the figure, this exercise results in a sawtooth period that is not regular and there is no clear correlation between the requested pacing period and the actual period. The time trace of the central electron temperature is a combination of cycles spanning from 50 to 150 seconds, if the first crash at entry to H-mode and the last crash at the end of the flattop are not considered. Further analysis by changing the radial position with respect to the $q = 1$ surface has also resulted in unclear results. Although these simulations are probably not conclusive, they suggest that there is no evidence that sawtooth pacing is effective.

7.3 Commissioning of the EC system

The commissioning of the EC system will be done at 2.65T, in a pure helium plasma and in L-mode to take advantage of the large difference between O-mode and X-mode absorption. An L-mode plasma has been simulated assuming a prescribed electron density profile, with line averaged value of $2.25 \times 10^{19} \text{m}^{-3}$, 100% helium, 2% berillium and 10^{-5} fraction of tungsten.

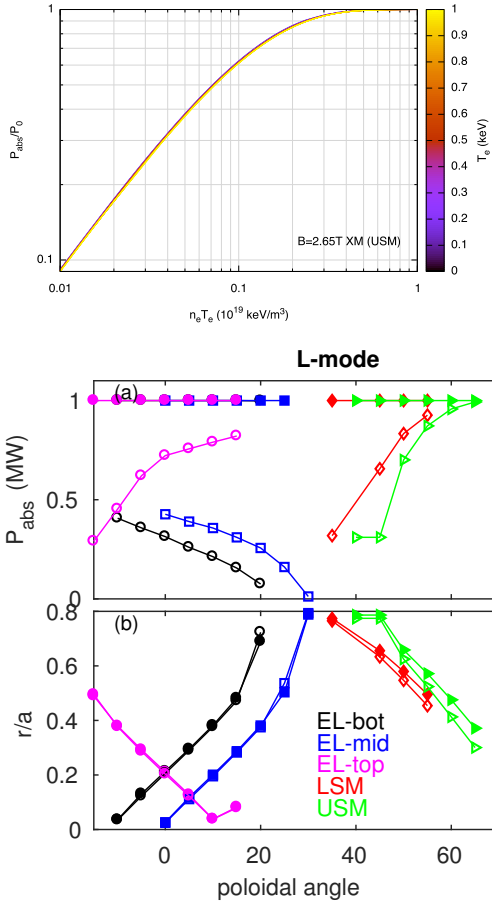


Figure 7.7: Left: absorbed power as a function of the plasma pressure for $B_T = 2.65\text{T}$. The color code indicates the expected fluctuation in the local temperature (courtesy of L. Figini, IFP Milano). Right: fraction of absorbed power and deposition location in a L-mode plasma at 2.65T simulated with TRANSP, for X-mode (solid) and O-mode (open) polarization.

necessary to detect temperature fluctuations in this plasma where it is expected that turbulence will contribute significantly to the fluctuations at these radii and the signal to noise ratio of the ECE diagnostics will therefore be reduced.

Figure 7.7(top) shows the fraction of absorbed power as a function of the plasma pressure and, in color scale, the expected local variation of the temperature (figure provided by Lorenzo Figini, Istituto di Fisica del Plasma, CNR Milano). The curve has been obtained with X-mode polarization at a magnetic field of 2.65T. The sensitivity of the ECE diagnostic on ITER is of the order of $\delta T/T \simeq 10^{-3}$ for a sampling rate of 500 Hz and it scales with the square root of the sampling rate, thus a frequency of 2 kHz would provide a sensitivity of $\delta T/T \simeq 2 \times 10^{-3}$. Figure 7.7(bottom) shows the results from a scan of the poloidal angle during the flattop phase for the two co-current mirrors from the Equatorial Launcher and for the Upper Launcher. Solid symbols indicate X-mode polarization, open symbols indicate O-mode polarization. For all mirrors there is a large difference between the absorption in X-mode and O-mode. In order to detect sufficient emission from the ECE diagnostic the power deposition profile should be localized, a condition that is satisfied by the Upper Launcher. As shown in the figure, the smallest poloidal angles, which correspond to outer radial deposition and narrower power and current density profiles, also have the largest differences in the absorbed power. Based on the local values of the density and temperature profile, deposition inside $\rho = 0.85$ satisfies the condition $n_e T_e \geq 1.0$, thus a poloidal angle of 35-40 degrees for the LSM and of 40-45 degrees for the USM does provide the maximum difference between the two polarizations. Based on the data provided by Figini, the local variation of the temperature should be sufficient to be detected by the ECE diagnostic even assuming a signal to noise ratio degraded by 10%. These qualitative conclusions should be verified by ray-tracing codes coupled to Fokker Planck solvers for assessment of the minimum number of gyrotrons

8 H&CD power management in hydrogen plasmas

Operation in hydrogen plasma is foreseen for demonstration of access to H-mode and for commissioning - among the others - of the disruption mitigation scheme. The power threshold for access to H-mode is unfavorable in hydrogen plasmas, since it depends on the inverse of the hydrogenic mass species. At 2.65T and 7.5MA, the power threshold from the ITPA scaling [10] is 40MW for densities of $n_e \simeq 2.7 \times 10^{19} \text{m}^{-3}$ ($0.45n_G$), and increases up to 60 MW for densities of $n_e \simeq 4.7 \times 10^{19} \text{m}^{-3}$ ($0.75n_G$). The latter is close to the minimum density admissible for injection of full energy hydrogen beam sources. The maximum NBI power that can be used in this plasma, to stay below tabulated values of shine through power, is 13 MW at the lower density and full power at the higher density, although impurity seedings would be needed to reduce the shine-through on accounting of uncertainties in the time evolution of the density profile peaking and line-averaged value.

On account of radiation losses, and for the power inside the separatrix to be at least 25% above the H-mode power threshold, operation at $0.45n_G$ would need the full available power of 20MW of EC and 20MW of IC in addition to the NBI, under the assumption that less than 20% of the IC power is dissipated in the SOL. This would leave no reserved power to handle emergencies, such as one of the systems fails. Operation at higher density can benefit from the use of full energy beam sources, but it also has higher H-mode threshold power and it thus again all the available power would be required to sustain H-mode, leaving no reserved power for handling of system failures.

It has been observed that first pass absorption of IC waves is low in hydrogen plasmas and

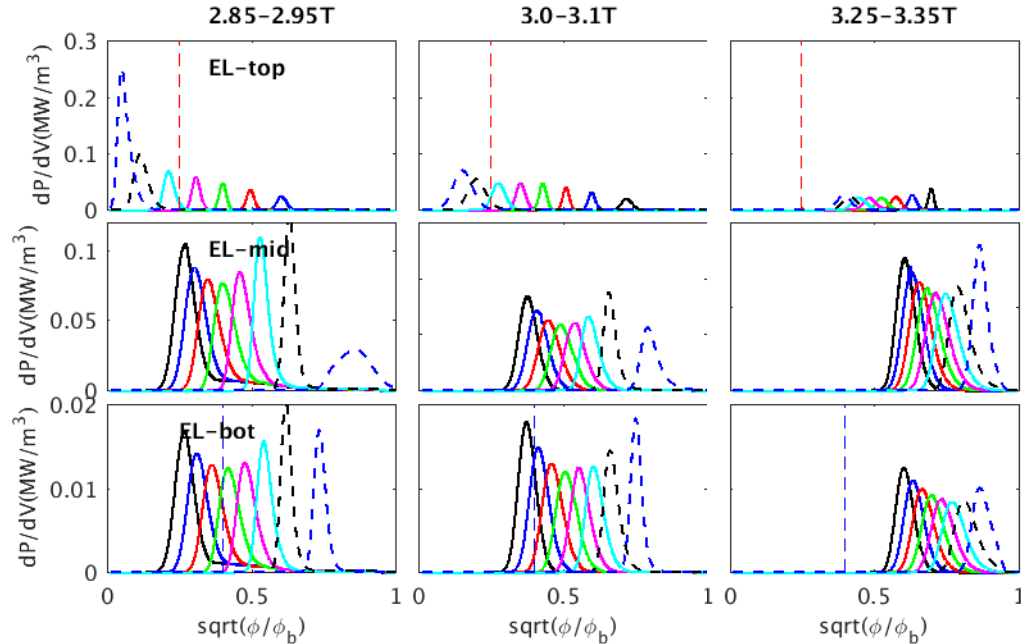


Figure 8.1: Power density profiles for the three EL mirrors, calculated in the flattop phase, for three values of the magnetic field and for a 100% hydrogen plasma. The dashed blue lines indicate the position of the $q = 1$ resonant surface, the dashed red lines limit the radial region inside $\rho = 0.25$.

no good heating scheme exists [4, 52, 53]. If the purpose is demonstration of access to H-mode, it probably does not matter whether the fraction of first pass is low, provided there is sufficient power inside the edge barrier to sustain the high confinement regime. The compatibility of the IC heating in this plasma with the SOL losses should be addressed to assess the coupling of the IC power to the plasma. It has been suggested that increasing the toroidal magnetic field up to 3.0-3.3 T and injecting a very small fraction of ^3He would significantly improve the first pass absorption of IC waves, operating at 40MHz [53]. By using a mix of hydrogen and helium with up to 10-15% fraction of helium would benefit from the three-ion scheme heating that has been recently proposed [58]. Unless the fraction of helium is increased significantly, the power threshold for access to H-mode is not going to change, thus increasing the magnetic field would not be favorable for the demonstration of access to H-mode. Moreover, operation at magnetic field around 3.0T and above would prevent the EC waves from being absorbed inside mid-radius, as discussed in Sec.5, and shown in Fig.8.1. If the EC system cannot be used, then the total usable power at 3.0-3.3T is even lower than the usable power at 2.65T, where multi-pass absorption of the IC waves might actually not be a real show-stopper.

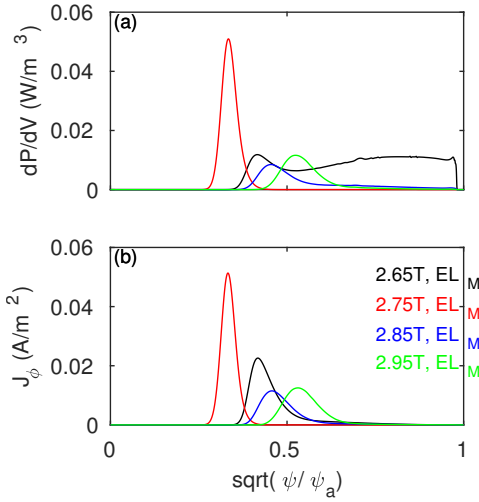


Figure 8.2: power (top) and current (bottom) density profiles for X-mode polarization.

The top mirror of the EL, which is injecting in the counter-current direction and that is foreseen for deep core heating can access inside $\rho = 0.25$ only for magnetic field lower than 3.0T. Because of the radial accessibility of the EC system, operation above 2.9T is not recommended. If the maximum magnetic field is limited by the accessibility of EC waves inside mid-radius, the minimum magnetic field is instead limited by the presence of parasitic absorption on the third harmonics, as already discussed in the previous sections, and hydrogen plasmas are no exception. As shown in Fig.8.2, the risk of parasitic absorption on the third harmonics can be eliminated by increasing the magnetic field to 2.75T. For the same poloidal steering angle, this magnetic field provides the highest peak current density and the innermost deposition, while increasing the magnetic field further would move the absorption outward and decrease significantly the current density peak.

As shown in Fig.8.1, the innermost radial location that can be accessed by either the EL-bot or the EL-mid is about 0.4 at magnetic field of 3.0-3.1T, but it increases to 0.7 for higher magnetic field values, with current drive efficiency being reduced by a factor ten. The location of the $q = 1$ surface in these plasmas is shown as a reference. The figures report a range instead of a fix value because the magnetic equilibrium that is calculated depends on the evolution of plasma parameters and pressure profiles, thus for a requested initial $B_0 R_0$ values, depending on the location of the magnetic axis, uncertainties of 0.1T should be included in the final, calculated magnetic field. The contribution of the beam fast ions to the magnetic equilibrium in particular contributes to the differences and to the shift of the magnetic axis and this is larger for densities below 65% of the Greenwald limit. Already at magnetic field around 3.0T, the EL cannot access inside the $q = 1$ resonant surface, reducing considerably the capabilities of the system.

8.1 IC heating in Hydrogen plasmas

Figure 8.3 compares the heating profiles from 20MW of IC in hydrogen plasmas for three different assumptions on the heating scheme: (a) 55MHz frequency and ^3He minority heating at a fraction of 1% of the electron density (b) 42MHz frequency and heating on hydrogen thermal with $n_\phi = 19$ (c) 42MHz and heating on hydrogen thermal with $n_\phi = 29$. Combinations of hydrogen and helium have not resulted in simulations with improved absorption or significantly different features and are not discussed herein. The radial component of the real part of the electric field indicates that the damping of the IC waves is not strong and suggests that waves might undergo a regime of multi-pass absorption. The simulation that assumes minority heating on ^3He at higher frequency has the stronger absorption in the core, with dominant heating on the electrons. The simulation with lower n_ϕ has comparable heating on the electrons and on the ions, with broad profiles and absorption off-axis where the impurities have a resonance. The wave absorption on the fast ions is peaked off-axis, but it is very low and does not represent a problem for fast-ion orbit losses, although this assessment should be confirmed with self-consistent calculations of RF and fast ion synergy in time dependent simulations.

Similarly to Helium plasmas, also in hydrogen plasmas NTMs are predicted to be stable when the growth rate is calculated using the reduced models described in Sec.2. Therefore, methods for lengthening the sawtooth period are needed in order to commission the control system. As discussed in the previous section, increasing the magnetic field to 2.75 and up to 2.85T, improves the accessibility of the Equatorial Launcher by allowing the use of X-mode polarization over the entire range of poloidal steering angles. However, because of the higher power threshold for access in H-mode in Hydrogen, there is less flexibility in changing the electron density and neutral beam source to modify the contribution of the fast ion stabilizing effect in the terms that set the triggering criteria for the sawtooth crash in the Porcelli model. A way of modifying

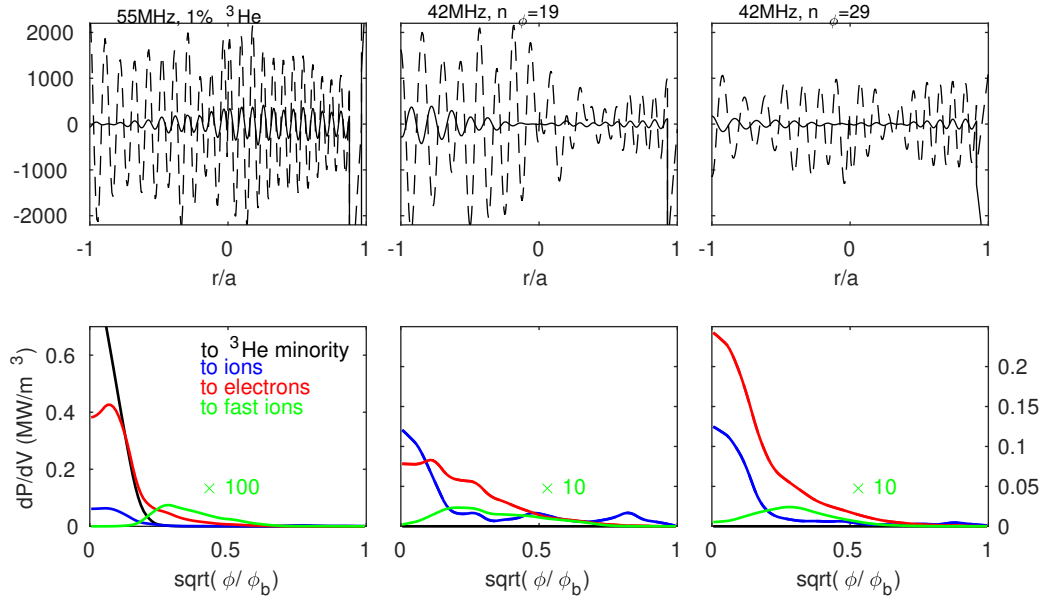


Figure 8.3: Top: radial component of the electric field for three different heating schemes. Bottom: heating profiles, calculated at 300s in the flattop phase. All cases have the same Neutral Beam and EC configuration and 20MW of injected IC power.

the sawtooth period in Hydrogen plasmas might exploit the effect of the heating profiles and current from the IC when the frequency and the toroidal mode number are changed. For a given configuration of the neutral beam, by modifying the electron and ion temperature profile with the IC waves, the EC heating and current drive efficiency would also be modified locally and the sawtooth cycle would therefore be modified by the total current profile. This is not how the IC has been initially envisioned to be used for sawtooth control, but it might provide an alternate method of achieving similar results while maintaining compatibility with the need for core heating.

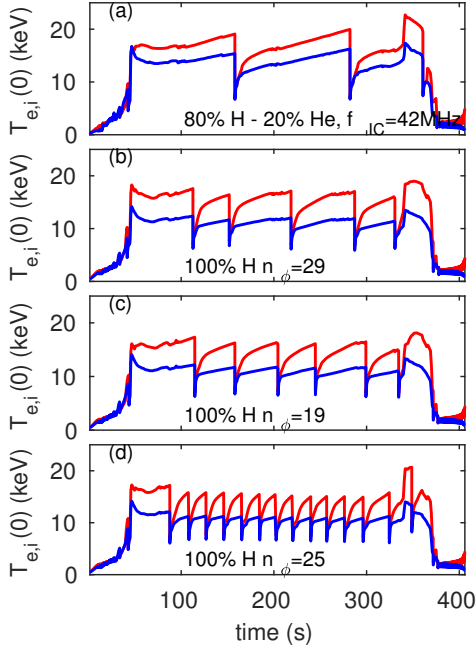


Figure 8.4: Evolution of the central temperature for different assumptions on the IC phasing.

Figure 8.4 shows the evolution of the central electron and ion temperature for four different assumptions on the IC heating scheme. All cases except one are assuming a pure hydrogen plasmas with 2% Berilium and up to 1.0×10^{-5} Tungsten, with additional injection of Argon to reduce the shine-through from the neutral beams. For the three cases with 100% hydrogen three values of the toroidal mode number are used, namely $n_\phi = 29$, which correspond to case 3 in table 3.3, $n_\phi = 19$, which corresponds to case 2 and $n_\phi = 25$, which corresponds to case 5 with both heating and current drive. In addition to these three cases, one case is assuming a mix of 80% hydrogen and 20% helium. This does not reduce the power threshold for access to H-mode, but reduces the density limits for shine-through, as reported in Table 7.1. From top to bottom, the case with a mix of helium and hydrogen has the longest period, then the period decreases when the antenna phasing is changed from heating-only configuration to heating and current drive. Although these results are not conclusive, they suggest that the options of combining the H&CD systems at half-field are numerous and that, at this lower current and density, the higher heating and

current drive efficiency of all systems should be exploited to design discharges that help in achieving the desired goals. As already noticed in the previous sections, there is no universal recipe as of how to use an individual system, but each discharge should be analyzed separately to optimize their synergy.

A plasma discharge with a very long sawtooth period - like the one shown in Fig.8.4(a) - would be suitable for the commissioning of the NTM control system. It would allow (a) testing the power switch between transmission lines from the EL to the UL in combination with real-time detection of the $n = 1$ magnetic perturbations (b) testing the accuracy of the alignment of the EC current peak with the $q = 1.5$ and of the $q = 2$ resonant surface, all by remaining within the maximum number of fatigue cycles of the system. It should be noted that the duration of the flattop phase could be reduced in order to fit a lower number of sawtooth cycles, as needed. Large sawtooth crashes like the one shown in the figure also causes a large shift of the $q = 1.5$ and $q = 2.0$ resonant surfaces, which would challenge the alignment. These are cases where a sweep across the resonant surface might be required.

9 Conclusions and Executive Summary

The principal aim of this task was to provide time-dependent analysis of the EC H&CD deposition profiles for the various plasma scenarios to assess the EC system primary functional aims, as listed in Table 1.1, then couple the results with the functional capabilities of the other H&CD systems for revising the global power management for the ITER scenarios. An EC system preliminary design review was performed in November 2012, wherein the review panel identified the need for additional EC H&CD analysis to ensure the EC system can achieve the desired objectives within reasonable delivered power limits. In addition, further analysis was required to assess the management of the injected power distributed over the various functions that may occur simultaneously in a plasma discharge.

The main conclusion of the research activity is that assessment of the Heating and Current Drive sources for ITER scenarios should be done case by case because details of the plasma evolution depend on how the external actuators are used together to tailor the current density profile, for given background plasma conditions like the electron density and the impurity content. There is no universal recipe as of how to use the individual systems, for example the phasing of the Ion Cyclotron antenna because the balance of electron vs ion heating has to be assessed taking into consideration how the IC heating is used in combination with the other systems and what the targets are.

An interface has been implemented in TRANSP to assess NTM control in ITER scenarios moving from the commissioning phase to the ELMy H-mode. Within the limits of the reduced models used herein, simulations indicate that there might not be sufficient time for the detection of the (2,1)-NTM, which grows fast and locks within seconds from this onset, typically at a width of about 8-10cm. Since the upper limit of the mechanical switch between transmission lines is 3 seconds, which is comparable to the time required for a full poloidal sweep of the Upper Launcher, approaches to control based on an active search for the magnetic island would be detrimental on ITER. A safer approach would require tracking the $q = 2$ resonant surface all time with a minimum amount of power and reserving power for handling of extraordinary cases, since the time required to turn-on a gyrotron is much lower than that needed to re-direct the power from another application. It is calculated that up to 5 MW should be used for pre-emptive control of the (2,1)-NTM in the flat-top and that up to two thirds of the total power should be invested for 20-50 seconds after the L-H transition and in the ramp-down phase before the H-L back transition. Similar conclusions hold for both operation at full field and for operation at half field in deuterium and in D-T plasmas.

While reserving the EC power for NTM control is excluding combined applications, it is found that in the ELMy H-mode plasma the capability of the EC system of tailoring the current profile is very limited. In particular, simulations indicate that the same approach to sawtooth pacing that is used on present-day experiments, based on the local modification of the magnetic shear, might not be effective in ITER where the stabilization of the fast ions dominates. Thus, at full field, sawtooth period pacing to control NTMs does not look like an attractive option. Also, it might be expected that NTMs in ITER are metastable and triggered spontaneously from either ELMs, tungsten impurity accumulation or magnetic turbulence fluctuations.

Approaches to sawtooth pacing through control of the global current profile and through fast ion effects look more promising than approaches based on modification of the magnetic shear. In

particular, at half-field, changing the neutral beam energy source, combined with operation at lower Greenwald fraction, can lengthen the sawtooth period by almost a factor three. Changing the IC frequency and phasing to use current drive and move the deposition from the core to 20% of the minor radius can modify the safety factor profile to design plasma discharges with very long sawteeth. While these simulations need to be verified and the models used validated against experiments, they indicate a wide flexibility in the use of the H&CD sources to engineering the plasma discharge. This approach still satisfy a need for deep core heating for control of impurity accumulation, with either one of the two IC antennas operated independently, or using the counter-current top mirror form the Equatorial launcher, the only one that can reach inside $\rho = 0.25$. Lengthening the sawtooth period is important to destabilize NTMs in those cases - like in helium and hydrogen plasmas - where NTMs would otherwise predicted to be stable.

Operation at half-field is limited by parasitic absorption on the third harmonics of the electron frequency resonance, which is Doppler-shifted inside the pedestal. Demonstration of access to H-mode and of NTM control is still possible at magnetic field of 2.65T, by changing the polarization of the Equatorial Launcher from X-mode to O-mode after the L-H transition. However, the range of poloidal angles that can be used is limited by the fast drop in the fraction of the absorbed power depending on the radial deposition. Also, it takes about three second for the polarization to be changed, thus it is important that the transition to H-mode is pre-programmed in feedforward to avoid back transition to L-mode, for example by selecting the energy source and carefully tuning the timing of the Neutral Beams with the density rise to avoid ahine-thru during this transient phase. Increasing the magnetic field to 2.75T would avoid the problem of parasitic absorption without compromising the capability of access to H-mode.

Operation above 2.85T is not recommended. While the ITER research plan is seeking to use a window between 2.65T-3.3T, increasing the magnetic field above a nominal value of 2.85T (this value accounts for variations of the magnetic axis due to fast ion pressure) would reduce the accessibility of the Equatorial Launcher in the core, in particular the top mirror, which is the innermost accessible.

Based on the simulations preformed and discussed herein, the following alternate path to operation at full field is proposed. While this approach is not entirely inline with the ITER plan of operating plasmas with full neutral beam sources at all values of magnetic field, it provides a step-wise procedure for the commissioning of the control. It is noted that operation at 1.8T is not included in the list below because this was not part of the contract.

1. commissioning of the EC system in helium plasmas, L-mode at half-field for O-mode and X-mode polarization check.
2. instead of following a track path to the ELMy H-mode plasma at constant q_{95} , it might be advisable to operate at constant magnetic field and change the current from low to high. This would gradually decrease the non-inductive fraction and q_{min} from above 2 down to unity and allow the study of Alfvénic stability, commission the NTM control separating a situation where NTM would be triggered spontaneously from one where NTM could be triggered by sawtooth. This approach would allow to test separately the tracking of the resonant surfaces for pre-emptive control and the poloidal steering and the switching between transmission lines.
3. Although ITER is targeting operation with full beam energy sources, it might be helpful to take advantage of operation at lower density to test shared actuator control applications, for tailoring of the current profile and the total beta, for optimization of the plasma stability, including Alfvénic instabilities in high q_{min} discharges with reversed magnetic shear.

4. Operation at intermediate values of the magnetic field looks not necessary. The window of operation around half-field is significantly reduced compared to the original plan and include one operating point at 2.65T-2.85T. The jump in magnetic field is large when moving to operation around full field and having two operating points close to each other does not look a sensible approach. It would be helpful to approach the 5.3T/15MA operational point as a scan in q_{95} from low current to high current. This would allow ITER to learn how to use the systems at full field, which might be particularly critical for NTM control, where complications would be added one at the time by moving from spontaneous NTMs that would be triggered in hybrid discharges to NTMs triggered by sawtooth crashes at lower q_{min} . The experience that JET will gain during DT operation as of how to optimize the access to hybrid and to the inductive H-mode will be valuable in this respect to validate the models and to prepare to ITER operation.

Bibliography

- [1] M.A. Henderson, G. Saibene, and G. Darbos. *Phys. Plasmas*, **22** 021808 (2015).
- [2] D. Farina, M.A. Henderson, L. Figini, and G. Saibene. *Phys. Plasmas*, **21** 061504 (2014).
- [3] D. Farina, M.A. Henderson, L. Figini, G. Ramponi, and G. Saibene. *Nucl. Fusion*, **52** 033005 (2012).
- [4] S.H. Kim, F.M. Poli, F. Koechl, E. Militello-Asp, A.R. Polevoi, R. Budny, T.A. Casper, A. Loarte, T.C. Luce, Y.-S. Na, M. Romanelli, M. Schneider, J.A. Snipes, P.C. de Vries, and The ITPA Topical Group on Integrated Operation Scenarios. *Nuclear Fusion*, **57** 086021 (2017).
- [5] Hawryluk R. An Empirical Approach To Tokamak Transport. In *Physics of Plasmas Close to Thermonuclear Conditions Proceedings of the Course Held in Varenna, Italy, 27 August-8 September 1979*, pages 19–46. Elsevier Ltd. (1981).
- [6] Waltz R.E. *et al. Phys. Plasmas*, **4** 2481 (1997).
- [7] Kinsey J.E. *et al. Fusion Sci. and Tech.*, **44** 763 (2003).
- [8] G. M. Staebler, J. E. Kinsey, and R. E. Waltz. *POP*, **12** 102508 (2005).
- [9] Tang WM. *Nucl. Fusion*, **26** 1605 (1986).
- [10] Martin YR *et al. Journal of Physics: Conf. Series*, **123** 012033 (2008).
- [11] Snyder P.B. *et al. Nucl. Fusion*, **51** 103016 (2011).
- [12] S.H. Kim, R.H. Bulmer, D.J. Campbell, T.A. Casper, L.L. LoDestro, W.H. Meyer, L.D. Pearlstein, and J.A. Snipes. *Nuclear Fusion*, **56** 126002 (2016).
- [13] Rutherford P.H. *Phys. Fluids*, **16** 1903 (1973).
- [14] W. Wehner and E. Schuster. *Nucl. Fusion*, **52** 074003 (2012).
- [15] Boyer M. *et al. Nucl. Fusion*, **55** 053033 (2015).
- [16] Boyer M. *et al. Nucl. Fusion*, **57** 066017 (2017).
- [17] Goumiri I. *et al. Nucl. Fusion*, **56** 036023 (2016).
- [18] Poli E. *et al. Nucl. Fusion*, **55** 013023 (2015).
- [19] N. Bertelli, D. De Lazzari, and E. Westerhof. *Nucl. Fusion*, **51** 103007 (2011).
- [20] Sauter O. *et al. PPCF*, **52** 025002 (2010).
- [21] Poli E *et al. Comput. Phys. Commun.*, **136** 90 (2001).
- [22] Poli E *et al.* 2017.
- [23] E. Fredrickson, M. Bell, R. V. Budny, and E. Synakowski. *POP*, **7** 4112 (2000).

- [24] Houlberg W A *et al. POP*, **4** 3230 (1997).
- [25] White R.B., Monticello D. A., Rosenbluth M.N., and Waddell B.V. *Phys. Fluids*, **20** 800 (1977).
- [26] de Blank H.J Westerhof E. and Pratt J. *Nucl. Fusion*, **56** 036016 (2016).
- [27] Chang Z. *et al. POP*, **5** 1076 (1998).
- [28] Fredrickson E.D, McGuire K.M., Goldston R.J., Bell M.G., Grek B., Johnson D.W., Morris A.W., Stauffer F.J., Taylor G., and Zarnstorff M.C. *Nucl. Fusion*, **27** 1897 (1987).
- [29] Fredrickson E.D. *Phys. of Plasmas*, **9** 548 (2002).
- [30] De Lazzari D. *et al. Nucl. Fusion*, **49** 075002 (2009).
- [31] Fitzpatrick. *POP*, **2** 825 (1995).
- [32] Wilson H. *et al. POP*, **3** 248 (1996).
- [33] Gorelenkov N. *et al. POP*, **3** 3379 (1996).
- [34] D. Farina. *Fusion Sci. Technol.*, **52** 154 (2007).
- [35] M.A. Henderson, R. Chavan, and R. Bertizolo *et al. Fusion Sci. Techn.*, **53** 139 (2008).
- [36] G. Ramponi, D. Farina, M.A. Henderson, E. Poli, G. Saibene, and H. Zohm. *Fusion Sci. Techn.*, **52** 193 (2007).
- [37] Zohm H. *et al. PPCF*, **49** B341 (2007).
- [38] Lin-Liu Y.R., Chan V.S., and Prater R. *POP*, **6** 3934 (2008).
- [39] RJ *et al* Goldston. *J. Comput. Phys.*, **43** 61 (1981).
- [40] A. Messiaen *et al. Nucl. Fusion*, **50** 025026 (2010).
- [41] T. Casper, Y. Gribov, A. Kavin, V. Lukash, R. Khayrutdinov, H. Fujieda, C. Kessel for the ITER Organization, and ITER Domestic Agencies. *Nucl. Fusion*, **54** 013005 (2014).
- [42] C.E. Kessel, D. Campbell, Y. Gribov, G. Saibene, G. Ambrosino, R.V. Budny, T. Casper, M. Cavinato, H. Fujieda, and R. Hawryluk *et al. Nucl. Fusion*, **49** 085034 (2009).
- [43] Sauter O. *et al. POP*, **4** 1654 (1997).
- [44] Chang Z. *et al. Phys. Rev. Lett.*, **74** 4663 (1995).
- [45] Chang Z and Callen J D. *Nucl. Fusion*, **2** 219 (1990).
- [46] J. A. Snipes *et al. FED*, **87** 1900 (2012).
- [47] E. Poli *et al. PPCF*, **52** 12402 (2010).
- [48] Muraglia M *et al. PRL*, **107** 095003 (2011).
- [49] Ishizawa A and Nakajima N. *POP*, **17** 072308 (2010).
- [50] Hornsby W A *et al. PPCF*, **57** 54018 (2015).

- [51] F. M. Poli *et al.* *Nucl. Fusion*, **58** 016007 (2018).
- [52] S.H. Kim *et al.* In *Proceedings of 41st EPS Conf. on Plasma Physics* (2014).
- [53] M. Schneider *et al.* *EPJ, RF topical conference* (2017).
- [54] Ye.O. Kazhakov *et al.* *Nucl. Fusion*, **55** 032001 (2015).
- [55] M J Singh, D Boilson, A R Polevoi, Toshihiro Oikawa, and Raphael Mitteau. *New Journal of Physics*, 19 055004 (2017).
- [56] F. Rytter *et al.* *Nucl. Fusion*, **53** 113003, (2013).
- [57] Militello-Asp E *et al.* Iter fuelling requirement and scenario development for h, he and dt through jintrac integrated modelling. In *2016 IAEA Fusion Energy Conference* (2016).
- [58] Ye.O. Kazakov *et al.* *Nucl. Fusion*, **55** 032001 (2015).

Princeton Plasma Physics Laboratory Office of Reports and Publications

Managed by
Princeton University

under contract with the
U.S. Department of Energy
(DE-AC02-09CH11466)

P.O. Box 451, Princeton, NJ 08543
Phone: 609-243-2245
Fax: 609-243-2751

E-mail: publications@pppl.gov

Website: <http://www.pppl.gov>